BERGISCHE
UNIVERSITÄT
WUPPERTAL

Fakultät für
Mathematik und Naturwissenschaften

Institut für Atmosphären- und Umweltforschung

Experimental and theoretical study of the reactions of atmospheric relevant epoxides with OH radicals and chlorine atoms

Dissertation

zur Erlangung des akademischen Grades eines

Doktor der Naturwissenschaften (Dr. rer. nat.)

vorgelegt von

Carmen María Tovar Ramos

unter Leitung von

Prof. Dr. Peter Wiesen

Wuppertal, Juli 2025

Eidesstattliche Erklärung

Hiermit versichere ich, dass ich die Arbeit selbstständig verfasst, keine anderen als die angegebenen Quellen und Hilfsmittel benutzt sowie Zitate kenntlich gemacht habe.

Wuppertal, Juli 2025

Einverständniserklärung

Ich bin damit einverstanden, dass meine Abschlussarbeit wissenschaftlich interessierte Personen oder Institutionen zur Verfügung gestellt werden kann. Korrektur- oder Bewertungshinweise in meiner Arbeit dürfen nicht zitiert werden.

Wuppertal, Juli 2025

Hinweis zum Einsatz von Künstlicher Intelligenz

Zur sprachlichen Optimierung (Klarheit, Kohärenz, Stil) wurde ein KI-Sprachmodell (ChatGPT, OpenAI GPT-4) unterstützend eingesetzt. Inhaltliche Erarbeitung, Forschung, Datenanalyse und Schlussfolgerungen sind ausschließlich das Werk der Autorin. Der Einsatz erfolgte im Einklang mit den Richtlinien zur wissenschaftlichen Integrität der Bergischen Universität Wuppertal.

Danksagung

Meinen tiefsten Dank richte ich an meine Mutter, die stets der Antrieb in meinem Leben war und mir die Kraft gegeben hat, jeden meiner beruflichen Erfolge zu erreichen. Mein Bruder Julio ist mein persönlicher Engel, dessen Unterstützung und Liebe mich immer begleiten. Ebenso danke ich meinen Geschwistern Sandra und Gustavo, deren Liebe mir in jedem Schritt den Mut gegeben hat, weiterzugehen. Ein besonderer Dank gilt auch meiner Nichte Gaby für ihre Zuneigung, die mir stets Freude bereitet hat. Schließlich möchte ich meinem Vater danken, der diesen Erfolg nicht mehr miterleben kann, aber immer an mich geglaubt hat und dessen Vertrauen mich weiterhin inspiriert.

Zusammenfassung

Diese Studie untersucht die Reaktivität und das kinetische Verhalten ausgewählter Epoxide – Cyclohexenoxid (CHO), 1,2-Epoxyhexan (12EHX), 1,2-Epoxybutan (12EB), trans-2,3-Epoxybutan (tEB) und cis-2,3-Epoxybutan (cEB) – gegenüber Hydroxylradikalen (OH) und Chloratomen (Cl). Als dominierendes atmosphärisches Oxidationsmittel spielt das OH-Radikal eine zentrale Rolle beim Abbau dieser Epoxide und fördert deren Umwandlung in sekundäre organische Aerosole (SOA) sowie andere niedrigflüchtige Verbindungen. Chloratome, obwohl primär in maritimen und anthropogen belasteten Regionen präsent, zeigen ebenfalls hohe Reaktivität und beeinflussen somit die atmosphärische Verweilzeit und Reaktionswege dieser Spezies.

Die Oxidation von Cyclohexenoxid erfolgt über multiple Pfade unter Beteiligung von OH-Radikalen und Cl-Atomen. Dabei entstehen bedeutende Oxidationsprodukte wie 2,3-Epoxycyclohexanon, 2,3-Epoxycyclohexanol, 2-Cyclohexen-1-on, Pentandial, Formaldehyd und Ameisensäure, die in dieser Arbeit identifiziert wurden. Hervorzuheben ist die Bildung von Ameisensäure über die Oxidation von R-CHOH-Radikalen, ein Prozess, der unabhängig von NOx-Konzentrationen abläuft und somit auf alternative Oxidationspfade jenseits der klassischen NOx-abhängigen Photochemie hinweist. Die Bildung von Ameisensäure, einer gering flüchtigen Verbindung, unterstreicht die Relevanz solcher Prozesse für die Säurebilanz von Wolken- und Aerosolwasser sowie für die SOA-Bildung.

Ein detailliertes Verständnis der mechanistischen Pfade der Cyclohexenoxid-Oxidation ist entscheidend, um atmosphärische Chemie-Modelle zu verbessern und die umweltrelevanten Auswirkungen der Epoxidoxidation adäquat zu bewerten.

Abstract

This study explores the reactivity trends and kinetic behavior of various epoxides, including cyclohexane oxide (CHO), 1,2-epoxyhexane (12EHX), 1,2-epoxybutane (12EB), trans-2,3-epoxybutane (tEB), and cis-2,3-epoxybutane (cEB), in relation to their interactions with hydroxyl radicals and chlorine atoms. As the predominant atmospheric oxidant, the OH radical plays a fundamental role in the degradation of these epoxides, facilitating their transformation into secondary organic aerosols (SOAs) and other low-volatility compounds. Similarly, chlorine atoms, although primarily concentrated in marine and polluted environments, exhibit significant reactivity toward these species, thereby influencing their atmospheric lifetime and altering their reaction pathways.

The oxidation of cyclohexane oxide via multiple pathways, primarily involving reactions with chlorine atoms and hydroxyl radicals, has been investigated in more detail. These oxidation processes result in the formation of several significant oxidation products, including 2,3-epoxycyclohexanone, 2,3-epoxycyclohexanol, 2-cyclohexen-1-one, pentanedial, formaldehyde, and formic acid, which have been identified in this study.

A notable feature of the oxidation of cyclohexane oxide evaluated in this study, is the production of formic acid via R-CHOH radicals' oxidation, which occurs irrespective of NOx levels. This highlights alternative oxidation pathways that extend beyond traditional NOx-dependent photochemistry. The production of formic acid, a compound characterized by its low volatility, highlights the broader atmospheric implications of hydrocarbon oxidation processes occurring in aqueous phases. This transformation plays a crucial role in the atmospheric chemical budget, influencing both secondary organic aerosol formation and the acidity of cloud and aerosol water. Understanding this pathway is essential for accurately representing the fate of organic compounds and their contribution to atmospheric chemistry.

Given the crucial role of these oxidation products, understanding the mechanistic pathways involved in cyclohexane oxide oxidation is essential for refining atmospheric chemical models and assessing the broader environmental impacts of epoxide oxidation.

Contents

1 Introduction

Epoxides are significant atmospheric constituents formed through various pathways and sources. One of the primary sources of epoxide emissions is the oxidation of isoprene, a five-carbon diene emitted predominantly from the biosphere, which accounts for more than 40% of nonmethane hydrocarbon emissions. Under pristine conditions, isoprene is oxidized by the hydroxyl radical (OH) to form hydroxyhydroperoxides, which further react to produce dihydroxyepoxides and reform OH, contributing nearly 100 teragrams of carbon per year to the atmosphere in the form of these epoxides (Paulot et al., 2009). Additionally, in urban environments with high levels of nitrogen oxides (NOx), isoprene photooxidation leads to the formation of methacrylic acid epoxide (MAE), a precursor to secondary organic aerosols (SOA) (Lin, Zhang, et al., 2013a). Another significant source of epoxides is the autoxidation and photochemical oxidation of olefins, which are substantial components of automobile exhaust. These processes result in the formation of various oxygenated aliphatics, including epoxides, which have been identified as carcinogenic and thus are of concern for air pollution control (Duuren, 1972). Furthermore, oxygenated volatile organic chemicals (OVOCs) like acetone, which can be emitted from terrestrial plant canopies, oxidation of dead plant material, biomass burning, and oceans, also contribute to the atmospheric pool of reactive compounds that can lead to epoxide formation (Potter et al., 2003). The formation of epoxides from isoprene and other hydrocarbons is crucial for understanding the link between gas-phase degradation and the formation of organic aerosols, which have significant implications for public health and climate systems (Claeys, 2010). Therefore, the major sources of epoxide emissions include biogenic emissions from isoprene, anthropogenic emissions from automobile exhaust, and various natural and anthropogenic sources of OVOCs.

1.1 Composition of the atmosphere

Earth's atmosphere consists of multiple regions, each distinguished by distinct temperature patterns as a function of altitude. This layered structure reflects the complex thermal dynamics governing the Earth's atmospheric system. The lowest layer, known as the troposphere, extent from the Earth's surface to approximately 15 kilometers and is distinguished by a decline in temperature as altitude increases (Wayne, 1985). The troposphere exhibits significant vertical mixing as a result of the presence of warm, less dense air situated beneath colder, denser air. Furthermore, the vast majority of atmospheric water vapor, clouds, and precipitation can be located within the troposphere of Earth. The boundary layer, which spans 0.5-2.0 km, is characterized by a complex and chemically active air mass resulting from the interaction of turbulent weather systems and both natural and anthropogenic emissions. The tropopause, the boundary between the troposphere and stratosphere, is located at an altitude of 10 - 15 km, varying with latitude and time of year.

The stratosphere, characterized by an inverted temperature gradient, is situated above the tropopause and ranges in altitude from approximately 15 to 50 kilometers. Due to the thermal inversion present in this layer, the movement of substances across the tropopause and the vertical diffusion within the stratosphere take place at considerably slow speeds. Similarly, one can view the stratosphere as a boundary that is situated above the troposphere. The rise in temperature with increasing height in the stratosphere can be attributed to a sequence of significant photochemical reactions.

The mesosphere, situated above the stratosphere, spans from the stratopause to approximately 80 to 90 km in altitude, experiencing a decline in temperature with increasing altitude until reaching the mesopause, which marks the lowest temperature point in the atmosphere. Referred to as the thermosphere, the area beyond the mesopause exhibits elevated temperatures attributed to the absorption of high-energy, short-wavelength radiation by N_2 and O_2. Within the upper mesosphere and lower thermosphere lies the ionosphere, a zone where ions are generated through the process of photoionization (Wayne, 1985)

1.1.1 Oxygenated volatile organic compounds

Oxygenated volatile organic compounds (OVOCs) represent a significant portion of the Volatile Organic Compounds (VOCs) released into the atmosphere, originating from both natural and anthropogenic sources. Among the anthropogenic sources of OVOCs, vehicular transportation, solvent utilization, residential heating, and industrial activities play crucial roles (Legreid, Reimann, et al., 2007; Placet et al., 2000; Sawyer et al., 2000). Biogenic emissions of OVOCs primarily originate from the growth of vegetation, plant residue, and the combustion of biomass (Mellouki et al., 2015). Also, OVOCs are generated within the atmosphere through the oxidation of various hydrocarbons that exist in the atmospheric environment. Environmental monitoring efforts often struggle to distinguish emissions from biogenic sources, evaporation, and secondary sources of oxygenated volatile organic compounds (OVOCs), such as the oxidation of non-methane hydrocarbons (NMHCs) (Legreid, Lööv, et al., 2007). (NMHCs) are identified as a primary origin of OVOCs (Atkinson, 2000; Mellouki et al., 2015; Read et al., 2012). Numerous atmospheric and environmental factors complicate the differentiation of emissions from diverse sources. For example, the eastern Mediterranean experiences high concentrations of primary and secondary gaseous pollutants, such as ozone, carbon monoxide, and reactive nitrogen, largely due to the downward motion of subsiding air and the reduced mixed layer depth, which limits the atmosphere's ability to dilute contaminants (Dayan et al., 2017). Also, seasonal variations also play a crucial role, as different months bring varying meteorological conditions, such as temperature, humidity, and wind speed, which influence the levels of pollutants like PM10, sulfur dioxide, nitrogen dioxide, carbon monoxide, and ozone (Cichowicz et al., 2017).

A vast group of chemical reactions arising from the oxidation of OVOCs are significantly involved in the generation of ozone and secondary organic aerosols. The products resulting from the oxidation of OVOCs are not only detected in heavily polluted regions but also in remote areas. An investigation recently carried out in a coastal suburban zone in Hong Kong revealed that over 77.4 percent of the species monitored were OVOCs.

In the same investigation, a notable presence of isoprene and OVOCs was identified during the autumn season. This phenomenon can be attributed to the increased photochemical activity that occurs during this specific time frame (Hui et al., 2023).

The epoxides studied in this work are cyclic OVOCs that have been very little studied. These epoxides are directly emitted from sources such as chemical industries, gasoline production, combustion processes, and engine exhaust (Fokin & Wu, 2006; Hereijgers et al., 2012; Kolb et al., 2001). Epoxides emissions can also be attributed to secondary atmospheric reactions, including the reaction of O (^{3})P with isoprene, which may occur with a yield approaching 80% (Atkinson, Aschmann, et al., 1994; Paulson et al., 1992b).

1.1.2 Reactive species

In a "clean" tropospheric environment, excited oxygen O(^{1}D) atoms react with water vapor to generate hydroxyl (OH) radicals, which serve as the primary oxidizing agent in the troposphere. These OH radicals regulate the atmospheric lifetime of numerous species, and their potential to contribute to climate change, air pollution, and ozone formation (Atkinson, 1997; DeMore, W.B. et al., 1997) according with the following reactions:

$$O_3 + h\nu(\leq 336\,nm) \rightarrow O_2 + O(^1D)$$

$$O(^1D) + M \rightarrow O(^3P) + M$$

$$O(^3P) + O_2 + M \rightarrow O_3 + M$$

$$O(^1D) + H_2O \rightarrow 2OH$$

The OH radicals react with Organic Volatile Compounds (VOCs) regenerating OH radicals by propagation chain in a very complex cycle. The major initiation sources of the OH radical in the atmosphere are the photolysis of O_3, formaldehyde (HCHO) and nitrous acid (HONO) in the presence of NOx (Elshorbany et al., 2010). Another source of OH radicals is the ozonolysis of alkenes. However, in the lower atmosphere, HONO is the major primary source of OH radicals (Acker et al., 2006; Dusanter et al., 2009; Elshorbany et al., 2009, 2010; Ren et al., 2003, 2006).

The OH radical has a calculated average global abundance of about 106 radicals/cm^3 (Prinn et al., 2005).

Conversely, molecular chlorine is an important precursor of chlorine atoms, a highly reactive species in the atmosphere. Chlorine can be emitted daytime from coal combustion (Riedel et al., 2013), water facilities (Riedel et al., 2012), and through different photochemical processes (Impey et al., 1997; Liao et al., 2014; X. Liu et al., 2017; Priestley et al., 2018). Molecular chlorine can be quickly photolyzed to release two Cl atoms during the daytime, and its production through heterogeneous reactions is a key step in the O_3 destruction over Antarctica during

austral spring (Solomon et al., 1986). Although, chlorine is a reactive specie found to typically peak during nighttime, it is also observed during daytime in elevated levels (17-450 pptv) (Peng et al., 2022).

Cl atoms can strongly influence atmospheric abundances of relevant trace gases such as methane and ozone (O_3) and is potentially a major removal process for alkanes and other VOCs (Atkinson, 2000; Peng et al., 2022). Atomic chlorine is known to destroy ozone (O_3) through catalytic cycles (L. T. Molina & Molina, 1987; M. J. Molina & Rowland, 1974). According to a recent study, the Cl atoms account for 59% of daily integrated oxidation of non-methane alkanes, 16% of aromatics, 13 % of aldehydes, and 9 % of dialkenes. Besides, the reactions of Cl atoms with VOCs produce RO_2 radicals, which are recycled to form HO_2 and OH radicals, thereby collectively increasing the average mixing ratios of OH, HO_2, RO_2 radicals by ~4%, ~17%, and 27%, respectively (Peng et al., 2022).

The role of chlorine atoms (Cl) in atmospheric oxidation is not just limited to the marine boundary layer, where they are produced through heterogeneous reactions which involve sea salt. Instead, the importance of this oxidant includes coastal and continental urban areas, debt to the presence of precursors as $ClNO_2$ and Cl_2 formed for anthropogenic pollution. Chlorine atoms play a significant role in atmospheric photochemistry, contributing approximately 9% as a primary source of radicals (Young et al., 2014).

By comparison, nitrate radicals (NO_3) play a crucial role as atmospheric oxidants for organic species during nighttime. Unlike the daytime, when hydroxyl radicals (OH) and chlorine atoms (Cl) are the primary oxidants, at night, NO_3 becomes the dominant oxidizing agent for volatile organic compounds (VOCs), including isoprene, monoterpenes, and other terpenoids.

While the reaction rate of NO_3 with VOCs is typically lower than that of OH radicals, the nighttime oxidation by NO_3 still contributes significantly to the overall atmospheric oxidation of organic compounds.

1.2 Chemistry of the troposphere

The chemistry of the troposphere is characterized by complex interactions involving various gases and reactive species, with significant implications for atmospheric composition and air quality. The troposphere, the lowest layer of Earth's atmosphere, contains most atmospheric trace gases and is a dynamic region where numerous chemical reactions occur, primarily driven by the hydroxyl radical (OH) (Derwent, R. G. et al., 1995). These reactions are crucial for the oxidation of trace gases, including volatile organic compounds (VOCs) and nitrogen oxides (NOx), which play a pivotal role in ozone formation and the overall oxidizing capacity of the troposphere (Akimoto, 2016).

Oxygenated organic compounds are in general more reactive than the alkanes from which they are derived and strongly affect atmospheric oxidation and compared to other hydrocarbons, are much more reactive towards atmospheric oxidants such as OH (Mellouki et al., 2015). In recent study, OVOCs were found to be the largest contributor to daytime OH reactivity (48.9%-51.5%) and the ozone formation potential (OFP) (48.2%-53.5%) (Hui et al., 2023). At the same time, photolysis of OVOCs is a primary source of the hydrogen oxide radicals HOx ($OH+HO_2$) and organic peroxy radicals (RO_2), promoting the production of peroxyacetyl nitrate (PAN, $CH_3C(O)OONO_2$) (Z. Liu et al., 2010, 2012; Singh et al., 1995). As established in (Min et al., 2011) the active role of OVOCs in the production of OH radicals can affect the oxidation ability of the atmosphere in a significative way. A recent study shows that OVOCs concentration and their effect on peroxy radicals, PAN, and ozone production are overestimated near the surface of earth in up to 76% in box models simulations compared with 1-D models. The vertical mixing and the huge amount of OVOCs reacting on the surface in the troposphere favors the photochemistry in the whole boundary layer (Qu et al., 2021).

(Huang et al., 2020) found a high contribution of OVOCs in regional pollution in North China and stated the urgence in the reduction of emissions of anthropogenic origin in the country. The reason is that anthropogenic and biogenic emissions contribute comparatively the same to pollution, but biogenic sources are uncontrollable.

1.2.1 Photo-oxidation

Atmospheric photooxidation is a complex process that plays a crucial role in atmospheric chemistry, influencing the formation of various oxidants and secondary pollutants. This includes the production of gas-phase hydrogen peroxide (H_2O_2) from the photooxidation of chromophoric dissolved organic matter (CDOMs) on particle surfaces, which can further oxidize sulfur dioxide to form sulfate, consequently contributing to acid rain and impacting the global radiation budget. Additionally, the photooxidation of volatile organic compounds like α-pinene and β-pinene leads to the formation of secondary organic aerosols (P. Liu et al., 2021).

Epoxides can be formed through the photooxidation of isoprene, a common biogenic volatile organic compound. Under high nitrogen oxides (NOx) conditions, methacrylic acid epoxide (MAE) is identified as a precursor to isoprene-derived SOA, highlighting the importance of epoxides in urban atmospheric chemistry (Lin, Zhang, et al., 2013a). This process is supported by computational chemistry and air quality model simulations, which align with field observations, suggesting that MAE chemistry is significant in urban areas with high isoprene emissions(Lin, Zhang, et al., 2013a).

When these compounds are oxidized in the presence of NOx, they lead to the formation of secondary organic aerosols (Kaminski et al., 2017). The oxidation of β-pinene, for instance, involves complex radical chemistry, including the formation of OH and HO_2 radicals, which are crucial for maintaining the atmospheric oxidative capacity.

However, models frequently underestimate the concentrations of these reactive species, implying the existence of unaccounted-for sources of hydroperoxyl radicals, potentially originating from new reaction pathways involving alkoxy radicals(Kaminski et al., 2017).

1.2.2 OH chemistry

Hydroxyl radicals are often referred to as the 'atmosphere's detergent' due to their crucial role in the degradation of a diverse array of pollutants, including volatile organic compounds, carbon monoxide, and methane (Stevenson et al., 2020). As highly reactive oxidizing agents, OH radicals initiate degradation processes for a wide range of organic compounds, including epoxides. The primary interaction between OH radicals and epoxides occur through hydrogen abstraction or addition to the epoxide ring, leading to the formation of various reaction intermediates. For example, in the case of isoprene-derived epoxides, studies have shown that gas-phase OH radical reactions significantly impact their fate, often competing with aerosol-phase processing. These reactions tend to form secondary organic aerosols or lead to further oxidation products depending on environmental conditions like temperature and humidity (Jacobs et al., 2013). The reactivity of epoxides toward OH radicals is influenced by the specific structure of the epoxide compound. Computational investigations have revealed that certain epoxide isomers, such as epoxybutanes, exhibit varying reactivities due to differences in their molecular configurations (Daimari et al., 2024). In greater depth, our recent studies have indicated a potential mechanism for evaluating the reactivity of epoxides with different radicals in the atmosphere. This reactivity would not solely depend on their molecular configuration, but rather on the pseudo-ethylenic nature of the epoxides (Tovar et al., 2021, 2022).

Also, the existence of epoxides within the atmospheric environment plays a significant role in the generation of additional hydroxyl (OH) radicals via a multitude of mechanisms. This phenomenon carry several critical implications, including the increase of the oxidative potential of the atmosphere (Lelieveld et al., 2016), the facilitation of secondary organic aerosol synthesis (Surratt et al., 2010), and the influence on both regional and global atmospheric chemistry (Hallquist et al., 2009). Epoxides exhibit notable reactivity and can engage in diverse transformations in the atmosphere that either directly or indirectly yield OH radicals (Peeters et al., 2014).These mechanisms frequently involves the reaction of epoxides with pre-existing oxidants or the breakdown of epoxides to form novel radicals.

1.2.3 Cl atoms chemistry

Recent investigations have revealed that the concentrations of reactive chlorine species are elevated beyond prior estimations, indicating that the atmospheric chlorine chemistry is more substantial than previously acknowledged. Chlorine radicals have the capacity to undergo reactions with hydroperoxy (HOx) radicals and nitrogen oxides (NOx), thereby modifying the oxidative capacity of the atmosphere. Experimental investigations under low-NOx conditions utilized isoprene and chlorine as the primary sources of VOCs and oxidants. Following the complete consumption of isoprene, the observed yields of SOA varied from 7 to 36 %, demonstrating a decline with prolonged photooxidation and aging of the SOA. The formation of particulate organochlorides was reported. In the same study, multi-generational chemical processes were identified, including ions indicative hydroperoxides, chloroalkyl hydroperoxides, isoprene-derived epoxydiol (IEPOX), and hypochlorous acid (HOCl), signifying secondary OH production and the consequent chemistry arising from Cl-initiated reactions. This study is an evidence of the SOA formation resulting from the chlorine-initiated oxidation of isoprene (D. S. Wang & Ruiz, 2017). In another recent study, a chemistry module was developed, which was integrated into an MCM box model to assess the effects of nitryl chloride ($ClNO_2$), a byproduct of nocturnal halogen activation by nitrogen oxides (NO_X), on the subsequent day's atmospheric photochemistry. By employing constraints from recent observational data gathered at a coastal site in Hong Kong, southern China, the modeling analyses indicate that the Cl radicals generated from the photolysis of $ClNO_2$ may significantly enhance the atmospheric oxidative capacity, volatile organic compound (VOC) oxidation, and ozone (O_3) formation, particularly during the early morning hours (Xue et al., 2015). Recent investigation also showed that the atmospheric oxidation capacity significantly influenced by chlorine, even surpasses the impact of hydroxyl radicals during the morning hours in Leicester. Sensitivity analyses indicate that the enhanced consumption of volatile organic compounds due to active gas-phase and aqueous-phase chlorine chemistry leads to an increase in the concentrations of OH, hydroperoxyl, and organic peroxy radicals near sunrise (Soni et al., 2023).

Part A:

Cumulative Part

2 Experimental and theoretical study of the reactivity of a series of epoxides with chlorine atoms at 298 K

Reproduced from:" Carmen M. Tovar, Alexander Haack, Ian Barnes, Iustinian Gabriel Bejan and Peter Wiesen: Experimental and theoretical study of the reactivity of a series of epoxides with chlorine atoms at 298 K, Phys. Chem. Chem. Phys., 2021, 23, 5176. DOI: 10.1039/d0cp06033j" with permission from the PCCP Owner Societies.

Evaluating the reactivity of epoxides in the gas phase is very important due to their wide distribution in the atmosphere, potential health implications and atmospheric impact. The kinetic rate constants for the oxidation of epoxides have been very little studied until now. From the experimental data obtained in this work it has been observed that there is an increase in reactivity towards chlorine atoms as a CH_2 group is added to the hydrocarbon chain. The Structure Activity Relationship (SAR) method usually provides a good approximation of the rate constant for a wide series of compounds especially for those without complex structure and multiple organic functions. However, a good determination of the factors included in SAR estimations depends largely on the database of these compounds, which in the case of epoxides is very limited. The SAR estimation method also does not take into account other possible factors that could affect reactivity, such as the geometry of the molecule. The aim of this work is to further evaluate the reactivity of epoxides with chlorine atoms using experimental determinations, theoretical calculations and SAR estimations. For this, rate coefficients have been measured at 298± 2 K and 1000 ±4 mbar pressure of synthetic air in a 1080 l Quartz Reactor (QUAREC) and a 480 l Duran glass reactor for the reaction of chlorine atoms with cyclohexene oxide (CHO), 1,2-epoxyhexane (12EHX), 1,2-epoxybutane (12EB), trans-2,3-epoxybutane (tEB) and cis-2,3-epoxybutane (cEB). Theoretical calculations for the reactions studied are in good agreement with our experimental findings and provide insights about the position of the H atom abstraction and reactivity trends for a series of epoxides. The importance of taking into consideration geometrical distribution and the ring influence to improve SAR calculations is discussed.

2.1 Introduction

Epoxides are the simplest known oxygen-containing heterocycles. They are widely distributed in the atmosphere from anthropogenic sources and have important applications in chemical industries due to their strong proton affinity. They are often used as intermediates in the synthesis of various industrial polymers, and also in electroplating, lithium batteries, polymers and gasoline production (Abraham et al., 1982; Altway et al., 2015; Belaribi et al., 2015; Malik et al., 2016; Pang et al., 2015).

Furthermore, cycloaliphatic epoxides like cyclohexene oxide (CHO), are one of the major types of epoxy resins utilized in coatings industry (Wallington, Dagaut, et al., 1988).

Epoxides are used as well in fine chemistry, in the production of pharmaceuticals, perfumery, plasticizers and pesticides (Grigoropoulou et al., 2003; Oyama, 2008). CHO can be enantio-selectively converted into chiral 1,2-amino-cyclohexanol or 1,2-diaminocyclohexane, which are both building blocks for the preparation of natural and synthetic biologically active molecules like amino acids (Ager et al., 1996; Anaya de Parrodi, 2006).

Whereas 1,2-epoxyhexane (12EHX) is used as a passivating agent for core–shell aluminium nanoparticles,(Jelliss et al., 2013) 1,2-epoxybutane (12EB) has applications in the chemistry of the modification of carboxylic acid ends groups in swollen polymer particles (e.g. in poly butylene terephthalate, PBT) in supercritical fluids(Pagliaro, 2006) and is applied in the production of surfactants and as stabilizer for chlorinated hydrocarbon solvents and gasoline additives (*Re-Evaluation of Some Organic Chemicals, Hydrazine and Hydrogen Peroxide (Part 1, Part 2, Part 3). IARC Monographs on the Evaluation of Carcinogenic Risks to Humans Volume 71*, 1999).

Cyclic ethers are also formed in the initial reactions of alkyl radicals with molecular oxygen in combustion and pre-combustion processes that occur at moderate temperatures. They represent a significant part of the oxygenated pollutants found in the exhaust gases of engines (Auzmendi-Murua & Bozzelli, 2014). Cyclohexene oxide has been detected in the oxidation

and auto-ignition of cyclohexene by rapid compression between 600 K to 900 K and 0.7 MPa to 1.4 MP (Lemaire et al., 2001).

Recent studies have shown an increasing interest in the atmospheric oxidation processes with chlorine atoms (McGillen et al., 2020).

Epoxides contribute in significant amounts to reaction products of the chemical degradation of VOCs in the atmosphere. The formation of cyclic ethers is considered as an important product in the OH radical initiated oxidation of aromatic compounds (Schwantes et al., 2017), isoprene (Paulot et al., 2009) in the ozonolysis of furans (Li et al., 2018), sesquiterpenes (Richters et al., 2016) and biomass derived alcohols (Almatarneh, Elayan, Abu-Saleh, et al., 2019). Isoprene-derived epoxides can make up a major proportion of the atmospheric SOA in many continental local areas(Hu et al., 2015; Worton et al., 2013).

A recent study has reported the annual global isoprene emission for about 500 to 750 Tg isoprene (440 to 660 Tg carbon) using MEGAN ranges (Guenther et al., 2006). Extensive studies of SOA formation in the south-eastern United States have identified epoxide intermediates as key species in the formation of isoprene-derived SOA (Budisulistiorini et al., 2013, 2015; Lin, Knipping, et al., 2013; Lin, Zhang, et al., 2013b; Paulot et al., 2009; Surratt et al., 2010; Xu et al., 2015). Global simulations estimate a flux of up to 100 Tg of carbon per year of the dihydroxy epoxides derived from isoprene photooxidation(Paulot et al., 2009).

The atmospheric degradation mechanism for many compounds is still unclear, with poor carbon balance.

Prior to evaluating the impact that these compounds have on the atmosphere, it is important to know their reactivity and structural properties, which can be key in the elucidation of reaction mechanisms. Previous studies suggest that the addition of an ether linkage to an alkane leads to a weakening of the C–H bonds adjacent to the ether site. Whether the enhancement in reactivity is restricted to the C–H bonds located near the ether linkage, or whether the enhancement extends further down the molecule is difficult to ascertain given the data currently available in a series of aliphatic ethers with OH, Cl and NO_3 (J. Calvert et al., 2011).

Our goal in this work is to gain insight into how geometrical distribution and ring tension can influence the reactivity of epoxides towards chlorine atoms. Five representative epoxy compounds were selected to develop kinetic calculations to evaluate the reactivity along the hydrocarbon chain. Later, theoretical calculations were developed to deepen the influence of the ring and ether group but considering the geometrical configuration of the molecule, which cannot be properly evaluated with experimental measurements alone.

These insights could improve future SAR calculations and explain the reactivity of epoxide in a more accurate way. These observations will also be useful to feed the atmospheric models for this kind of compound that has been until now very little studied. To the best of our knowledge, this is the first kinetic and theoretical investigation of these reactions.

2.2 Methods

2.2.1 Experimental Methods

Experiments have been performed in a 1080/Quartz reactor (6 m) and a 480/Duran glass reactor (3 m) under the following conditions: (298 ± 2) K and (1000 ±4) mbar total pressure of synthetic air. Fourier Transform Infrared Spectroscopy (FTIR) equipped with a liquid nitrogen cooled mercury–cadmium–telluride detector with a resolution of 1 cm^{-1} has been employed for reactants monitoring.

The 3 m reactor consists of a cylindrical Duran glass vessel (3 m length, 45 cm dia.) closed at both ends by Teflon coated aluminium end flanges. Integrated on the metal flanges are ports for the inlet of reactants into the reactor and for the collection of samples from the reaction mixtures for further analysis. Other accessories, like a mixing fan to ensure homogeneity of the reaction mixtures and a capacitance manometer, are also located on the flanges. Arranged concentrically around the outside of the reactor are 32 super actinic fluorescent lamps (Philips TLA 40 W/05, $300 \leq \lambda \leq 450$ nm, $\lambda_{max} = 360$ nm). The vacuum (ca. 10^{-3} mbar) is maintained by means of a Leybold turbo-molecular pump, model RUVAC WZ 151 (500 $m^3 h^{-1}$), backed by a Leybold double stage rotary fore pump, model D40B (200 $m^3 h^{-1}$). The reactor is equipped with

built-in White mirror systems, which were usually operated at total path lengths of 51.6 m for the acquisition of the IR spectra.

Barnes et al. (Barnes et al., 1994) provided a detailed description of the 6 m reactor, and in a more recent publication(Barnes et al., 2016) the system has been described as follows: the reactor consists of two quartz glass tubes with an inner diameter of 47 cm and a wall thickness of 5 mm. The reactor can be evacuated to 10^{-3} mbar using a pumping system consisting of a turbo-molecular pump backed by a double stage rotary fore pump. Homogeneous mixing of the reactants in the reactor is ensured by magnetically coupled Teflon mixing fans located inside the reactor. Two types of lamps are available to photo-dissociate the radical/atom precursors: 32 super actinic fluorescent lamps (Philips TL 05/40 W: $320 \leq \lambda \leq 480$ nm, $\lambda_{max} = 360$ nm) and 32 low-pressure mercury lamps (Philips TUV/40 W, $\lambda_{max} = 254$ nm). The lamps are wired in parallel and can thus be switched individually.

They are distributed evenly around the photo reactor to ensure homogeneous irradiation within the reactor. A White type multiple-reflection mirror system set at a total optical path length of (484.7 ± 0.8) m is mounted inside the photo reactor.

This optical system was used for sensitive monitoring of reactants and products in the IR spectral range 4000–700 cm^{-1}. A Nicolet Nexus FT-IR spectrometer equipped with a KBr beam splitter, and a liquid nitrogen cooled mercury–cadmium–telluride (MCT) detector is used to record IR spectra with a spectral resolution of 1 cm^{-1}.

A Globar was used as IR light source. All mirrors are gold coated to increase reflectivity efficiency. Typically, 60 interferograms were co-added per spectrum over a period of approximately 1 minute and 15–20 such spectra were recorded per experiment.

2.2.2 Relative rate method

Rate coefficients for the reactions of Cl atoms with epoxides were determined using the relative rate method(Finlayson-Pitts & Pitts, 2000) in which the relative disappearance rates of the epoxides compared with different reference compounds were monitored in the presence of Cl atoms.

The photolysis of Cl_2 with the fluorescent lamps was used to generate Cl atoms:

$$Cl_2 + \lambda\nu\ (320 < l > 480\ nm) \rightarrow 2Cl \qquad (1)$$

Reaction mixtures consisting of a reference organic compound, the sample epoxide and the radical precursor compounds, diluted in synthetic air, were prepared in the reactor and left to mix prior to photolysis for approximately 15 min. Measured amounts of the reagents were flushed into the reactor under reduced pressure by a stream of synthetic air and the reactor was then filled with synthetic air to atmospheric pressure.

Typical photolysis times ranged from 15 to 20 min. In the presence of the chlorine atoms the epoxide under investigation and the reference compound are consumed by the following reactions:

$$Cl + Epoxide - Products\ (k_{epoxide}) \qquad (2)$$

$$Cl + Reference - Products\ (k_{reference}) \qquad (3)$$

Provided that the reference compound and the epoxides are lost only by reactions (2) and (3), then it can be shown that:

$$ln\left\{\frac{[Epoxide]_0}{[Epoxide]_t}\right\} = \frac{k_{Epoxide}}{k_{reference}} ln\left\{\frac{[Reference]_0}{[Reference]_t}\right\} \text{ (I)}$$

where, [Epoxides]0, [Reference]0, [Epoxide]t and [Reference]t are the concentrations of the epoxides and reference compound at times t=0 and t, respectively and $k_{epoxide}$ and $k_{reference}$ are the rate coefficients of reactions (2) and (3), respectively.

In order to test for possible loss of the reactants through photolysis and wall deposition, mixtures of the reactants in nitrogen or air in the absence of chlorine were irradiated for 30 min. Photolysis and wall deposition was found to be negligible for all epoxides and the reference compounds. Additionally, various experiments were performed to assess possible loss of the reactants and references via reaction with molecular chlorine. No significant direct reaction of the epoxides with molecular chlorine was observed on leaving the compounds in the dark in the reactor for at least the reaction time duration.

The initial mixing ratios of the oxidant precursor molecular chlorine in the experiments performed in the 6m reactor, were typically ~5 ppmv, and ~42 ppmv in the 3m reactor. The initial mixing ratios for the epoxides and reference compounds are shown in Table I (supplementary information).

All epoxy and reference compounds used in this study were obtained from Sigma Aldrich and used without further purification. The stated purities were as follows: cyclohexene oxide 98%; 1,2-epoxyhexane 97%; 1,2- epoxybutane 99%; trans-2,3-epoxybutane 97%; cis-2,3-epoxybutane 97%; propylene 99%; methacrolein 95%; butane 99% and ethylene 99,5%. Synthetic air has been provided by Messer GmbH with a 99.999%.

2.2.3 Computational methods

All calculations were conducted with the Gaussian16 program package (Frisch et al., 2016). GaussView6 (Dennington, Roy et al., 2019) together with a standard text editor were used to create input files and analyze output files. We used density functional theory (DFT) applying the B3-LYP (Becke, 1993; Lee et al., 1988) exchange-correlation function with Grimme's GD3-BJ empirical dispersion corrections (Grimme et al., 2011) to account for long range interactions. We chose the def2-TZVPP (Weigend & Ahlrichs, 2005) basis set for all atoms because of its generality and good triple-zeta quality. All SCF energies were converged within a threshold of 10^{-8} Hartree, corresponding to „tight convergence".

All stationary geometries, i.e., minimum as well as transition state structures, were optimized with „tight convergence" criteria (in Hartree/Bohr: Max force=1.5E-^{5}, RMS force=1.0E^{-5}, Max

displacement=6.0E^{-5} and RMS displacement=4.0E^{-5}) and normal mode were optimized with tight convergence criteria and normal mode analysis was performed to check the correct number of imaginary frequencies (zero for minima, one for transition states). It was also checked whether the movement along the imaginary mode in the transition state structures corresponds to the expected reaction path. The harmonic frequencies of the normal modes were used to calculate thermochemical data, i.e. free reaction enthalpies, Δ_R G.

Potential energy surface (PES) scans, using the same level of theory (except that the default geometry convergence criteria), were conducted to either find initial guesses for transition states or minimum energy paths for the H-abstraction by the chlorine atom. This was done by gradually changing one coordinate (e.g. elongation or shortening of a bond distance) while allowing all other geometrical parameters to relax. For the H-abstractions, however, some angles were held constant to model, for example, a linear approach of the chlorine atom onto the C-H bond.

2.3 Results and discussion

Figure 1 shows the exemplary plots of the rate coefficients of cyclohexene oxide (CHO), 1,2-epoxyhexane (12EHX), 1,2-epoxybutane (12EB), *trans*-2,3-epoxybutane (*t*EB) and *cis*-2,3-epoxybutane (*c*EB) according to eq I, obtained for the gas-phase reaction of chlorine atoms with different reference compounds using 3m reactor. Very good linear plots with almost zero intercepts were obtained for all epoxy compounds, which confirms that no interferences are indicated in the rate constant determination.

The average rate coefficient ratios ($k_{epoxide}/k_{reference}$) obtained from the slopes of these plots from a minimum of at least two experiments for each compound are given in. Very good agreement between the rate coefficients obtained using two or three different reference hydrocarbons have been observed. Figure 2 shows the experiments performed for 1,2-epoxybutane in the presence of chlorine atoms using both reactors. It is worth mentioning that the rate coefficients obtained were almost identical.

The errors quoted in for the average $k_{epoxide}$ include the 2σ statistical error from the linear regression analyses of the plots with an additional 35% uncertainty contribution in the recommended values of the reaction rate coefficients for the reaction of the reference compounds with chlorine (J. Calvert et al., 2011).

Table 2 compares the experimental rate coefficients with the values obtained by a SAR estimation method and those found in the literature for other epoxy compounds. The third column in Table 2 shows the rate coefficient, k_{SAR}, predicted from the structure-reactivity relationship (SAR) method (Aschmann & Atkinson, 1995) that has been tentatively applied for the epoxides studied by using the factor F(O)=1.18 (Middala et al., 2011; Notario et al., 2000) and F(O)=1.45 (J. Calvert et al., 2011). This factor corresponds to the calculated influence of the ether group on the rate constant. In the SAR method, the calculation of the rate constants depends only on the identity of the substituents bonded to these groups. As can be seen in Table 2 the SAR predicted values for the rate coefficients are in reasonable agreement with the experimentally determined values of the present study.

From the rate coefficients in

Table 1 it can be derived that the methyl group (i.e. propylene oxide) added to the cyclic ether moiety (ethylene oxide) increases up to 6 times the reactivity of the epoxy compounds. Furthermore, 2,3-epoxybutane shows a doubled reactivity towards chlorine atoms by comparison with propylene oxide. This enhanced reactivity can be attributed mainly to the additional methyl group attached to the ethylene oxide heterocyclic ring. Table 3shows the rate coefficients of the reaction of different ethers and epoxides towards chlorine atoms, where ethers and epoxides of the same number of carbons, increase their reaction rate coefficient as the number of CH_2 groups adjacent to ether group increases. In order to try to elucidate the reason for this reactivity trend in the epoxy compounds we calculated thermochemical data and minimum energy paths on the potential energy surface (PES) for each compound, which gives us an important insight about the likelihood of each H abstraction reaction by chlorine atoms.

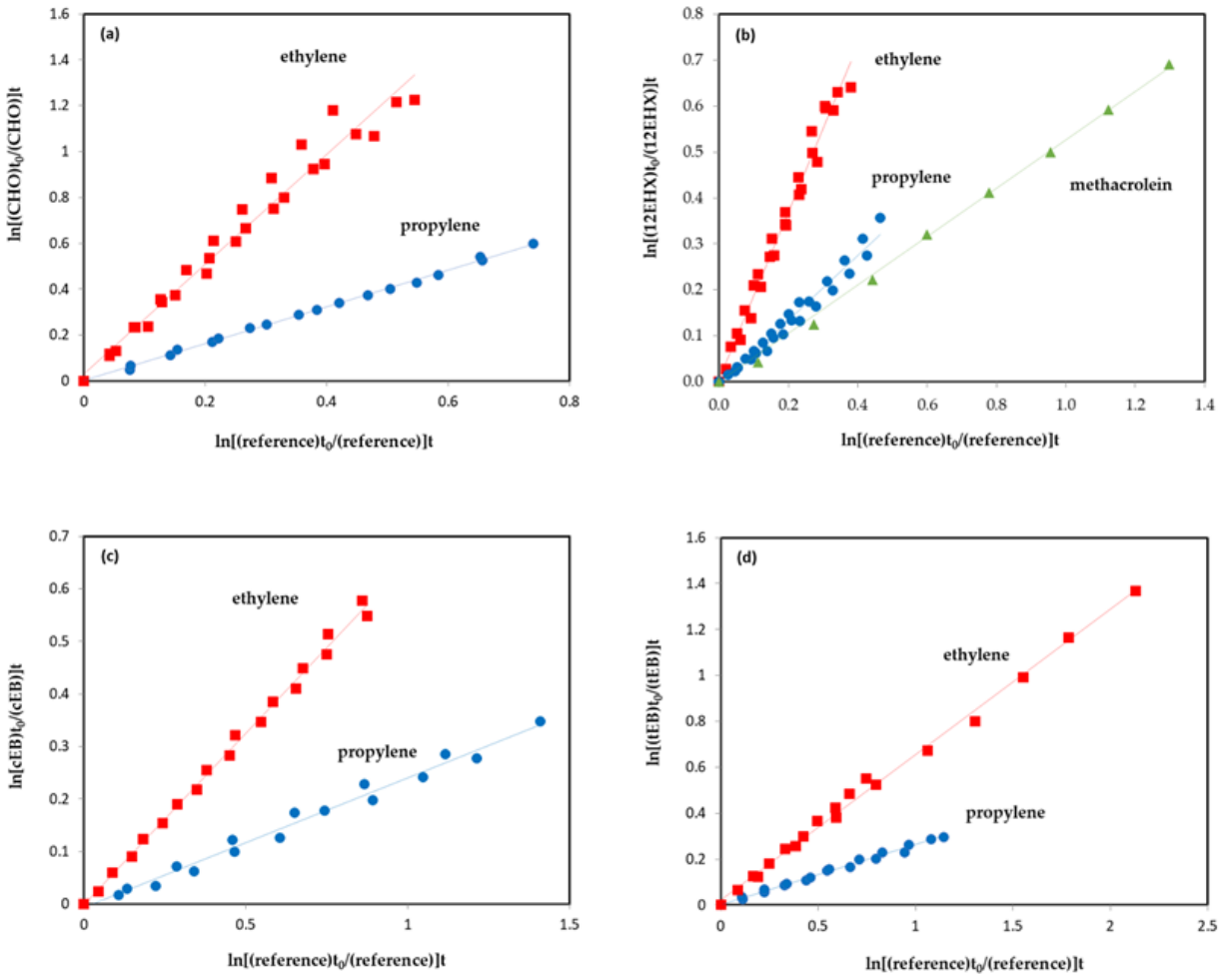

Figure 1 - Rate coefficients for the reaction of chlorine atoms with (a) cyclohexene oxide; (b)1,2-epoxy hexane; (c) cis-2,3-Epoxybutane; (d) tras-2,3-epoxybutane using ethylene, methacrolein and propylene as reference compounds.

For the PES scans, we picture the potential energy as a function of the difference of the Cl-H and H-C distances, which gives us a coordinate covering the two important geometrical parameters that change during the reaction. Values smaller than zero correspond to a long Cl-H and short H-C bond (reactant channel), values larger than zero correspond to a short Cl-H and long H-C bond (product channel). For the following discussion, we will consider that for *cis*-2,3-epoxybutane and *trans*-2,3-epoxybutane H1 is the hydrogen atom of the CH group directly attached to the ring (position α) and H_2 is one of the hydrogen atoms of the CH_3 group next to the ring (position β).

Table 1 - Measured rate coefficient ratios, $k_{epoxide}/k_{reference,}$ and the rate coefficients for the reactions of chlorine atoms with epoxides at (298 ±2) K derived from these ratios.

Epoxide	Structure	Reference	$K_{epoxide}/k_{reference}$	$k_{epoxide}$ (cm^3 $molecule^{-1}$ s^{-1})
Cyclohexene Oxide		Propylene	0.803±0.007	(2.17±0.24)×10^{-10}
		Ethylene	2.394±0.073	(2.63±0.72)×10^{-10}
		Average		(2.40±0.76)×10^{-10}
1,2-epoxyhexane	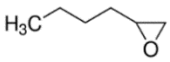	Propylene	0.707±0.022	(1.91±0.22)×10^{-10}
		Ethylene	1.821±0.042	(2.00±0.55)×10^{-10}
		Methacrolein	0.539±0.006	(1.40±0.16) ×10^{-10}
		Average		(1.77±0.61)×10^{-10}
1,2-epoxybutane	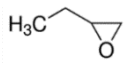	Propylene	0.324±0.013	(8.65±1.02)×10^{-11}
		Ethylene	0.746±0.012	(8.21±2.24)×10^{-11}
		Average		(8.43±2.46)×10^{-11}
trans-2,3-epoxybutane		Propylene	0.261±0.053	(7.03±0.79)×10^{-11}
		Ethylene	0.633±0.009	(6.96±1.91)×10^{-11}
		Average		(6.99±2.06)×10^{-11}
cis-2,3-epoxybutane	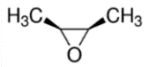	Propylene	0.247±0.007	(6.66±0.77)×10^{-11}
		Ethylene	0.652±0.009	(7.17±1.96)×10^{-11}
		Average		(6.92±2.11)×10^{-11}

In the case of the 1,2-epoxybutane, we will use H0 for one of the hydrogen atoms of the CH_2 group directly attached to the ring. Similarly, H1 is the hydrogen atom of the CH group directly attached to the ring (position α) and H2 is the H atom abstracted for the CH_2 next to the ring (position β) in the aliphatic chain Figure 3.

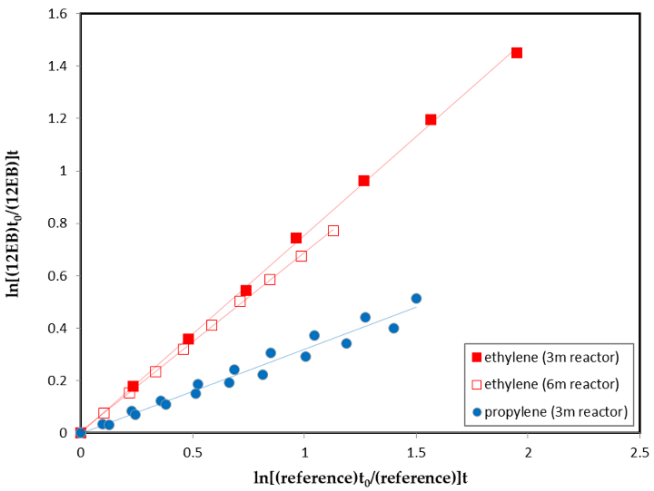

Figure 2 - Rate coefficients for the reaction of 1,2-epoxybutane towards chlorine atoms with ethylene and propylene as reference compounds (using 6m and 3m reactors).

The H atom abstraction paths for H1 and H2 of *cis*-epoxybutane and *trans*-epoxybutane are shown in Figure 4. Firstly, it can be observed that decreasing the Cl-H distance is accompanied by a monotonically decrease of the potential energy from its asymptotic value and no TS is visible. This is true for all abstraction reactions considered here. This is why the discussion about the rate constants have to focus on the form of the minimum energy paths and the energies of the reactant and product channels.

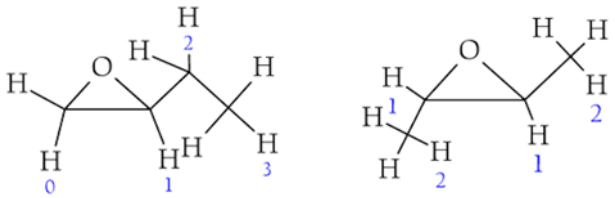

Figure 3 - Diagram of the possible hydrogen atoms considered for the abstraction channels.

Comparing the shape of the reaction paths for the H1 and H2 abstractions, it can be noticed that the former has only one minimum lying in the reactant channel and the latter has two, each in the reactant and product channels.

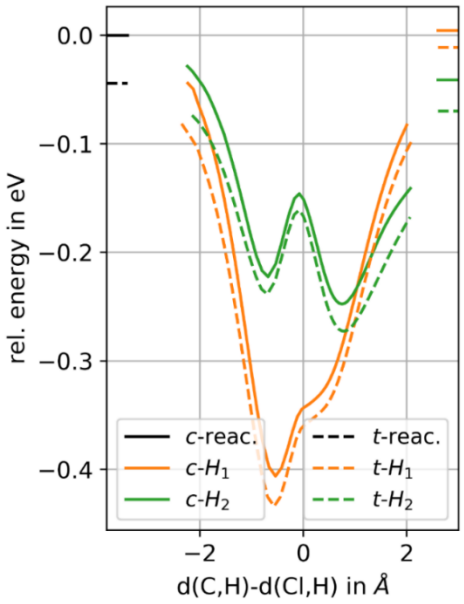

Figure 4 - Potential energy surface (PES) scans, for the H atom abstraction from cis/trans-2,3-epoxybutane by chlorine atoms.

Assuming an approach of Cl and the formation of a metastable pre-reactive complex, in the H1 case, it will mostly remain in the reactant channel and in the H2 channel there will be a distribution between the two minima, slightly favouring the product channel one due to its lower energy. If the pre-reactive complex falls apart, this configuration will strongly influence in which direction the reaction occurs. Considering also the energy of both channels leads to the conclusion that for H1 the abstraction reaction is less likely than for H2 because in the latter the product channel is more populated and the energy of the products is lower than of the reactants.

Regarding the difference between *cis*- and *trans*-epoxybutane the PES scans show no significant difference for both H1 and H2, which is in good agreement with the experimental findings, i.e. that the rate constants are almost identical. This is supported by the Gibbs free reaction enthalpies for the cis and trans isomer, which are -22 kJ/mol and -25 kJ/mol for H1 and -30 kJ/mol and -32 kJ/mol for H2, respectively.

The reason for the second minimum and for the lower energy of the products can be explained by the Walsh model (Rosowsky, 1964; Walsh, 1947, 1949). It is founded in the premise that carbon atoms in ethylene oxide approach the sp^2 state, its CH_2 units being therefore pseudo-ethylenic in character (Rosowsky, 1964).

It has also been shown that such conjugation does not occur if the π orbitals of the unsaturated groups cannot orient themselves with their axes parallel to the plane of the epoxide ring (Cromwell & Hudson, 1953) Figure 5. It follows, therefore, that the orbitals in the epoxide ring, which are responsible for the conjugation, must lie in the plane of the ring (and not above and below as in the benzene case).

Accordingly, with the Walsh configuration, one orbital from each carbon atom overlaps with an atomic orbital of oxygen to form the molecular orbital, and two electrons of oxygen move into this orbital. The remaining four electrons populate the delocalized molecular orbitals, which are in the plane of the ring. These latter orbitals are formed by sideways overlapping of

atomic p orbitals, and their presence accounts for the conjugating ability of the epoxide ring (Parker & Isaacs, 1959).

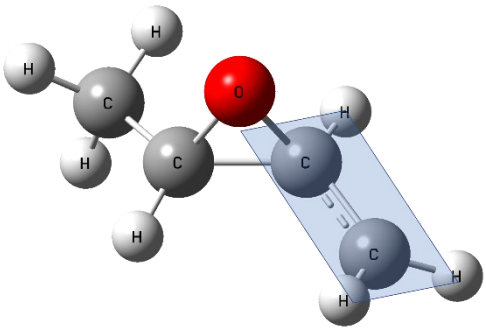

Figure 5 - Geometry of trans-2, 3-epoxybutane showing the plane of the epoxy ring associated to the conjugation

Coulson and Moffit proposed a similar structure. They purposed a structure that was called a "bent bond". In this structure the ring atoms do not lie along the lines of greatest electron density of the atomic orbitals from the neighbouring atoms (Coulson, C., A. & Moffitt, W., E., 1949; Coulson & Moffitt, 1947). If we consider the case of cis/trans–epoxybutane, when the compound has lost one H of the CH_3 group, it becomes trigonally (sp^2) hybridized, facilitating the possible formation of a double bond with the singly-occupied p-orbital after abstraction of H. Indeed, the optimized geometry shows the CH_2 group aligning in such a way that the three hydrogens and two carbons lie within one plane indicating a double bond character of the C-C bond (Figure 5). This aspect could explain the favoured abstraction of H2 (β-position).

The effect of the side chain can be studied by comparing the minimum energy paths of *cis/trans*-epoxybutane and 1,2-epoxybutane (Figure 6). The same effects observed above can be seen for the asymmetric compound: only the H2 abstraction path has a (significant) minimum in the product channel and the product energy is much lower than for the other channels indicating a strong preference toward an abstraction in β-position. In particular, an abstraction of H0 is very unfavorable since in addition to the weak population of the product channel, the energy of the products is even higher than for H1.

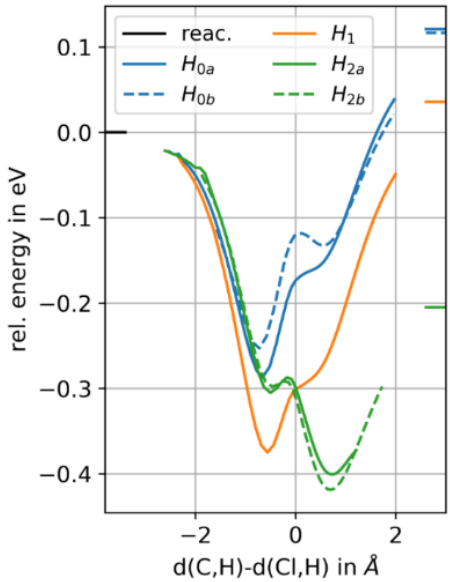

Figure 6 - Potential energy surface (PES) scans, for the H atom abstraction from 1,2-epoxybutane by chlorine atoms

Comparing now the paths for the H2 abstraction, it can be seen that the second minimum (lying in the product channel) is significantly lowered in the asymmetric compound compared to the symmetric ones. The metastable reaction adduct thus strongly populates the product channel increasing the likelihood of the abstraction. This is in agreement with the experimental data, where the rate constant for the 1,2-epoxybutane is significantly larger than for the cis/trans isomers. This effect could be explained by a stabilizing effect of the adjacent CH_3 group, which can contribute to the π-interaction through its own p-orbitals to a certain degree (+I effect). The preference of the H2 abstraction is also supported by the thermochemistry of the products. The Gibbs free reaction enthalpies for H0a/b, H1 and H2 are -14 kJ/mol, -14 kJ/mol, -22 kJ/mol and -50 kJ/mol, respectively.

We did not calculate energy paths for 1,2-epoxyhexane because of the difficulties due to its flexible nature. However, the increased rate constant (Table 1) compared to 1,2-epoxybutane can be explained by the longer sidechain and thus a stronger +I effect. Additionally, hydrogens in γ, δ, … position can be abstracted as well, increasing the overall rate. The likelihood of these reactions will be discussed below.

Having a cyclic compound, i.e. cyclohexene oxide (Figure 7) the rate constant increases again compared to 1,2-epoxyhexane, despite having the same number of carbons. From Figure 8 it becomes clear that, again, H2 abstraction is favored over H1 abstraction (e and a describe atoms in equatorial and axial position). The side chain again contributes to an energetically low product channel minimum having thus a high population density. Terming H3 the H atoms of the CH_2 group in γ-position, it can be seen that they have two minimum as well.

Table 2 - Comparison of the rate coefficients for the reaction of Cl atoms with range of epoxides from the present study with literature data and SAR predictions.

Epoxides	**Structure**	**k_{SAR}**	**$k_{epoxide}$ (cm^3 $molecule^{-1}$ s^{-1})**	**Technique**	**Reference**
Cyclohexene Oxide		2.09×10^{-10a} 2.31×10^{-10b} 2.08×10^{-10c}	**$(2.40\pm0.76)\times10^{-10}$**	RR-FTIR	This work
Ethylene Oxide		3.10×10^{-12a} 4.15×10^{-12b} 7.25×10^{-10c}	$(2.9\pm0.24)\times10^{-12}$ $(4.6\pm0.60)\times10^{-12}$ $(5.2\pm0.60)\times10^{-12}$ **$(4.9\pm0.63)\times10^{-12}$**	$RR(C_2H_6)$ $RR(C_2H_5Cl)$ $RR(CH_3OCHO)$ Average	(Bartels, Hoyermann, & Lange, 1989) (Ponomarev, Hurley, & Wallington, 2002) (Ponomarev, Hurley, & Wallington, 2002) (Calvert, Mellouki, Orlando, Pilling, & Wallington, 2011)
Propylene Oxide		2.89×10^{-11a} 2.63×10^{-11b} 2.62×10^{-10c}	**$(3.0\pm0.70)\times10^{-11}$**	RR-FTIR	(Middala, Campbell, Olea, Scruggs, & Hasson, 2011)
1,2-epoxyhexane	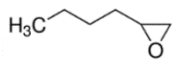	1.98×10^{-10a} 2.12×10^{-10b} 1.84×10^{-10c}	**$(1.77\pm0.61)\times10^{-10}$**	RR-FTIR	This work
1,2-epoxybutane	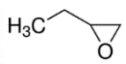	9.45×10^{-11a} 9.75×10^{-11b} 9.21×10^{-10c}	**$(8.43\pm2.46)\times10^{-11}$**	RR-FTIR	This work
trans-2,3-epoxybutane	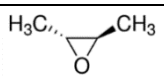	5.47×10^{-11a} 4.84×10^{-11b} 5.25×10^{-10c}	**$(6.99\pm2.06)\times10^{-11}$**	RR-FTIR	This work
cis-2,3-epoxybutane	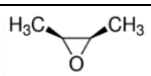	5.47×10^{-11a} 4.84×10^{-11b} 5.25×10^{-11c}	**$(6.92\pm2.11)\times10^{-11}$**	RR-FTIR	This work

Additionally, their exit channel is energetically lower than the reactant asymptote, hence, although not as likely as the H2 abstraction, this pathway is also feasible, contributing to the overall rate. Assuming this behavior being similar in 1,2-epoxyhexane would explain the larger rate constant compared to 1,2-epoxybutane. However, since cyclohexene oxide has four H atoms in β-position compared to only two in 1,2-epoxyhexane, the increased rate from linear to cyclic can be explained as well.

Table 3 - Comparison of rate coefficients for the reaction of Cl with ethers and epoxides at room temperature.

Ether	*K* (10^{-11} cm^3 molecule^{-1} s^{-1})	Epoxide	*K* (10^{-11} cm^3 molecule^{-1}s^{-1})
CH_3OCH_3	(13.0 ± 2.0)[a]		(0.5 ± 0.1)[b]
$CH_3CH_2OCH_2CH_3$	(25.0 ± 3.0)[a]		(6.9 ± 2.1)[c]
		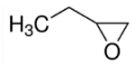	(8.4 ± 2.4)[c]
$CH_3(CH2)_2O(CH_2)_2CH$	(36.0 ± 4.0)[a]	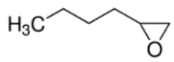	(17.7 ± 6.1)[c]

a Notario et al 2000; b Calvert et al2011; c this work

We investigated further reaction steps for the decomposition of cyclohexene oxide as can be seen in Figure 9.

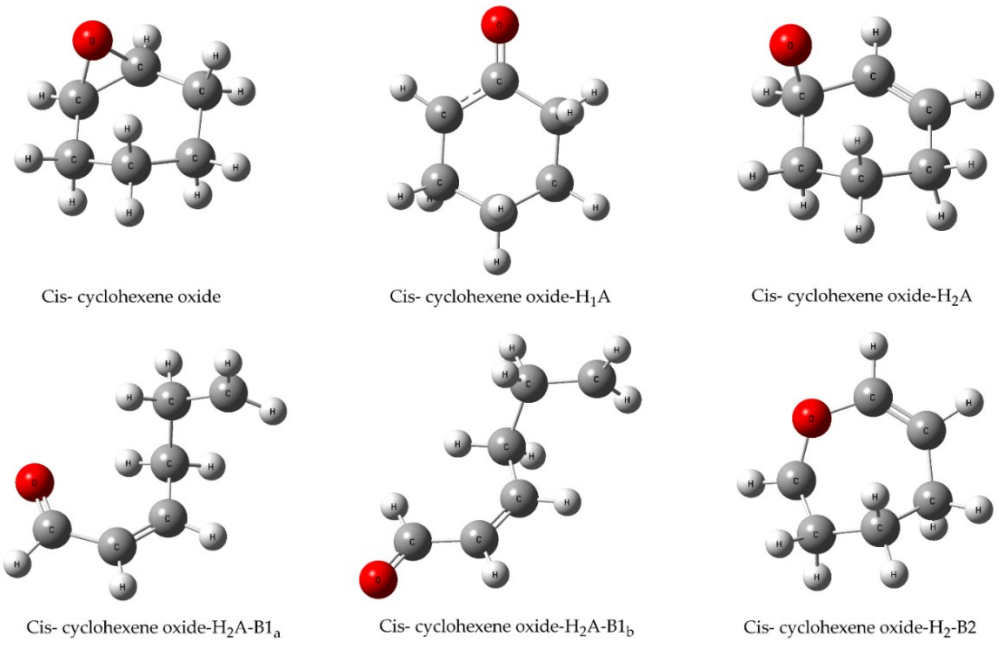

Figure 7 - Geometries of the cis conformer of cyclohexene oxide during the H abstraction reaction in the presence of chlorine atoms, optimized under the B3LYP-GD3BJ/def2-TZVPP. The coordinates of all structures can be found in the supporting information.

Experiments are being developed to analyze the decomposition products as well, giving us the opportunity to test the above discussions by comparing the measured and calculated decomposition products.

The intramolecular changes now all proceed through TSs and hence their likelihood can be discussed with the concept of these barrier heights. In Figure 9, all pathways containing an "A" corresponds to opening of the epoxide ring (breaking of a C-O bond) while "B" containing paths correspond to opening of the carbon ring (breaking of a C-C bond). Following the H2 abstraction, the epoxide ring opens through a low TS to form the compound H2-A. Although compound H1-A is very stable due to the delocalization of the free electron over three atoms (see Figure 7), we argue that due to kinetic effects regarding first the H abstraction and second the epoxide opening, the H2-A compound is more likely to be observed in experimental data. An H3 abstraction can only be followed by high transition states making progression along this pathway questionable.

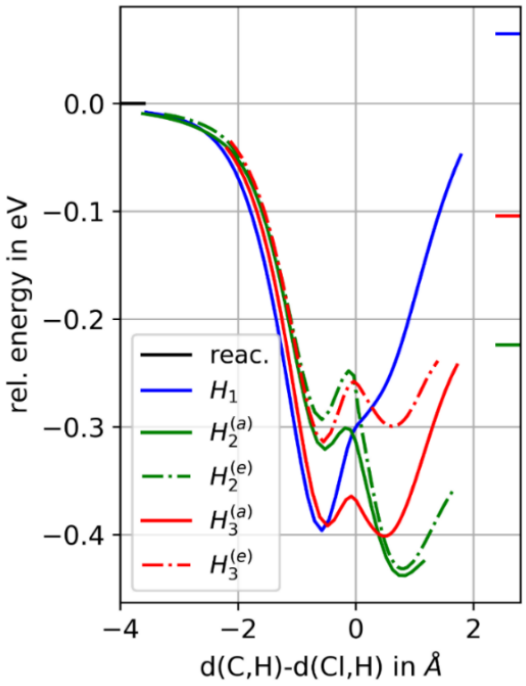

Figure 8 - Potential energy surface (PES) scans, for the H atoms abstraction from cyclohexene oxide by chlorine atoms.

We thus believe that the H2-A compound will be the most likely one, probably further decomposing into the H2-AB1 products having a conjugated π system over four atoms (see Figure 7).

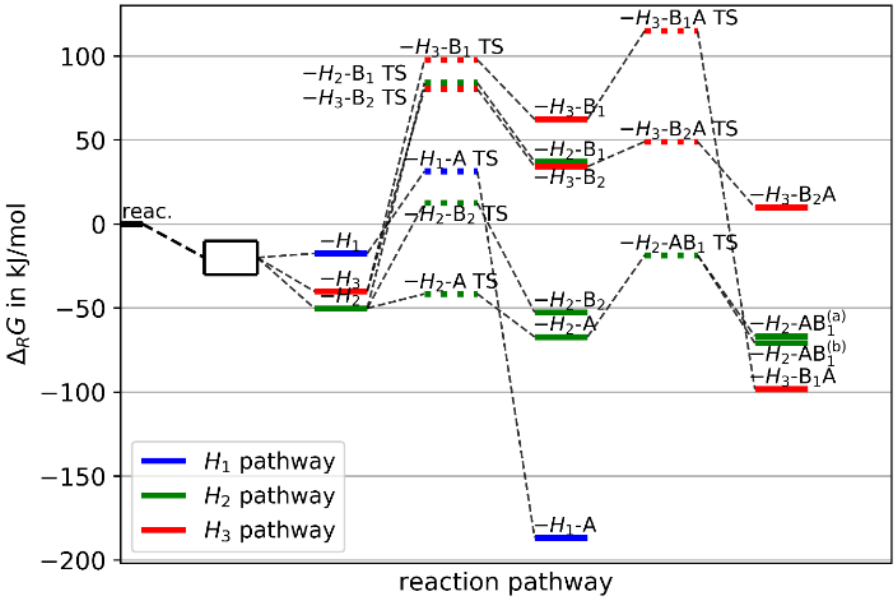

Figure 9 - Pathways of H atom abstractions from the cis conformer of cyclohexene oxide (CHO) reacting with chlorine atoms, see Figure 13 for the explanation of acronyms.

In terms of reactivity trends, the CH_2 groups near to the ring are prone to form double bonds after the abstraction of a hydrogen atom and then orient themselves easily with their axes of π orbitals parallel to the plane of the epoxide ring, making the reaction faster. Also, if we compare the reactivity of cyclohexene oxide with 1,2–epoxyhexane with the same number of C atoms, we can see that $k_{CHO} > k_{12EHX}$ (Table 2). Also, previous studies shows that the electron density in the oxygen atom in ethylene oxide is unusually low compared to that in acyclic and larger cyclic ethers (Searles et al., 1953; Searles & Tamres, 1951), that could add to the explanation why the reactivity of cyclohexene oxide is higher.

Conclusions

From the results of this work, it can be seen that ethers and epoxides of the same number of carbon atoms increase their reaction rate coefficient as the number of CH_2 groups adjacent to ether group increases.

According to the Structure-Activity Relationships (SAR) method, the rate coefficients at a primary, secondary and tertiary site on an organic species are modified by substituent factors F(X) corresponding to different functional groups that account for the activating or deactivating effects of neighboring groups. Comparing the reactivity between aliphatic ethers and epoxides, there is a sharp decrease in the reactivity that could be attributed to the effect of the ring.

Through the theoretical calculations performed in this work for epoxides up to 6 carbon atoms, we present a possible explanation to the reactivity trends observed experimentally and the importance of the selectivity in the reaction of epoxides towards chlorine atoms. The presence of the ring will affect the molecule in a complex manner, and both, ring and ether group have to be considered as a unity to properly evaluate the reactivity of these compounds. Therefore, as explained before, the sites in the molecule are more reactive in β-position when the carbon atoms in ethylene oxide approach the sp^2 state and its CH_2 units are pseudo-ethylenic in character. That conjugation does not occur if the π orbitals of the unsaturated groups cannot orient themselves with their axes parallel to the plane of the epoxide ring. Such a geometric

arrangement in the epoxy molecule would be necessary to allow the abstraction of a hydrogen in the molecule in a preferential way, thus increasing the reactivity of the reaction, as demonstrated here for the molecules under study.

Further investigation into the reaction mechanism products of these compounds will help further improve the knowledge of the nature and reactivity of this type of compounds.

3 Kinetic studies of the OH Reactions with a series of epoxides

Reproduced from:" Carmen Maria Tovar, Ian Barnes, Iustinian Gabriel Bejan and Peter Wiesen: Kinetic study of the atmospheric oxidation of a series of epoxy compounds by OH radicals, Atmos. Chem. Phys., 22, 6989–7004, https://doi.org/10.5194/acp-22-6989-2022" with permission from the ACP Owner Societies.

3.1 Abstract

In this work, we study the kinetics of the gas-phase reactions of hydroxyl radicals with cyclohexene oxide (CHO), 1,2-epoxyhexane (EHX), 1,2-epoxybutane (12EB), trans-2,3-epoxybutane (*t*EB) and cis-2,3-epoxybutane (*c*EB) using the relative rate technique. The experiments were conducted at (298 ± 3) K and (760 ± 10) Torr (1.01 ± 0.01) × 10^5 Pa) total pressure of synthetic air using different reference compounds in a 1080 L Quartz Reactor (QUAREC) and a 480 L Duran glass chamber. The following room temperature rate coefficients (cm3 molecule−1 s−1) were obtained: $k_{1(OH+CHO)}$ = (5.93 ± 1.13) × 10^{-12}, $k_{2(OH+EHX)}$ =(5.77±0.83)×10^{-12}, $k_{3(OH+12EB)}$ = (1.98±0.29)×10^{-12}, $k_{4(OH+cEB)}$ = (1.50±0.28)×10^{-12} and $k_{5(OH+tEB)}$ =(1.81±0.33)×10^{-12}. Except for previous studies on 1,2-epoxybutane and cyclohexene oxide, this is, to the best of our knowledge, the first kinetic study of the reaction of these compounds with OH radicals. We discuss the discrepancies found between the values obtained from the present study with values estimated from the structure–activity relationship method (SAR). Our findings indicate that pseudo-ethylenic character in the epoxy ring is an important factor to be included in the improvement of the SAR estimation method. Atmospheric lifetimes, reactivity trends and atmosphere implications are discussed considering the epoxy compound rate coefficients obtained in the present study.

3.2 Introduction

Oxygenated volatile organic compounds (OVOCs) play an important role in atmospheric chemistry and have an impact on climate and human health (J. Calvert et al., 2011).

From those OVOCs emitted from either biogenic or anthropogenic sources, cyclic ethers, except for furans (Li et al., 2018; Villanueva et al., 2009), have received very little attention. Epoxides, as the simplest cyclic ethers, are an important and valuable class of raw materials and intermediates for the chemical industry. They can polymerize for the production of homo- and copolymers as polyethers, polyols and polycarbonates (Hereijgers et al., 2012).

Epoxides are considered a key element in "click" chemistry (Fokin & Wu, 2006; Kolb et al., 2001). They are also relevant in the field of pharmaceutical applications because of their potential as protease inhibitors against several diseases like cancer, stroke, and parasitic or viral diseases (Otto & Schirmeister, 1997; Powers et al., 2002; Schirmeister & Klockow, 2003). A relatively new utilization of epoxides, which could have huge atmospheric implications and an impact on climate change, is their potential use for carbon capture and storage, i.e. the chemical fixation of CO_2 in the form of cyclic carbonates in the presence of various catalysts (Andrea & Kerton, 2021; Appaturi et al., 2021; Guo et al., 2021; F. Zhang et al., 2020; Zou & Hu, 2017).

Epoxides are known to be formed from the reaction of $O(^3P)$ with isoprene at nearly 80 % yield (Atkinson, Aschmann, et al., 1994; Paulson et al., 1992a). In the atmospheric ozonolysis of isoprene, epoxide yields of about 2 %–3 % were observed (Atkinson, Arey, et al., 1994). A few percent of epoxide formation have been reported from α-pinene ozonolysis as well as from the reaction of 1,2-dimethyl-1-cyclohexane with ozone (Alvarado et al., 1998). (Atkinson, Arey, et al., 1994) concluded that epoxide formation is a process occurring in the ozonolysis of most terpenes and cycloalkenes. Low yields of isoprene derived epoxides have also been observed from the gas-phase nitration of isoprene (Skov et al., 1994).

Furthermore, in indoor pollution studies the formation of epoxides from the heterogeneous oxidation of volatile organic compounds (VOCs) with gas-phase ozone has been reported (Zhou et al., 2017). Other compounds could also form epoxides during their gas-phase

chemical degradation by OH radicals and ozone. More recent theoretical and mechanistic studies report epoxide formation during the gas-phase ozonolysis of methylbutenol and sabinene via the Criegee degradation mechanism (Almatarneh, Elayan, Abu-Saleh, et al., 2019; Almatarneh, Elayan, Altarawneh, et al., 2019; G. Calvert et al., 2000).

Epoxides are responsible for up to 10 % of the open-ring products from the degradation of aromatic hydrocarbons in the presence of OH radicals according to the MCM (Master Chemical Mechanism) model (Jenkin et al., 2015). In the past, benzene oxide has been reported as an epoxide-type product in the reaction of benzene with OH radicals (Klotz et al., 1997, 2002). In addition, a theoretical study has reported epoxide formation in the OH-radical-initiated oxidation of dimethylphenol isomers (Sandhiya et al., 2013).

Secondary organic aerosols (SOAs) constitute a substantial portion of the total ambient aerosol particles, which mainly originate from biomass burning and atmospheric reactions of volatile organic compounds (VOCs) (Kanakidou et al., 2005). Epoxides can polymerize easily, leading to the growth of SOA (Gao et al., 2004). A recent study shows that the yield of epoxides from the reaction of aromatic compounds with OH radicals is probably dependent on the abundance of NO, HO_2 and RO_2 in the reaction system (Vereecken, 2018). This aspect represents an uncertainty in atmospheric models to reliably estimate the expected SOA formation from reactive epoxide uptake by aerosols (Paulot et al., 2009). The presence of epoxides in SOA is highly probable for conditions prevailing in the atmosphere, leading to higher hygroscopicity of particles with potential cloud condensation nuclei activity by conversion to organosulfates through an acid-catalysed mechanism (Fuzzi et al., 2015).

Isoprene-derived epoxides are very important intermediates, which could explain at least in part the composition of ambient SOA both in urban areas (Lin, Zhang, et al., 2013b) and remote regions (Jacobs et al., 2013; Paulot et al., 2009; Shrivastava et al., 2019; Stropoli et al., 2019).

The toxicity of ultrafine particles such as SOA is not only related to their atmospheric concentration but also to the nature and chemical properties of both the precursors and the

formed SOA components (Jiang et al., 2019). In this sense, epoxides are of great concern because the epoxy functional group can act as an electrophile in its interaction with DNA and nucleosides, producing carcinogenic and mutagenic damage (Ehrenberg & Hussain, 1981).

The kinetic and mechanistic data available on the gas phase reactions of epoxy compounds with the atmospheric oxidants OH and NO_3 radicals, O_3, and chlorine atoms are very scarce. For the compounds investigated in the present study, there is only one previous relevant study towards chlorine atoms at 298 K (Tovar et al., 2021). Two studies have reported the rate coefficients of the reaction of 1,2-epoxybutane towards OH radicals (El Othmani, Ren, Mellouki, et al., 2021; Wallington, Dagaut, et al., 1988), and more recently cyclohexene oxide with OH radicals have been measured as a function of temperature (El Othmani, Ren, Mellouki, et al., 2021).

In the present study we have performed, for the first time, a kinetic study of the reaction of OH radicals with 1,2-epoxyhexane, trans-2,3-epoxybutane and cis-2,3-epoxybutane at 298 K using the relative rate method.

Since several of the rate coefficients for the reactions of epoxides with OH radicals have been measured in the present study for the first time and cannot be compared with literature values accordingly, we have applied different approaches for the estimation of structure–activity relationship (SARs) for the compounds studied in this work.

3.3 Methods

The experiments were performed in two different environmental chambers, namely a 1080 L quartz–glass photoreactor and a 480 L Duran glass chamber. These two photoreactors are briefly described below.

3.3.1 Indoor simulation chamber-480 L

This reaction chamber consists of a cylindrical Duran glass vessel (3 m length, 45 cm diameter) closed at both ends by Teflon-coated aluminium end flanges. Integrated on the metal flanges are ports for the inlet of reactants into the chamber and for the collection of samples from the reaction mixtures for further analyses. Other accessories, like a mixing fan to ensure homogeneity of the reaction mixtures and a capacitance manometer, are also located on the flanges. Arranged concentrically around the outside of the reactor are 32 super actinic fluorescent lamps (Philips TLA 40 W, $300 \leq \lambda \leq 460$ nm, $\lambda_{max} = 360$ nm). The vacuum (ca. 10^{-3} mbar) is maintained by means of a Leybold turbo-molecular pump, model RUVAC WZ 151 (500 $m^3 h^{-1}$), backed by a Leybold double-stage rotary fore pump, model D40B (200 $m^3 h^{-1}$).

A White-type mirror system mounted inside the reactor is set to an overall optical path length of 51.6 m. The analysis of the reactants was done during the experiments by in situ FTIR (Fourier transform infrared) long-path spectroscopy using a resolution of 1 cm^{-1}. The FTIR spectrometer (Nicolet Magna 520) and the transfer mirror system are covered with a protective box and are permanently purged with dry air to remove water vapour. The spectrometer is directly controlled by the OMNIC software, which is provided by Nicolet.

3.3.2 Indoor simulation chamber-1080 L

A detailed description of the reactor can be found in the literature (Barnes et al., 1994). Briefly, the reactor consists of the two quartz–glass tubes with an inner diameter of 47 cm and a wall thickness of 5 mm. The reactor has a total length of 6.2 m. Silicone rubber rings are used for all the glass–metal connections as well as for metal–metal connections.

The reactor is connected to a turbo molecular pump system by which an end vacuum of 10^{-3} mbar can be achieved.

A total of three fans are used for homogeneous mixing of compounds within the reactor. Different types of inlets are mounted on the end flanges for the introduction of chemicals and for pressure measurements.

The beam from an FT-IR spectrometer is coupled via a transfer mirror system into the reactor through KBr windows located in one of the end flanges. A White-type mirror system (base path length (5.91 ± 0.01) m), mounted inside the reactor, is used for multiple reflection of the infrared beam within the reactor before it reaches the detector. Reactants were monitored in situ in the reactor in the infrared using 82 traverses of the beam, which is equivalent to a total optical path length of (484.7 ± 0.8) m. All spectra in this work were recorded with a spectral resolution of 1 cm^{-1}.

The FTIR spectrometer NICOLET NEXUS was used, which is equipped with a liquid nitrogen-cooled (77 K) mercury–cadmium–tellurium (MCT) detector. A Globar was used as IR light source. All mirrors are gold-coated to achieve optimum reflectivity.

Two different types of lamps (32 each) are installed around the reactor. They are mounted alternatively around the reactor to ensure homogeneity of the light intensity within the reactor. The first type, 32 superactinic fluorescent lamps (Philips TL05 40 W: 300–460 nm, max. intensity at ca.360 nm) and 32 low-pressure mercury vapour lamps (Philips TUV 40 W: max. intensity at 254 nm), can be used to irradiate the reaction mixture.

Typically, 64 interferograms were co-added per spectrum over a period of approximately 1 min, and 15–20 such spectra were recorded per experiment.

3.4 Relative rate method

The relative rate method was used to determine the rate constant of the OH-radical-induced oxidation of the epoxy compounds.

The photolysis of CH_3ONO in the presence of NO was used to produce OH radicals:

$$CH_3ONO + h\nu\ (\lambda \sim 360\ nm) \rightarrow CH_3O + NO$$

$$CH_3O + O_2 \rightarrow CH_2O + HO_2$$

$$HO_2 + NO \rightarrow NO_2 + HO$$

The concentrations or mixing ratios were measured from the exact amount of the compound added to the chamber. The liquids and gases were injected into the chamber via a septum using a gas-tight syringe in a flow of air with the reactor being under reduced pressure. The glass–steel inlet system was heated up to 60 °C to ensure the addition of the entire amount of epoxides and reference compounds into the reactor. After addition and filling the chamber to (760 ± 10) Torr (1.01 ± 0.01) × 10^5 Pa) pressure of synthetic air, up to 15 infrared spectra (15 min) were recorded to prove the constant concentration of the compounds in the chamber. These tests

were performed not only to check if there is a diffusion of the injected compounds from the inlet into the chamber, but also to evaluate the potential wall deposition of the added compounds to correct the rate coefficients for additional loss processes. Any diffusion from the inlet would affect the linearity of the kinetic plots, which otherwise would not have been obtained. The different epoxides and reference compound employed in the present study did not show wall loss during the time of the experiment.

In the presence of the OH radical, the corresponding epoxide and reference compound are consumed by the following reactions:

$$OH + Epoxides \rightarrow Products \quad (k_{Epoxide}) \quad (4)$$

$$OH + Reference \rightarrow Products \quad (k_{Reference}) \quad (5)$$

Provided that the reference compound and the epoxide are lost only by reactions (4) and (5), then it can be shown that:

$$ln\left\{\frac{[Epoxide]_0}{[Epoxide]_t}\right\} = \frac{k_{Epoxide}}{k_{Reference}} ln\left\{\frac{[Reference]_0}{[Reference]_t}\right\} \text{ (II)},$$

Where $[Epoxide]_0$, $[Reference]_0$, $[Epoxide]_t$ and $[Reference]_t$ are the concentrations of the corresponding epoxy compound and reference compound at times t = 0 and t, respectively, and $k_{Epoxide}$ and $k_{Reference}$. are the rate coefficients of reactions (R4) and (R5), respectively.

To test for a possible loss of the reactants through photolysis, mixtures of the reactants in air in the absence of methyl nitrite were irradiated for 30 min, and photolysis was found to be negligible for both the epoxide and the reference compounds. Additionally, various tests were performed to assess possible loss of the reactants via deposition on the chamber walls, and no significant wall loss of the epoxy compounds and references was observed, leaving the compounds in the dark in the reactor.

Table 4 - Initial mixing ratios used in the 1080 L reactor and 480 L reactor for the epoxide and reference compounds in parts per million by volume (ppmv; 1 ppm = 2.46 × 1013 molecule cm−3) at (298 ± 3) K and (760 ± 10) Torr ((1.01 ± 0.01) × 105 Pa) of total pressure of air. The mixing ratios have been estimated from injections of the compounds into the reaction chambers and provide information about the amount of compounds used in this study.

	Initial mixing ratios (ppmv)	
Compounds	***Reactor (1080 l)***	***Reactor (480 l)***
Epoxides		
cyclohexene oxide	6	17
1,2-epoxyhexane	6	28
1,2-epoxybutane	6	23
cis-2,3-epoxybutane	3	28
trans-2,3-epoxybutane	3	23
Reference compounds		
Propylene	4	8
Butane	4	-
iso-propyl acetate	1	9
sec-butyl acetate	1	9
Ethylene	4	21
methyl nitrite (OH radical precursor)	8	84

A minimum of two experiments for each epoxide compound were performed in this study, and up to three reference compounds were used. Reference compounds were chosen based on similar reactivity as epoxides and suitability for FTIR subtraction procedures. Conversion of

epoxides and reference compounds through the reaction with the OH radical was achieved up to 50 %. Initial mixing ratios used in the 1080 L reactor for the epoxides and reference compounds were as follows (in ppmv with 1 ppmv = 2.46×10^{13} molecule cm^{-3} at (298 ± 3) K and (760 ± 10) Torr ((1.01 ± 0.01) × 10^5 Pa) of total pressure of synthetic air): epoxides between 3–6 ppmv and reference compounds between 1 and 4 ppmv, as shown in Table 4. Concentrations used for the reactions performed in the 480 L reactor were up to 8 times higher. Around 8 ppmv CH_3ONO was added in the 1080 L reactor and up to 10 times more in 480 L reactor. All epoxy and reference compounds used in this study were obtained from Sigma Aldrich and used without further purification. The stated purities were as follows: cyclohexene oxide, 98 %; 1,2-epoxyhexane, 97 %; 1,2-epoxybutane, 99 %; *trans*-2,3 epoxybutane, 97 %; *cis*-2,3-epoxybutane, 97 %; propylene, 99 %; butane, 99 %; iso-propyl acetate, 99.6 %; sec-butyl acetate, 99 %; and ethylene, 99.5 % and 99.985 % for synthetic air, which was from Messer.

3.5 Results and discussion

The experimental data from the kinetic experiments are plotted according to Eq. (1I). Figure 10 shows the results obtained for the rate coefficient determinations from the OH-radical initiated oxidation of cyclohexene oxide using ethylene, propylene and isobutene as reference compounds; 1,2-epoxyhexane using ethylene and propylene as reference compounds; 1,2 epoxybutane using ethylene and iso-propyl acetate as reference compounds; *trans*-2,3-epoxybutane using sec-butyl acetate, ethylene and propylene as reference compounds; and *cis*-2,3-epoxybutane using sec-butyl acetate, iso-propyl acetate and butane as reference compounds. The selection of the reference compounds employed in the kinetic study was constrained by the experimental technique since it is required to identify the infrared absorption bands which do not overlap with other infrared absorption features from reaction mixture. All plots showed very good linearity despite the difficulties in handling the epoxides and subtracting the IR spectra.

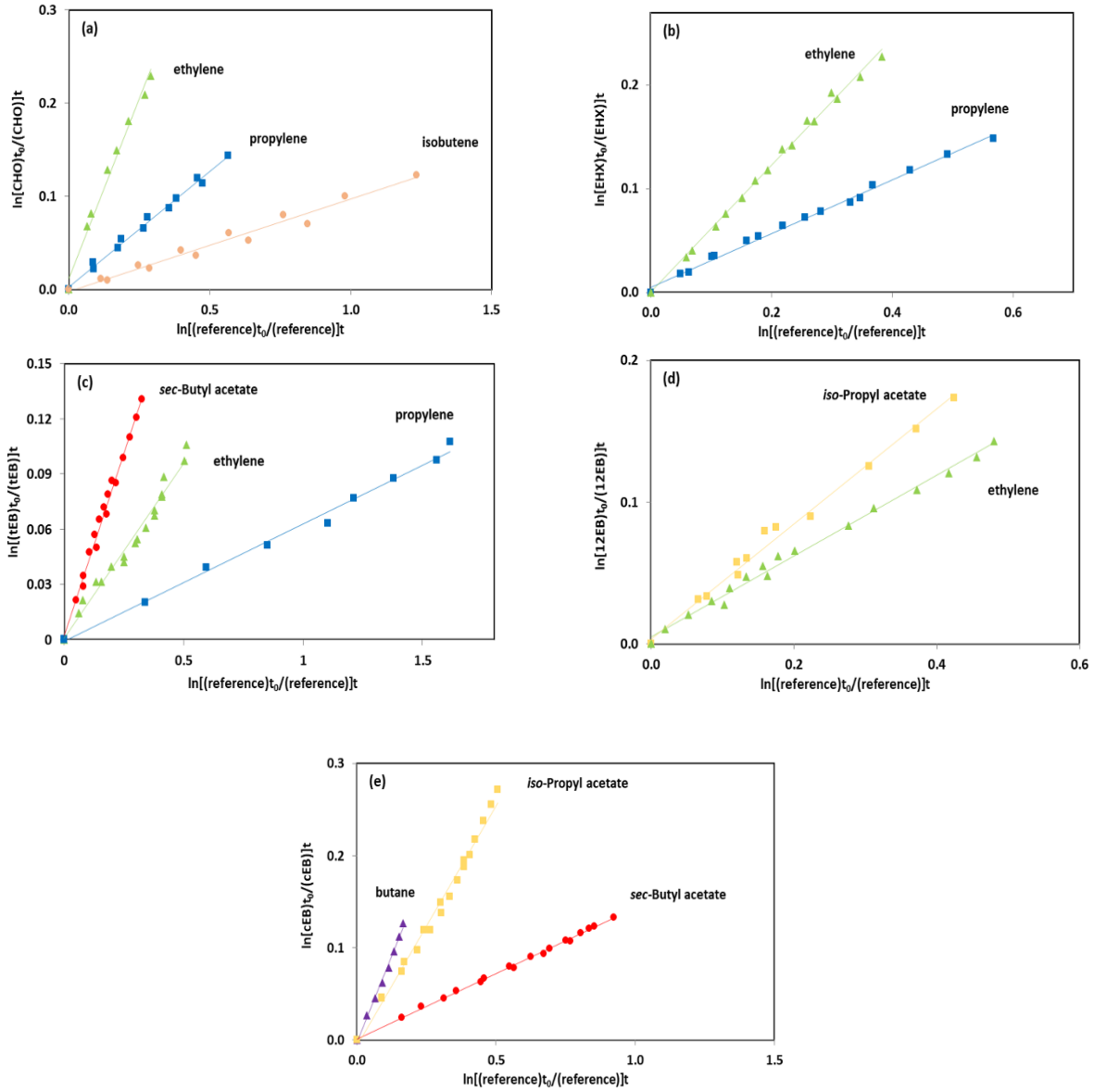

Figure 10 - Kinetic data for the reaction of OH radicals with (a) CHO, (b) EHX, (c) tEB, (d) 12EB and (e) cEB using ethylene, butane, sec-butyl acetate, iso-propyl acetate and propylene as reference compounds.

The rate coefficients $k_{Epoxide}$ given in Table 5 were put on an absolute basis using the following values for the reactions of the reference compounds (cm^3 molecule^{-1} s^{-1}): $k_{(OH+propylene)} = (2.44 \pm 0.37) \times 10^{-11}$ (*IUPAC Task Group on Atmospheric Chemical Kinetic Data Evaluation*, n.d.), $k_{(OH+ethylene)} = (8.52 \pm 0.13) \times 10^{-12}$ (J. G. Calvert et al., 2015), $k_{(OH+isobutene)} = (5.10 \pm 1.33) \times 10^{-11}$ (*IUPAC Task Group on Atmospheric Chemical Kinetic Data Evaluation*, n.d.), $k_{(OH+iso\text{-}propyl\ acetate)}$

= (3.72 ± 0.29) × 10^{-12} (Wallington, Liu, et al., 1988), $k_{(OH+sec\text{-}butyl\ acetate)}$ = (5.65 ± 0.59) × 10^{-12} (Wallington, Liu, et al., 1988) and $k_{(OH+butane)}$ = (2.38±0.24) ×10^{-12} (McGillen et al., 2020).

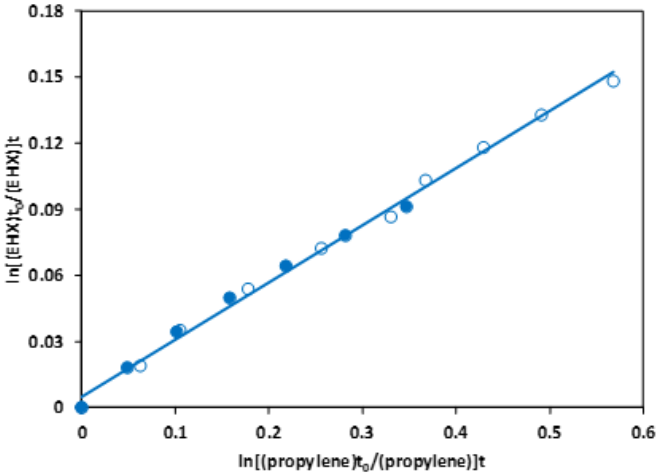

Figure 11 - Kinetic data for the reaction of OH radicals with EHX using propene as reference compound performed in 480 l reactor (●) and 1080 l reactor (○).

The rate coefficients obtained using two simulation chambers are in perfect agreement as shown in Figure 11, which is a comparison of the data for EHX using propylene as reference compounds. The linearity observed in Figure 11 was the same for all epoxides where we had the opportunity to perform the kinetic studies in both reactors with OH radicals and chlorine atoms. Therefore, considering they are the same family of compounds, we concluded the results are reproducible in both reactors. Accordingly, we plotted the data together for all the epoxides, regardless of the reactor where the experiment was performed.

The rate coefficient ratios $k_{Epoxide}/k_{Reference}$ obtained from linear regression analyses of these plots are summarized in Table 5. The rate coefficients are averages from the experiments, with each reference compound from the experiments performed in both reactors (cm^3 $molecule^{-1}$ s^{-1}): $k_{1(OH+CHO)}$ = (5.93 ± 1.13) × 10^{-12}, $k_{2(OH+EHX)}$ = (5.77 ± 0.83) × 10^{-12}, $k_{3(OH+12EB)}$ = (1.98±0.29)×10^{-12}, $k_{4(OH+cEB)}$ = (1.50±0.28)×10^{-12} and $k_{5(OH+tEB)}$ = (1.81 ± 0.33) × 10^{-12}.

All the rate coefficients obtained in this study, except those for 12EB and CHO, were measured for the first time.

The errors presented in Table 5 for the individual value of the slope $k_{Epoxide}/k_{Reference}$ represent 2σ of the least-squares fit of the data. The epoxides rate constants are placed on an absolute basis using different reference rate constants for which a uniform error of 10 % was applied, considering that the corrections for possible secondary processes (e.g., dilution, wall losses) were not necessary in the present study (Atkinson, 1986b). Thus, the errors quoted for individual rate constants of epoxides comprise the 2σ statistical errors resulted from lineal regression analysis of the plots and an additional 10 % contribution from the errors attributed to the recommended values of the rate constants for the reference compounds. The final rate constant has been calculated as an average of the individual rate constant, with the error calculated using the arithmetic calculation of the error propagation.

Table 5 - Measured rate coefficient ratios, kEpoxide/kReference, and the rate coefficients for the reactions of OH radical with epoxides at (298 ± 3) K derived from these ratios.

Epoxide	Reference compound	$k_{Epoxide}/k_{Reference.}$	$k_{Epoxide}$ (cm^3 $molecule^{-1}$ s^{-1})
CHO	Propylene	0.258±0.009	(6.28±0.66) ×10^{-12}
	Ethylene	0.751±0.038	(6.40±0.72) ×10^{-12}
	Isobutene	0.099±0.005	(5.13±0.57) ×10^{-12}
	Average		**(5.93±1.13) ×10^{-12}**
EHX	Propylene	0.259±0.004	(6.33±0.64) ×10^{-12}
	Ethylene	0.612±0.009	(5.21±0.53) ×10^{-12}
	Average		**(5.77±0.83) ×10^{-12}**
12EB	*iso*-Propyl acetate	0.406±0.011	(1.51±0.16) ×10^{-12}
	Ethylene	0.286±0.006	(2.43±0.25) ×10^{-12}
	Average		**(1.98±0.29) ×10^{-12}**
*t*EB	*sec*-Butyl acetate	0.398±0.009	(2.25±0.23) ×10^{-12}
	Ethylene	0.190±0.007	(1.62±0.17) ×10^{-12}
	Propylene	0.064±0.002	(1.56±0.16) ×10^{-12}
	Average		**(1.81±0.33) ×10^{-12}**
*c*EB	*iso*-Propyl acetate	0.518±0.012	(1.93±0.20) ×10^{-12}
	sec- Butyl acetate	0.142±0.001	(0.80±0.08) ×10^{-12}
	Butane	0.745±0.022	(1.77±0.18) ×10^{-12}
	Average		**(1.50±0.28) ×10^{-12}**

3.5.1 Correlation between the rate coefficients of the reaction of epoxides with OH radicals and chlorine atoms

The abstraction route defines the main reaction pathway of the epoxides with OH radicals. For epoxide series, it is likely to define a correlation of the rate coefficients from their reaction with OH radicals and chlorine atoms. Similar correlations were observed for the series of alkanes, saturated alcohols and acyclic ethers (J. Calvert et al., 2011). Figure 12 presents a log–log correlation plot between the Cl atoms and OH radical rate coefficients with epoxides for the series of propylene oxide, 1,2-epoxyhexane, 1,2-epoxybutane and both isomers of 2,3-epoxybutane. A very clear correlation (R^2 =0.9935) described by the relation $\log_{10}[k_{(Cl+epoxides)}] = 0.718 \times \log_{10}[k_{(OH+epoxides)}] - 1.685$ was obtained. The compounds ethylene oxide and cyclohexene oxide are represented in Figure 12 but are not included into the correlation plot, although including the cyclohexene oxide, the log–log correlation would change to $\log10[k_{(Cl+epoxides)}] = 0.788 \times \log10[k_{(OH+epoxides)}] - 0.852$ with (R^2 = 0.978). The reactivities of the epoxides with OH radicals and Cl atoms are clearly correlated for the series of epoxides. However, the log–log correlation for epoxides is different to the one presented by (J. Calvert et al., 2011) and described by the relation $\log10[k_{(Cl+alkanes)}] = 0.521 \times \log10[k_{(OH+alkanes)}] - 3.670$ with (R^2 = 0.85) for the series of alkanes with those two atmospheric oxidants. In addition, the log–log correlation for the series of ethers and alcohols with these two oxidants presented by (J. Calvert et al., 2011) described by the relation $\log_{10}[k_{(Cl+ether/alcohol)}] = 0.634 \times \log_{10}[k_{(OH+ether/alcohol)}] - 2.710$ with (R^2 = 0.72) is in better agreement with the log–log correlations obtained in this study for epoxides.

The log–log correlation plot can be used to predict rate coefficients. For example, the rate coefficient for the reaction of propylene oxide with chlorine atoms which has not been measured to date can be derived based on the proposed correlation, $k_{(propylene\ oxide+Cl)} = 3.04 \times 10^{-11}$ cm^3 molecule^{-1} s^{-1}. However, the knowledge of rate coefficients for the reactions of epoxides with atmospheric oxidants is still very limited.

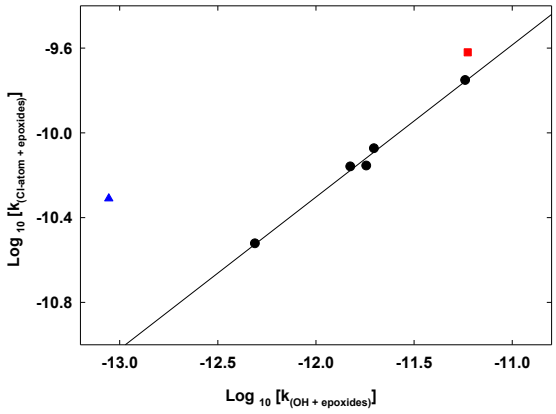

Figure 12 - Double logarithmic plot (log10) of the rate coefficients for the reaction of Cl-atoms versus the reaction of OH-radicals with the epoxides (propylene oxide, 1,2-epoxybutane, trans-2,3-epoxybutane, cis-2,3-epoxybutane, 1,2-epoxyhexane). The solid line represents the unweighted least-squares fit to the data. Cyclohexene oxide is represented by the red square while ethylene oxide is represented by a blue triangle. Both were not included into the least squares fit.

3.5.2 Structure-activity relationship (SAR) calculations for epoxides

To date, the rate coefficients of hundreds of new compounds have been studied under laboratory conditions with different atmospheric oxidants. However, there are still many compounds for which the data are still very scarce, such as for cyclic ethers.

There are several methodologies to estimate the rate coefficients towards OH radicals. One of them is quantum theoretical calculations, useful for reactions which are very difficult to study directly in the laboratory. Another approach is the structure–activity relationship (SAR) method, which relies solely on the structure of the organic compounds and the effect of this structure on the reactivity. Both methodologies are critical to predict the chemical reactivity and physical behavior of compounds where direct data are not available. The SAR estimation method applied for the epoxide type compounds studied in the present work treats the rate of abstraction from a group within an epoxide molecule. In the case of H atom abstraction from C–H bonds, the calculation of the overall H atom abstraction rate constants is based upon the estimation of $–CH_3$, $–CH_2–$ and > CH– group rate constants.

The $–CH_3$, $–CH_2–$ and > CH– group rate constants depend on the substituents influence around those groups.

For example, in the case of an α position, $k(CH_3\text{-}X) = k_{prim}F(X)$; $k(X\text{-}CH_2\text{-}Y) = k_{sec}F(X)F(Y)$; and $k(X\text{-}CH(Y)(Z)) = k_{tert}F(X)F(Y)F(Z)$, where k_{prim}, k_{sec} and k_{tert} are the rate constants per $–CH_3$, $–CH_2–$ and> CH– group for a "standard" substituent; X, Y and Z are the substituent groups; and F(X), F(Y) and F(Z) are the corresponding substituent factors (Atkinson, 1986a, 1986b, 1987). The validity and usefulness of a SAR depend on many factors, such as the amount and type of input data, reliability of prediction, scope of applicability and ease of implementation (Vereecken, 2018).

The rate constant of the reactions with OH radicals obtained in this work were used to derive reactivity trends towards the OH radical. Also, five different approaches have been used in the SAR estimations to evaluate the most suitable method to predict the reactivity of this series of epoxides towards OH radicals. The results obtained are described in more detail below.

For isomers it has been observed that within the experimental error limits, the rate coefficients for the reaction of *trans*-2,3-epoxy butane with OH radicals are slightly different than for *cis*-2,3-epoxybutane. Table 3 shows the result of the SAR calculations for the epoxide reactions by using different factors from the literature for the total rate constant estimation. Method (a), (Kwok & Atkinson, 1995), used the substituent factor F(–OR) = 6 to describe the effect of one or two α–ether linkages, with the influence of a β–ether linkage. Method (b), (J. Calvert et al., 2011), also took into consideration the influence of a β-ether linkage and a factor F(–OR) = 4.13. Method (c), (J. G. Calvert et al., 2015), is similar to method (a) and (b) but assumes a factor F(–OR) = 8.4.

Comparing these approaches with the experimental results, for 1,2-epoxybutane, the estimated value using method (a), (Kwok & Atkinson, 1995), is the closest to the experimental value. However, it is not the case for cis and trans isomers, where a small deviation is observed.

The SAR estimation using (d), (Middala et al., 2011), proposed a corrected factor for ring strain, assuming that the effect of the presence of oxygen on the ring might have been underestimated. However, as shown in Table 6, the experimental data obtained in this work differ in most of the cases from the values predicted by SAR using this approach.

The SAR estimation using (e), (Jenkin et al., 2018b), proposes an improved new set of three rate coefficients for H atom abstraction for C atoms adjacent to ether linkages.

These new sets of the rate coefficients are applied independently of neighboring group substituent factors. Our experimental results show that the rate coefficient of 1, 2-epoxybutane is lower than the rate coefficient calculated with this approach. The rate coefficient calculated for cyclohexene oxide with this approach is the lowest with respect to all experimental values of epoxides and by other SAR estimation methods.

The influence of the ether group seems not to be the same for epoxides of the same number of carbon atoms with differences in the symmetry. Factors like geometrical disposition and neighbor groups could explain the H atom abstraction in places far from the ether linkage.

In less substituted epoxides, such as propylene oxide, the approaches presented by (Kwok & Atkinson, 1995) and (J. Calvert et al., 2011; J. G. Calvert et al., 2015) are the closest to the experimental values determined in this work.

There are discrepancies between the values calculated by different approaches of the SAR estimation method, as is shown in Table 6 . In addition, there is no SAR estimation method that consistently generates a value close to the experimental value for all compounds which have been studied in the present work. These discrepancies had already been observed since the first SAR approximations for cyclic ethers, and they could be attributed to the limited database that still exists for this kind of compound (Jenkin et al., 2018a; Kwok & Atkinson, 1995). In general, all these approaches were developed to fit the behavior of cyclic alkanes, with one factor being attributed to ring strain and the presence of an ether group.

Table 6 - Comparison of the rate coefficients for the reaction of OH radicals with the epoxides investigated in this study with the literature data and SAR predictions. $k_{Epoxide}/k_{SAR}$

Epoxide	k_{SAR}	$k_{Epoxide}/k_{SAR}$	$k_{Epoxide}$ (cm^3 $molecule^{-1}$ s^{-1})	Reference
Cyclohexene Oxide 	[a] 6.37×10^{-12}	0.93	**$(5.93\pm1.13)\times10^{-12}$**	This work
	[b] 6.14×10^{-12}	0.97	**$(6.51\pm0.65)\times10^{-12}$**	(El Othmani, Ren, Mellouki, et al., 2021)
	[c] 6.31×10^{-12}	0.94		
	[d] 5.81×10^{-12}	1.02		
	[e] 1.02×10^{-11}	0.58		
Ethylene Oxide 	[a] 2.80×10^{-13}	0.31	**$(0.88\pm0.25)\times10^{-13}$**	(J. Calvert et al., 2011)
	[b] 1.89×10^{-13}	0.47		
	[c] 3.54×10^{-13}	0.25		
	[d] 0.77×10^{-13}	1.14		
	[e] 8.85×10^{-14}	0.99		
Propylene Oxide 	[a] 0.59×10^{-12}	0.83	**$(0.49\pm0.52)\times10^{-12}$**	(Wallington, Liu, et al., 1988)
	[b] 0.46×10^{-12}	1.07	**$(0.30\pm1.00)\times10^{-12}$**	(Middala et al., 2011)
	[c] 0.67×10^{-12}	0.73	**$(0.47\pm0.24)\times10^{-12}$**	(Virmani et al., 2020)
	[d] 0.28×10^{-12}	1.75		
	[e] 5.43×10^{-12}	0.90		
1,2-epoxyhexane 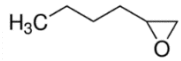	[a] 4.64×10^{-12}	1.24	**$(5.77\pm0.83)\times10^{-12}$**	This work
	[b] 4.48×10^{-12}	1.29		
	[c] 4.15×10^{-12}	1.39		
	[d] 3.97×10^{-12}	1.45		
	[e] 6.34×10^{-12}	0.91		
1,2-epoxybutane 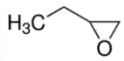	[a] 1.81×10^{-12}	1.09	**$(1.98\pm0.29)\times10^{-12}$**	This work
	[b] 1.65×10^{-12}	1.20	**$(1.90\pm0.67)\times10^{-12}$**	(Wallington, Dagaut, et al., 1988)
	[c] 1.83×10^{-12}	1.08	**$(2.20\pm0.02)\times10^{-12}$**	(El Othmani, Ren, Bedjanian, et al., 2021)
	[d] 1.45×10^{-12}	1.37		
	[e] 2.96×10^{-12}	0.67		
trans-2,3-epoxybutane 	[a] 0.92×10^{-12}	1.97	**$(1.81\pm0.33)\times10^{-12}$**	This work
	[b] 0.73×10^{-12}	2.48		
	[c] 0.99×10^{-12}	1.83		
	[d] 0.49×10^{-12}	3.69		
	[e] 9.98×10^{-13}	1.81		
cis-2,3-epoxybutane 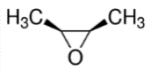	[a] 0.92×10^{-12}	1.63	**$(1.50\pm0.28)\times10^{-12}$**	This work
	[b] 0.73×10^{-12}	2.05		
	[c] 0.99×10^{-12}	1.52		
	[d] 0.49×10^{-12}	3.06		
	[e] 9.98×10^{-13}	1.50		

Calculated using the SAR estimation of (a) (Kwok and Atkinson, 1995), (b) (Calvert et al., 2011), (c) (Calvert et al., 2015), (d) (Middala et al., 2011), (e) (Jenkin et al., 2018)

3.5.2.1 Pseudo-ethylenic character in the epoxy ring as the main factor affecting SAR estimation

The kinetics, reactivity trends and thermochemistry of *cis*- and *trans*-2,3-epoxybutane, 1,2-epoxybutane, 1,2-epoxyhexane and cyclohexene oxide initiated by Cl atoms were previously discussed (Tovar et al., 2021). The series of epoxides were theoretically investigated using density functional theory (DFT), applying the B3-LYP exchange–correlation function with Grimme's GD3-BJ empirical dispersion corrections. The calculation results showed that the abstraction channels of β-CH_2 sites are dominant for all epoxides under study.

As we explained in (Tovar et al., 2021), the sites in the molecule are more reactive in β position when the carbon atoms in ethylene oxide approach the sp^2 state and its CH_2 units are pseudo-ethylenic in character. That conjugation does not occur if the π orbitals of the unsaturated groups cannot orient themselves with their axes parallel to the plane of the epoxide ring. Such a geometric arrangement in the epoxy molecule would be necessary to allow for the abstraction of a hydrogen in the molecule in a preferential way, thus increasing the reactivity of the reaction.

In Sect. 4.4.2, we discuss the rate coefficients experimentally calculated for the same series of epoxides towards OH radical and the estimated rate constants of epoxides with a total of two to six carbon number using different SAR approaches. In these estimations, different substituent factors were applied. In the following discussion, we present the possible theoretical reasons these SAR estimations could differ between them and with respect to the experimental values based in novel theoretical and experimental studies, which confirms our previous findings.

From Table 7, we can assess the influence of the ring size over a series of cyclic ethers. In this way, the cyclic ether reactivities towards OH radicals increase with ring size (k in 10^{-12} cm^3 $molecule^{-1}$ s^{-1}) ($k_{oxirane}(C_2H_4O) = (0.091 \pm 0.023)$) < ($k_{oxetane}(C_3H_6O) = (10.3 \pm 2.6)$) < ($k_{oxolane}(C_4H_8O) = (17.0 \pm 2.6)$); ($k_{oxane}(C_5H_{10}O) = (18.0 \pm 5.0)$).

For previous studies, we know that the electron ability in hydrogen bonding can act as a measure of the relative electron density (Tamres et al., 1954). The very low electron donor ability of substituted ethylene oxides, compared with other cyclic ethers, in hydrogen bonding has

already been shown in the past (Searles et al., 1953; Searles & Tamres, 1951). Thus, the oxygen in three-membered ring ethers is more electronegative than in larger ring ethers or in acyclic ethers. This observation can be explained from Walsh's proposal for the structure of ethylene oxide and cyclopropane (Walsh, 1949). Walsh's model implies a high electron density in the centre of the three-membered rings, which suggests that the exterior of such rings would have a lower electron density than normal for the atoms involved. This effect is explained for strained systems where the hybridized orbitals employed for a bonding attain maximum overlap in such a way that altered valence angles "bent bonds" are realized. Because the Walsh model does not correspond to the ground state of cyclopropane/epoxide, the description of bent bonds for cyclopropane by the Förster–Coulson–Moffitt model (Coulson, C., A. & Moffitt, W., E., 1949; Coulson & Moffitt, 1947; Förster, 1939) is the most frequently considered one (Wiberg, 1996).

More recently, the topological analysis of the electron density method (ED) is applied to describe the electron distribution within a compound (Bader et al., 1994; Coppens, 2005; Koritsanszky & Coppens, 2001; Kutzelnigg, 1993).

However, the ED method provides information on concentration and depletion of electrons but not on the pairing of electrons. In order to measure the electron pair localization, the electron ability indicator (ELI) is used (Kohout, 2004). A recent study presented by (Grabowsky et al., 2010) has introduced the ELI based on an X-ray diffraction experiment by means of the X-ray constrained wave function fitting procedure. The method was applied on a series of epoxide derivatives and clearly indicated outwardly bent bonds according to the Förster–Coulson–Moffit model.

Also, this study shows that the maxima of deformation density and the valence shell charge concentrations (VSCCs) in the Laplacian maps are located clearly outside the bond axes for both the C–O and C–C bond, and there are no maxima inside the ring. The Förster–Coulson–Moffit model makes use of hybrid orbitals with a relation between s and p character like sp^2 hybridization. This conducts to an orbital overlapping outside the direct bond axis forming three σ-type bonds. The orbitals used in these exterior bent bonds of the ring are in a favorable position for some overlap with p orbitals from adjacent atoms (Searles et al., 1953). The

involvement of sp^2-type orbitals in the epoxide ring instead of sp^3 like in normal single bonds suggests that the bonds are not saturated and can interact with π–electron systems (Grabowsky et al., 2010). Our recent study on the reactivity of a series of epoxides towards chlorine atoms in gas phase using quantum mechanical calculations agrees with these findings. As we discussed in (Tovar et al., 2021), if we consider the case of *cis*- and *trans*-epoxybutane, when the compound has lost one H of the CH_3 group, it becomes trigonally (sp^2) hybridized, facilitating the possible formation of a double bond with the singly occupied p-orbital after abstraction of H. This effect could explain the formation of acrolein from Cl-initiated oxidation of both *cis*-2,3-dimethyloxirane and *trans*-2,3-dimethyloxirane with yields of 36.49 ± 0.55 and 49.08 ± 1.29 at 650 and 800 K, respectively, in the work presented by Doner et al. (2021). The formation of the vinyl oxirane from β hydrogen abstraction and the subsequent formation of the keto hydro peroxy radical reported by (Christianson et al., 2021) for the oxidation of 1,2-epoxybutane also confirm this theory. In addition, one of the most abundant products reported in the same work, 2,2-bioxirane (31.44 ± 6.49) at 640 K, would also respond to the same reactivity trend, with abstraction in the β position being the most predominant.

This structural effect has also been observed experimentally with cyclopropyl ketones (Rogers, 1947), α- and β-epoxyketones (Cromwell & Graff, 1952; Walsh, 1949), ethylenimine ketones (Cromwell & Graff, 1952) and more recently in the acid-catalysed ring opening of epoxides (Oshima et al., 2008). Moreover, there is some evidence of a conjugation of the epoxy ring with substituents using methods like UV spectroscopy, heat of combustion and molecular orbital (MO) calculations (Parker & Isaacs, 1959; Starit et al., 1964).

Table 7 - Reactivity trends of the epoxy compounds towards OH radicals compared with their homologous alkanes, acyclic ethers and cycloalkanes with the same number of carbon atoms.

	Cyclic ether			***Alkane/cycloalkane***			***Acyclic ether***	
Ring size	**Structure**	**$k_{OH}\times10^{12}$ †**	**C Atoms**	**Compound**	**$k_{OH}\times10^{12}$ †**	**C atoms**	**Compound**	**$k_{OH}\times10^{12}$ †**
7 member	oxepane 	18.0[1]						
6 member	oxane 	12.0[1]	7	methylcyclohexane[1]  heptane[1]	9.26[1] 6.23[1]			
5 member	oxolane 	17.0[1]	6	2,3-dimethylbutane Hexane	5,86[1] 4.97[1]	6	di-n-propyl ether	20.0[1]
4 member	oxetane 	10.3[1]	5	2-methylbutane pentane	3.74[1] 3.76[1]	5	methyl-s-butyl-ether	9.67[1]
3 member	CHO 	5.93	4	Butane	2.38[1]	4	1-metoxypropane	9.91[1]
	EHX 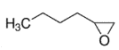	5.77						
	12EB 	1.98						
	*t*EB 	1.81						
	*c*EB 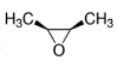	1.50						
	oxirane 	0,09						

† units: $cm^3molecule^{-1}s^{-1}$

[1](McGillen et al., 2020); (Recommended values of the most recent revision of database for the kinetics of the gas-phase atmospheric reactions of organic compounds).

3.5.2.2 Ring strain in epoxides

From Table 7, we can see that the epoxides are less reactive towards OH radicals than the analogous alkanes with the same number of carbon atoms: (k in 10^{-12} cm^3 $molecule^{-1}$ s^{-1}) ($k_{cEB(C4H8O)}$ = (1.50 ± 0.28)), ($k_{tEB(C4H8O)}$ = (1.81 ± 0.33)), ($k_{12EB(C4H8O)}$ = (1.98 ±0.29)) < ($k_{butane(C4H10)}$ = (2.38 ± 0.24)). The effect is more pronounced for epoxides with four carbon atoms than for those with six carbon atoms: ($k_{12EHX(C6H12O)}$ = (5.77 ± 0.83)) < ($k_{(C6H14)}$ = (5.86 ± 1.17)). The presence of a six-membered ring next to the epoxide group increases its reactivity ($k_{CHO(C6H10O)}$ = (5.93 ± 1.13)) > (k(C_6H_{14}) = (5.86 ± 1.17)).

Grabowsky et al. (2010) derived the experimental electron density of ethylene oxide from a multipole refinement of 100 K X-ray data and complemented it with density-functional calculations at experimental and optimized geometry. This study found that despite the high strain in the three-membered ring of ethylene oxide, most atomic and bond topological properties do not differ from comparable fragments in unstrained molecules. Grabowsky et al. (2010) concluded that the strained and unsaturated character of the epoxide ring is reflected in the populations of the bonds.

The three-membered ring strain is considered in the SAR estimations for its influence on the reactivity of epoxides.

However, this factor itself does not play a dominant role in the rate coefficients of the epoxides. The presence of the epoxy ring would affect the reactivity of epoxides because the CH group attached favors the π overlap (Figure 13).

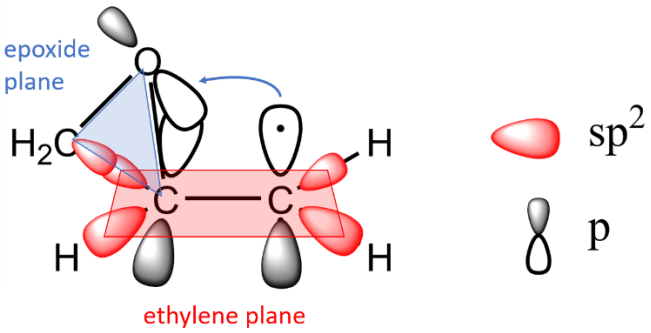

Figure 13 - Involvement of sp^2-type orbitals in the epoxide ring.

For this reason, the factors (F(O), F (three-member ring)) need to be treated specially in SAR and possibly as one single factor F (epoxy ring-β-CX) since their influence on the β carbon is very pronounced. Only then can one see the contributions of other groups, for example, linear, branched and rings on this basic structure. The reactivity trends observed in our previous (Tovar et al., 2021) and present work suggests that the rate constant of the β-channel could be the closest to the k_{total} determining the overall reaction rate. These aspects have not been considered in SAR estimates to date; therefore, new factors that include these complicated bond structures in epoxides need to be developed.

3.5.3 Improving SAR estimation for epoxides

To provide a new set of "corrected" factors, especially for F (epoxy ring-β-CX) that can be used for an improved SAR estimation for epoxides, a new set of theoretical calculations with OH radicals are recommended. These kinds of calculations are beyond the scope of this work. However, a possible approach should be conducted to expand the kinetic database of epoxides (experimental and theoretical) in a wide temperature range. Experiment and theory are highly complementary in this regard, and their combined application allows for alleviation of some of the shortcomings in both approaches; for theoretical work specifically, even a single experimental datum point often allows for the optimization of the potential energy surface (PES) or energy transfer parameters to allow for temperature (T) and pressure (P) extrapolations with strongly enhanced reliability (Vereecken et al., 2015).

A recent work by (Q. Wang et al., 2022) proposed a concept of a combined experiment–SAR–DFT method to theoretically discuss the abstraction reaction of a series of alcohols and ketones. A similar approach could be used for epoxides with some considerations.

As has been shown in (Tovar et al., 2021), the potential energy surface of chlorine atoms reacting with the series of epoxides possesses a barrierless reaction. For these cases, (Piletic et al., 2017) proposed to use the Master Equation Solver for Multi-Energy Reactions (MESMER v.4.0) in order to compute the energy-dependent microcanonical rate constants for all forward

and reverse reactions on the PES, with the option of computing the k(E)s using an inverse Laplace transform (ILT) technique. The k(E)s may be calculated using Arrhenius parameters from a fit of the temperature-dependent high-pressure rate coefficients.

A second method could include a semi-empirical method using the Arrhenius parameters in MESMER to fit phenomenological rate constants that are consistent with the experimentally measured rates. Our preliminary exploration of the PES of the series of epoxides towards chlorine atoms (Tovar et al., 2021) provides a hint of the complex structural analysis that must be developed in order to ensure more accurate rate coefficients and capture the reactivity trends of epoxides with the SAR estimation method.

Some studies have evaluated the temperature dependence for 1,2-epoxypropane and 1,2-epoxybutane towards OH radicals. (Virmani et al., 2020) found for the reaction with 1,2-propylene oxide a very small (or possibly no) dependence on temperature within the temperature range between 261–355 K. (El Othmani, Ren, Bedjanian, et al., 2021) showed for the reaction with 1,2-epoxybutane a very weak negative temperature dependence at $T \leq 285$ K and a transition toward a positive temperature dependence at $T \geq 295$ K. (El Othmani, Ren, Mellouki, et al., 2021)measured a stronger negative temperature dependence in the case of cyclohexene oxide. This behavior could suggest the existence of van der Waals complexes that can play a role in the reaction mechanisms of epoxides at lower temperatures. More theoretical research is needed to further elucidate these findings.

All the electronic structure calculations will serve as input for the kinetic rate calculations using MESMER or another similar approach.

Even with the clear correlation between the rate coefficients of epoxides with OH radicals and chlorine atoms shown in Sect. 3.1, detailed structural optimizations and vibrational frequency calculations are also recommended for the reactions of the epoxides towards OH radicals.

Parallel to the present work, product studies of the reactions presented here have been undertaken, to delve a little deeper into the reaction mechanisms of these reactions.

3.6 Atmospheric implications

Using the kinetic data obtained in the present work, in combination with daytime average radical concentrations, the estimation of the tropospheric lifetimes of the investigated compounds can be calculated using the following expression:

$$\tau_{OH/Cl} = 1/k_{OH/Cl}\,[OH/Cl].$$

Therefore, for a globally averaged [OH] of 1.13×10^6 radicals cm^{-3} (Lelieveld et al., 2016) the atmospheric lifetimes for cyclohexene oxide, 1,2-epoxyhexane, 1,2-epoxybutane, *trans*-2,3-epoxybutane and *cis*-2,3-epoxybutane are estimated between 1 to 7 d, as shown in Table 8.

According to the rate coefficients presented in (Tovar et al., 2021), and considering an estimated atmospheric concentration [Cl] of 2.3×10^3 atoms cm^{-3} (Young et al., 2014), an atmospheric lifetime between 21 and 73 d has been calculated for the epoxides. Accordingly, the reaction with OH radicals is the primary sink for epoxides in the atmosphere under these conditions.

However, in some cases, the atmospheric composition can be more than an order of magnitude more reactive with Cl than with OH (e.g Los Angeles during CalNex, where a maximum [Cl] of 8.7×10^3 atoms was measured; (Young et al., 2014)). In polluted continents during winter, $ClNO_2$ chemistry drives increases in ozone of up to 8 ppb (X. Wang et al., 2019).

In the laboratory and ambient SOA, epoxides are considered as potential precursors for sulfate esters, polyols, hydroxy nitrates and halides. Epoxide concentrations in the aerosol composition will be limited by the rates of the gas uptake process, which will be largely determined by the gas-phase epoxide concentration levels (Minerath et al., 2009; Minerath & Elrod, 2009), the uptake process and particle acidity. Higher acidity of aerosol particles would produce more efficient heterogeneous reactions of epoxides. A recent study suggests that heterogeneous reaction of some epoxides on acidic aerosols is faster and more efficient than gaseous reactions with atmospheric oxidants, and thus these reactions could represent the major removal pathway for epoxides (Lal et al., 2012). Additionally, in urban environments, the particle acidity can be significantly high, with pH between 0–5. Under such conditions, epoxides can react

rapidly, and the reaction products of the heterogeneous reactions could contribute to the growth of the SOA particles and to the possible modification of their physical and chemical properties (Q. Zhang et al., 2007). (Minerath & Elrod, 2009) have shown that 1,2-epoxybutane, which possesses slower hydrolysis, has an increasing lifetime with increasing pH. It is expected that even at higher pH, most of the epoxides will have time to react on SOAs. The monitoring and evaluation of emissions of this kind of compound in different ambient conditions, such as pH and different regimens of NOx, are recommended in rural and urban locations.

Table 8 - Comparison of the atmospheric lifetimes of epoxides towards OH radicals and chlorine atoms.

Epoxides	τ_{OH} (days)	τ_{Cl} (days)
cyclohexene oxide	1.7	20.9*
1,2-epoxyhexane	1.8	28.4*
1,2- epoxybutane	5.1	59.7*
trans-2,3-epoxybutane	5.7	71.9*
cis-2,3-epoxybutane	6.8	72.7*

∗ Calculated values using the rate coefficients of epoxides towards Cl atoms (Tovar et al., 2021).

3.7 Conclusions

The rate coefficients for the reaction of OH radicals with three different epoxides have been determined for the first time in this study. The rate coefficients for 1,2-epoxy butane and cyclohexene oxide are in very good agreement with previous studies (El Othmani, Ren, Bedjanian, et al., 2021; El Othmani, Ren, Mellouki, et al., 2021; Wallington, Dagaut, et al., 1988). A comparison of the reactivity trends from the gas-phase reaction of the epoxides obtained in this study showed a very good correlation with the reactivity trends of epoxides with chlorine atoms. Differences have been observed between the experimental OH rate coefficients and those obtained from SAR estimations. However, the values determined by the SAR method show some discrepancies dependent on the substituent factors, which were considered for the

calculations. Such discrepancies could be explained by taking into consideration the structural effect of the ring acting in conjunction with the oxygen atom and the pseudo-ethylenic character of the epoxy ring. From the atmospheric chemistry viewpoint, the rate coefficients from the present study would help to extend the database for the reaction of cyclic ethers under atmospheric conditions.

Part B:

Non-cumulative Part

4 Experimental Methods and Instrumentation

Simulation chambers provide a controlled environment that mimics atmospheric conditions, enabling researchers to investigate the complex interactions of gases and particles and analyse chemical reactions and particle formation through experimental methods and instrumentation.

Nitrogen oxides (NO_X=NO+NO_2) influence the distribution of volatile organic compound oxidation products by primarily affecting the fate of peroxy radicals (RO_2), a key intermediate generated during the atmospheric degradation of VOCs by major oxidants like hydroxyl radicals (OH), ozone (O_3), and nitrate radicals (NO_3). In the absence of nitrogen oxides, peroxy radicals predominantly react with hydroperoxy radicals (HO_2), yielding organic peroxides and other products, and to a lesser extent, undergo self- or cross-reactions, producing carbonyls, alcohols, and multifunctional species. However, in the presence of elevated nitrogen oxides, the dominant fate of peroxy radicals (RO_2) is to react with nitric oxide (NO), leading to ozone production and the formation of organic nitrates (X. Zhang et al., 2018). During the night, peroxy radicals also react with nitrate radicals, which are produced by the reaction between ozone and nitrogen dioxide. Additionally, the reaction of peroxyacyl radicals ($RC(O)O_2$) with nitrogen dioxide produces peroxyacyl nitrates, which constitute a significant reservoir of reactive nitrogen and a potentially important secondary organic aerosol precursor (Nguyen et al., 2015; Singh & Hanst, 1981).

Several chamber studies extensively investigated distinct chemical regimes, categorized as "high-NO", intermediate-NO and "low-NO" conditions. The findings from these chemical scenarios are widely incorporated into chemical transport models to represent key atmospheric processes in urban and pristine environments (X. Zhang et al., 2018). The laboratory chamber experiments are the primary source of data on the mechanistic understanding of oxidation and the secondary organic aerosol formation potential of volatile organic compounds (Cappa et al., 2013).

4.1 Atmospheric simulation chambers

The simulation of atmospheric chemical processes involves removing a complex array of interactions that lead to the observed concentrations of gaseous and particulate species in the atmosphere. These interactions occur over a wide spectrum of time scales, ranging from a few seconds to several days, and spatial scales, varying from less than a centimeter to many kilometers. They incorporate rapid homogeneous and heterogeneous reaction pathways, which occur alongside a constant background of trace species concentrations, the sporadic presence of aerosols and hydrometeor clouds, contaminant emissions, and air mixing processes that cause dilution. Simulation models are specifically adapted to conditions that favor extremely small temporal and spatial scales. Their primary goal is to isolate distinct chemical phenomena from the multitude of concurrent processes occurring in the atmosphere and its boundaries (Hidy, 2019).

Atmospheric chambers are vital tools in atmospheric chemistry, as they recreate environmental conditions to facilitate the examination of chemical processes. These sophisticated facilities allow researchers to investigate the behavior of gas-phase reactions, the generation of secondary organic aerosols (SOA), and the effects of various atmospheric components under controlled conditions. In this research, we will delve into the insights gained from these laboratory studies and their implications for understanding atmospheric chemistry and air quality.

Best practices in data analysis are imperative for accurately interpreting outcomes derived from chamber experiments, particularly in relation to gas-phase measurements and SOA yields (Seakins et al., 2023). The architectural design of these chambers must account for variables that affect the precision of results, thereby ensuring that findings can be relevantly extrapolated to authentic atmospheric conditions (Kiendler-Scharr et al., 2023). The progression of atmospheric chambers has substantially enhanced our comprehension of atmospheric chemistry, with ongoing advancements directed towards addressing emerging scientific challenges (Doussin, 2023).

During the assessment of the kinetics, reactivity trends, and reaction products of a series of epoxides in this study, a variety of atmospheric simulation chambers were employed, each equipped with different analytical techniques. This approach enabled the acquisition of complementary results, given the complexity of such studies, particularly in elucidating gas-phase reaction products.

4.1.1 Indoor simulation chamber (QUAREC)-1080 L (Wuppertal University)

The 1080 L chamber is comprised of two interconnected quartz-glass tubes, exhibiting an aggregate length of 6.2 m and an inner diameter measuring 0.47 m, which are joined together by a central flange. Both extremities are sealed with metal flanges that incorporate multiple ports designated for the introduction of reactants, the addition of bath gases, and the integration with analytical instruments. A total of 32 superactinic fluorescent lamps (Philips TL05 40W: 300–460 nm, with a peak intensity at approximately 360 nm) and 32 low-pressure mercury vapor lamps (Philips TUV 40W: peak intensity at 254 nm) may be employed to irradiate the reaction mixture. These lamps are configured in a parallel arrangement and are uniformly distributed around the reaction vessel (See Figure 28 in Illustrations.). The pumping apparatus comprises a turbo-molecular pump that is supported by a double-stage rotary fore pump. The chamber is subjected to a cleaning process between experiments, wherein it is evacuated to a pressure of 10^{-4} mbar for a minimum duration of 30 minutes. The cleanliness of the chamber is validated through Fourier-transform infrared (FTIR) spectroscopy. The homogeneity of the reaction mixtures is facilitated by three magnetically coupled Teflon mixing fans, which are strategically positioned on the terminal and central flanges. An optical mirror system of the White type is installed within the chamber to facilitate the monitoring of reaction mixtures through FTIR spectroscopy across the spectral range of 4000–700 cm^{-1} at a resolution of 1 cm^{-1}. The system, characterized by a base length of (5.91 ± 0.01) m, was utilized at 82 traverses, resulting in a cumulative optical path length of (484.7 ± 0.8) m. This extended path length enhances the detection of trace gas concentrations, enabling precise monitoring of low-abundance reactants and products. The gold mirror system is part of a White-type multiple-reflection system and is integral to the Fourier Transform Infrared (FTIR) spectroscopy setup

in the chamber. The gold mirrors require regular cleaning and calibration to maintain their high reflectivity and precision Figure 14. Also, ensuring their alignment within the multiple-reflection system is vital for optimal performance.

Spectra were acquired using a Nicolet iS50 instrument, which is equipped with a liquid nitrogen-cooled mercury-cadmium-telluride (MCT) detector.

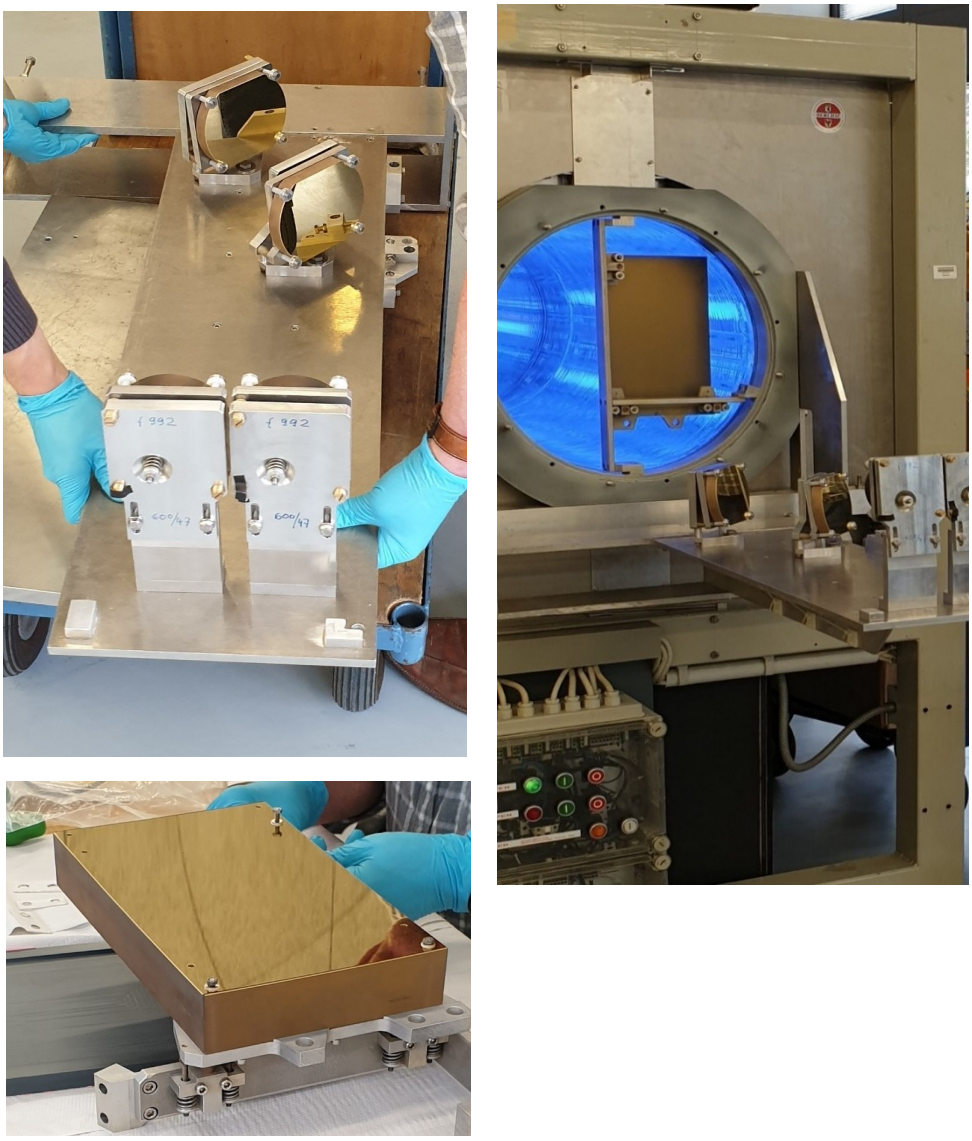

Figure 14 - The mirrors are coated with gold, which is highly reflective in the infrared (IR) range. Gold mirrors are chosen for their superior reflectivity and durability, minimizing IR light absorption and maximizing signal strength.

4.1.2 Indoor simulation chamber-480 L (Wuppertal University)

The chamber located within the Wuppertal laboratory is comprised of a borosilicate glass cylinder featuring a cumulative volume of 480 L, with dimensions measuring 3 m in length and an inner diameter of 0.45 m. The extremities of the tube are sealed with aluminum flanges that incorporate multiple ports designed for the introduction of reactants and bath gases Figure 15, as well as for sampling and monitoring instruments that assess the physical parameters within the chamber. To facilitate a uniform mixing of the reactants, a magnetically coupled fan is affixed to the anterior flange situated inside the chamber. A total of 32 fluorescent lamps (Philips TLA 40 W, with wavelengths ranging from 300 to 460 nm and a maximum intensity at 360 nm) are systematically installed in four boxes, evenly distributed around the chamber. The housings of the lamps are subjected to air cooling, and their internal surfaces are lined with reflective steel sheets. The individual operability of the lamps permits adjustments to the photolysis frequency, thereby modulating the radical concentration throughout the photolysis experiments. The vacuum system comprises a rotary vane pump in conjunction with a root pump, achieving a terminal vacuum of approximately 10^{-3} mbar. In a typical cleaning protocol conducted between two experimental runs, the chamber undergoes complete evacuation followed by refilling to a pressure of 200–300 mbar with synthetic air or nitrogen. This cleaning procedure is reiterated until it is assured that no residual signals from the preceding experiment are evident. The monitoring of reactants and products is accomplished through in situ FTIR spectroscopy. For this objective, a White-type mirror system (base length: 2.80 ± 0.01 m) is installed within the chamber and is connected to a Nicolet 6700 FTIR spectrometer equipped with an MCT detector. The operational configuration of the system involves 18 traverses, which results in a cumulative optical path length of 50.4 ± 0.2 m. FTIR spectra are captured within the spectral range of 4000–700 cm^{-1} at a resolution of 1 cm^{-1}.

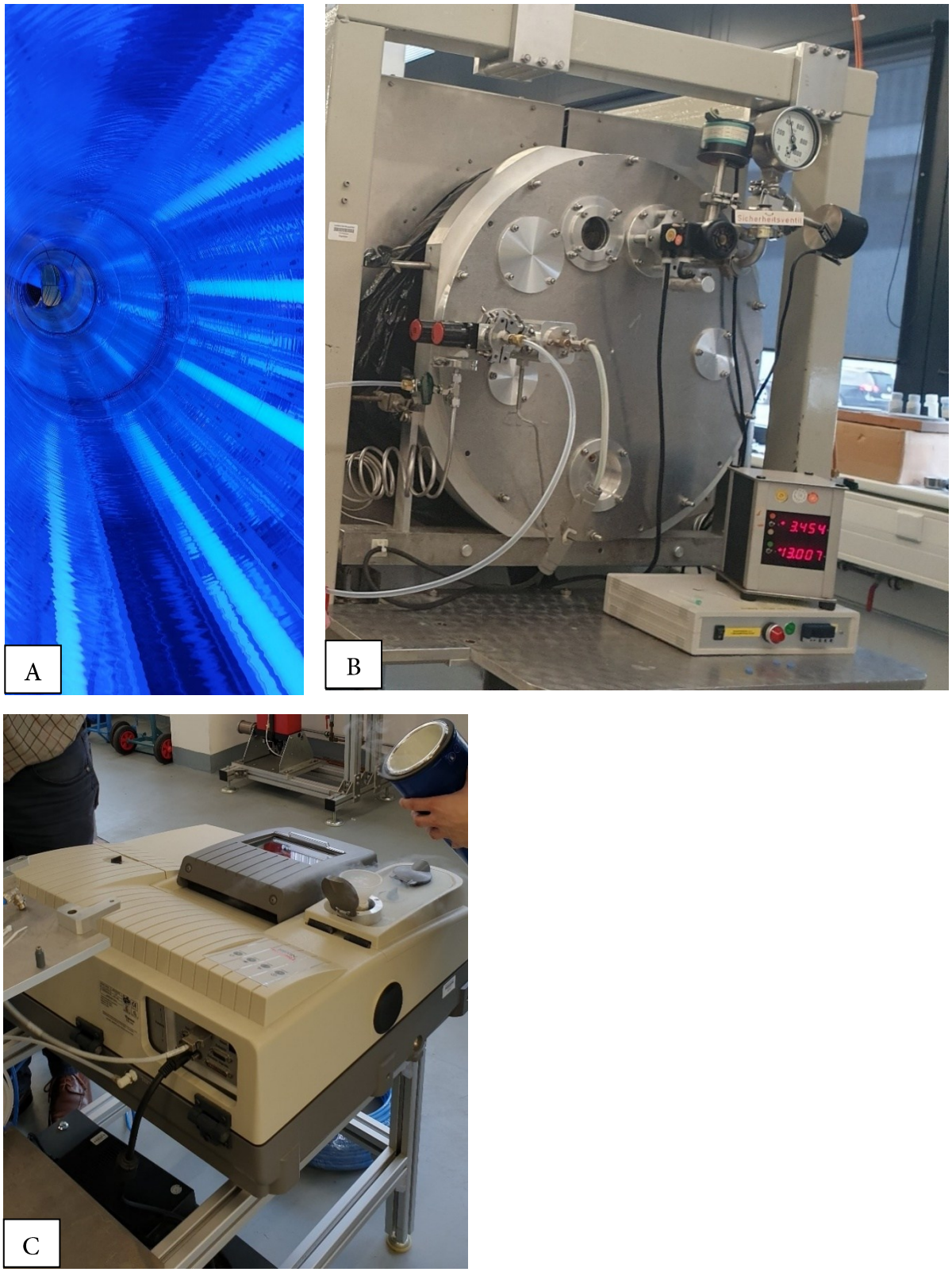

Figure 15 - A. fluorescent lamps. B. multiple ports designed for the introduction of reactants. C. Nicolet 6700 FTIR spectrometer.

4.1.3 Indoor simulation chamber (CSA)-7.3 m^3 (ICARE-ORLEANS)

The cubic indoor simulation chamber, with a volume of 7.3 m^3 is constructed from Teflon foil and is maintained at ambient temperature and a pressure of 760 Torr, utilizing purified air with a relative humidity of less than 2% (See Figure 29 in Illustrations). This chamber is encased in protective panels and features two roll-up doors (Figure 16), facilitating both maintenance activities and the execution of dark reactions. It houses 14 germicidal lamps (UV-A T-40 L, 40W, Viber Lourmat) that emit radiation at a wavelength of 254 nm, in addition to 24 black lamps (UV-A T-40 L, Viber Lourmat) operating at 365 nm, as well as 12 daylight lamps that emit wavelengths exceeding 300 nm (Orsam Ultra-Vitalux) (Figure 16). Two Teflon fans are incorporated within the chamber to promote the efficient mixing of reactants throughout the experimental procedures. For the introduction of liquid compounds, a specified volume of reactant is introduced into a custom-designed glass tube (gently heated when deemed necessary) and subsequently transported into the chamber using a stream of purified air, with the concentration being determined according to the ideal gas law (Figure 16).

For the introduction of gaseous compounds (for instance, the vapor of volatile organic compounds and other gas-phase entities such as nitrogen monoxide and nitrogen dioxide), a predetermined quantity of gases is initially introduced into a precisely calibrated cylinder (0.9 L) linked to two pressure sensors (0–10 Torr and 0–100 Torr, MKS Baratron). Subsequently, these gases are propelled into the experimental chamber utilizing a stream of purified air, and the concentration will be calculated utilizing the principles of the ideal gas law. Temperature and relative humidity metrics were systematically recorded by a combined sensor. To account for sampling flows and potential leaks, a continuous flow of purified air was supplemented throughout the duration of all experiments, thereby maintaining a slight internal overpressure and preventing any contamination from ambient air. Sulfur hexafluoride (SF_6) is introduced and employed to ascertain the dilution of the gas volume within the chamber. Following each experimental trial, the chamber is purged with purified air at a flow rate of approximately 250 L min^{-1} to eliminate any residual chemicals from the system.

4.1.3.1 Fourier transform infrared spectroscopy (FTIR)

A Fourier Transform Infrared (FTIR) spectrometer was integrated with the indoor simulation chambers used in this study—namely, the 480 L chamber, the QUAREC (1080 L), and the 7.3 m^3 chamber—to enable in situ gas-phase measurements. For the 7.3 m^3 chamber, the system utilizes dual symmetric transfer optics that guide the collimated infrared beam from the spectrometer to a White-type multi-reflection cell within the chamber and subsequently return the beam to the spectrometer. The system employs two symmetric transfer optics that direct the collimated infrared beam from the spectrometer to a White-type multi-reflection cell located inside the chamber and subsequently return the beam to the spectrometer. The long-path absorption setup within the chamber is based on a White cell configuration, utilizing gold-coated mirrors to ensure high reflectivity in the infrared (IR) region. The system includes adjustable alignment screws, allowing for straightforward modification of the optical path length. In this study, the FTIR spectrometer operated in the mid-infrared spectral range (4000–650 cm^{-1}), with an effective optical path length of 148 meters. Spectral data were acquired by co-adding 130 interferograms over a 5-minute measurement period, with a spectral resolution of 1 cm^{-1}.

In conventional Fourier Transform Infrared (FTIR) spectroscopic systems, infrared radiation generated by a source—typically a Silicon Carbide (SiC) Globar—is directed into an interferometer, which modulates the incident light. Following modulation, the radiation passes through a single optical compartment containing the sample and is subsequently focused onto a detector. The resulting signal, known as an interferogram, represents the cumulative summation (integral) of interference patterns produced by all individual wavelengths within the source spectrum. This interferogram is digitized during data acquisition and then mathematically converted into an infrared spectrum via the Fourier Transform (FT) process. Infrared (IR) spectroscopy measures the absorption of infrared radiation by a given substance, resulting in the excitation of molecular vibrations and rotations. According to vibration theory, these excitations occur at frequencies that correspond to those within the IR region of the electromagnetic spectrum. A molecule can absorb infrared (IR) radiation only if the dipole

moment corresponding to a particular atomic group changes during the vibrational motion. The intensity of the IR absorption band is directly proportional to the extent of this dipole moment variation. Furthermore, the infrared spectrum is conventionally categorized into three regions: near-infrared (NIR), mid-infrared (MIR), and far-infrared (FIR). Fundamental molecular vibrations primarily occur within the MIR region, while the NIR range primarily excites overtone and combination vibrations, along with backbone vibrations in large molecules and fundamental vibrations in molecules containing heavy atoms. At present, most infrared (IR) spectrometers used for mid-infrared (MIR) spectroscopy are based on the Fourier Transform Infrared (FTIR) method.

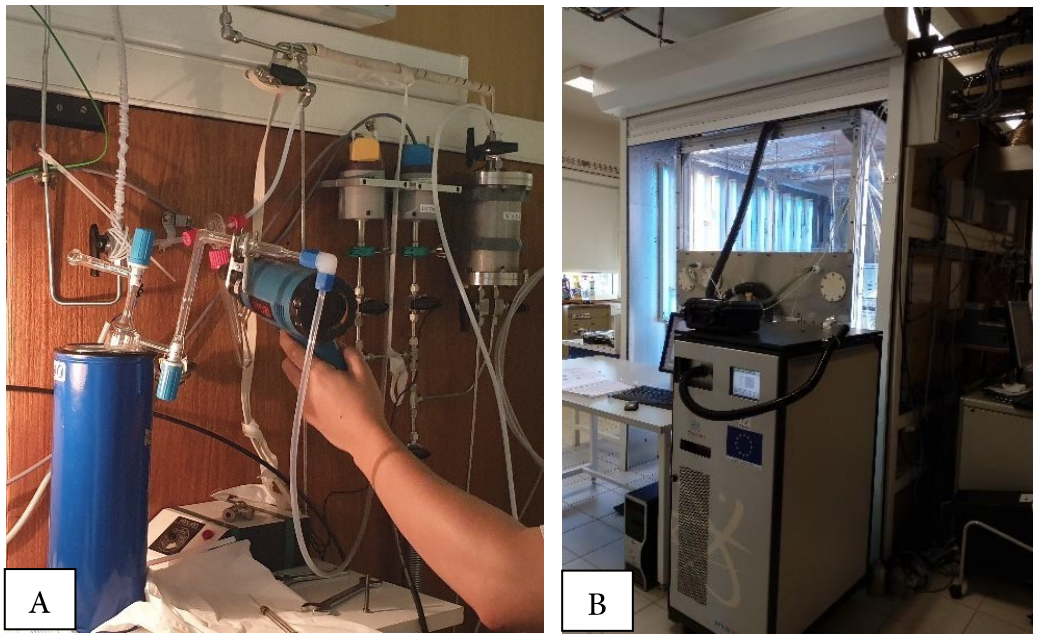

Figure 16 - A. introduction of the reactants into the chamber. B. Teflon foil cubic indoor simulation chamber. The chamber is encased in protective panels and features two roll-up doors.

In the experiments utilizing the 7.3 m^3 simulation chamber, the chemical analysis of the gas mixture was executed using an infrared spectrometer (specifically, the Nicolet 550 Magna FTIR spectrometer, that was integrated with a White-type multi-pass mirror cell (2 liters in volume and an optical path length of 10 meters). Infrared spectra were systematically recorded at five-minute intervals by co-adding 130 interferograms, maintaining a resolution of 1 cm^{-1}.

4.1.4 Outdoor simulation chamber (HELIOS) -90 m^3 (ICARE-ORLEANS)

Description of the chamber

The HELIOS chamber possesses a volume of 90 m^3, characterized by a surface-to-volume ratio of 1.2 m^{-1}. In conjunction with a suite of instruments, the primary objective of HELIOS is to assess the comparability of photochemical reactions under artificial illumination in contrast to natural sunlight. The HELIOS chamber has been strategically positioned on the rooftop of ICARE (CNRS, Orléans, France, Figure 17). Constructed in the form of a truncated hemisphere, the reactor is fabricated from a fluorine-ethene-propene (FEP) foil with a thickness of 250 µm (Vector Foiltec, GmbH, Bremen, Germany), which transmits between 88% and 95% of the light across the entire solar spectrum (Figure 18). It consists of 28 welded segments of foil, which are suspended from a central point within a framework of three half-arches. The reactor is inflated around a structural skeleton composed of 12 epoxy components. Acting as an internal reinforcement for the chamber, the epoxy framework provides protection, capable of withstanding wind velocities of up to 25 km/h. Teflon tubes encase the skeleton to mitigate friction between the reactor and the epoxy framework. At the apex, the skeleton is affixed to a valve that facilitates the expulsion of gases when the chamber undergoes flushing.

Figure 17 - HELIOS chamber ICARE (CNRS, Orléans, France)

Protective structure of the chamber

The chamber has been constructed within a framework that accommodates an 11-ton metallic enclosure, which is capable of being relocated along designated rails. Referred to as the "Light Box," one of the primary objectives of this mobile protective structure is to safeguard the reactor from adverse meteorological phenomena, such as precipitation, snowfall, and high-velocity winds. Xenon arc lamps are intended to be integrated within the enclosure, thereby facilitating the investigation of chemical reactions under controlled artificial radiation conditions. Ultimately, the Light Box enables maintenance activities within the chamber, extending to its uppermost areas, utilizing a ladder and a bridge that have been installed internally within the box.

Figure 18 - The foil with a thickness of 250 µm transmits between 88% and 95% of the light across the entire solar spectrum.

The protective enclosure can be repositioned in less than two minutes from one side of the roof to the opposite side, facilitated by two motors operating along the rails. A silent block is employed to mitigate the transmission of vibrations, induced by the movement of the box, to the structural integrity of the building. To further inhibit the propagation of vibrations to the chamber, the foundation of HELIOS has been elevated by several centimeters above the metallic framework that supports the Light Box. The chamber is affixed to an anti-vibration framework,

which comprises a layered assembly of a specialized IPN structure, firmly anchored to the building, industrial grating, and, at the apex, wood composite panels.

The structure has been perforated at four distinct locations, which serve as access points to the chamber from the laboratory situated within the building, beneath the reactor. These apertures are sealed with movable INOX plates. Concealed beneath a paper covering that matches the color of the wood panels, the plates are designed to facilitate the connection of various instruments located in the laboratory to the chamber. A Teflon-FEP foil, with a thickness of 500 µm, encases the floor of the chamber, ensuring that the entire chamber maintains uniform physicochemical properties.

4.1.4.1 Introduction to the working mechanism of the chamber

Injection and Mixing System

As illustrated in Figure 19, various methodologies are employed to introduce substances into the chamber, regardless of their physical state—liquid, gaseous, or solid. Liquid substances, under standard ambient conditions, are introduced into the chamber by administering a predetermined volume within a glass apparatus known as a bubbler, utilizing a syringe for precision. Subsequently, purified dry air is conveyed through the bubbler, which induces the volatilization of the compounds and facilitates their transfer to the reactor. If deemed necessary, the bubbler is subjected to gentle heating via a heat gun to augment the volatilization process of the compounds. Gaseous substances are introduced into HELIOS utilizing a 4.87 L stainless steel cylinder: this cylinder is charged with a specific pressure of the compounds and subsequently purged with pure dry air. To guarantee efficient mixing of the substances, two fans are strategically positioned within HELIOS. Aligned oppositely, these fans can achieve a maximum rotational speed of 50 Hz (3,000 rpm). During the experimental procedures, both fans were operated at a frequency of 20 Hz, resulting in an estimated mixing duration of less than 90 seconds. As part of the cleaning protocol, the chamber is purged with purified dry air at a flow rate of 800 L min-1 for an entire night prior to the commencement of any experimental activities.

Figure 19 - gas sample injection systems.

Air purification system

A sophisticated air purification system has been implemented to provide HELIOS with dry, uncontaminated air. This system consists of an oil-free compressor, an air dryer, and an air purification unit. In summary, approximately 390 cubic meters of oil-free air is produced hourly from the surrounding atmospheric air through pressurization processes (at 10 bar) facilitated by the oil-free compressor. The air undergoes a drying process via a dryer that employs absorption techniques without the application of heat, achieving an air flow rate of 420 m^3 h^{-1}. The air purification unit effectively removes all airborne pollutants, ensuring that the concentrations of O_3, SO_2, H_2S, COS, and NOx remain below 1 part per billion; similarly, the concentrations of hydrocarbons, methane, and carbon monoxide are maintained at a maximum of 5 parts per billion within the dried air.

Loss of gas-phase species

The depletion of gas-phase entities encompasses both dilution and wall loss phenomena. Dilution can transpire as a consequence of minor leaks and extensive sampling volumes, which may fluctuate in relation to the quantity and nature of apparatus engaged in sample extraction from the reactor. In every experimental trial, a low-reactive substance such as SF_6 was introduced as a tracer to monitor dilution effects. The concentration of SF_6 was quantifiable via Fourier Transform Infrared Spectroscopy (FTIR). The effects associated with chamber walls involve off-gassing of reactive species such as nitrogen oxides (NOx), generation of chamber-derived radicals like the hydroxyl radical (OH), and the depletion of species due to wall interactions (Carter et al., 1982). These factors may exert significant influence on gas-phase reactivity as well as secondary organic aerosol (SOA) formation.

4.1.4.2 Proton transfer reaction-time of flight-mass spectrometer (PTR-ToF-MS)

The PTR-ToF-MS, developed by Ionicon Analytik, is an analytical instrument specifically designed for the examination of volatile organic compounds (VOCs). In this chapter, the functionalities of the PTR-ToF-MS 8000 model will be described in detail, which operates in conjunction with HELIOS chamber and 7.3 m^3 simulation chamber. The PTR-ToF-MS apparatus fundamentally comprises four integral components: the ion source, the PTR drift tube, the Transfer Lens Systems, and the Time-of-Flight Mass Spectrometer (ToF-MS). The proton transfer reaction constitutes a form of soft chemical ionization (CI), which is a methodology employed for the generation of ions of the target compound (analyte, M) through ion-molecule interactions with reagent ions that are typically present in significantly higher concentrations than the analyte itself, and which are generated via electron ionization (EI) or irradiation of the reagent gas. The PTR-ToF-MS 8000 provides exceptional sensitivity and achieves detection limits at the parts-per-trillion by volume (pptv) level, enabling real-time monitoring and comprehensive mass spectral acquisition with high temporal resolution. Its sophisticated ion optics system minimizes background interference, improves sensitivity, and ensures excellent linearity across an extensive dynamic range. Unlike traditional electron ionization, the soft chemical ionization (CI) method produces reduced fragmentation—or in

some cases, no fragmentation—resulting in a generally simpler mass spectrum. The predominant ion-molecule reactions observed in chemical ionization encompass proton transfer (leading to the formation of AH^+ or $[A\text{-}H]^-$ ions), charge or electron transfer (resulting in the creation of $A^{+\bullet}$ or $A^{-\bullet}$ ions), hydride transfer (yielding $[A\text{-}H]^+$ ions), and the formation of adducts or complexes (which produces $[A + R]^+$ or $[A + R]^-$ ions). The PTR-ToF-MS 8000, developed by Ionicon Analytik GmbH, is among the most advanced commercial Proton Transfer Reaction Time-of-Flight Mass Spectrometry (PTR-ToF-MS) systems currently available. This instrument supports reagent ion chemistry using hydronium ions (H_3O^+) and, via its Selective Reagent Ionization (SRI) feature, also employs NO^+ and O_2^+ ions, enabling selective detection of volatile organic compounds (VOCs). The system achieves a high mass resolution greater than 4,000 full widths at half maximum (FWHM), typically ranging between 5,000 and 8,000 depending on operational parameters, and covers a broad mass-to-charge ratio (m/z) range from 1 to 50,000. It exhibits rapid response times under 100 milliseconds and detection limits below 15 parts per trillion by volume (pptv) for compounds such as benzene, with time-averaged limits reaching approximately 10 pptv for one-minute integrations. The PTR-ToF-MS 8000 incorporates an advanced hollow cathode ion source combined with a temperature-regulated drift tube, which ensures stable ion generation and minimizes clustering effects. Consequently, this instrument enables real-time, high-sensitivity VOC detection with quantitative precision suitable for a wide range of analytical applications. Chemical Ionization Mass Spectrometry (CIMS) is conducted utilizing both positively and negatively charged reactant ions. Furthermore, chemical ionization can be applied using any variety of mass spectrometers, including but not limited to quadrupole, magnetic, Time-of-Flight, Fourier transform ion cyclotron resonance (FTICR), and ion trap configurations.

The PTR-ToF-MS 8000 features an advanced hollow cathode discharge ion source specifically designed to generate high and stable hydronium ion (H_3O^+) currents, ensuring consistent ionization efficiency. A key aspect of the instrument's design is its Selective Reagent Ionization (SRI) capability, which enables rapid switching between multiple reagent ions, including H_3O^+, NO^+, O_2^+, Kr^+, and Xe^+. This flexibility significantly enhances selectivity and broadens the

range of detectable target compounds, allowing for tailored analytical strategies depending on the specific chemical characteristics of the sample being analyzed. In a sequential manner, H_3O^+ ions of elevated purity (reaching up to 98%) are generated from water vapor through the process of a hollow cathode discharge, as follows:

$$e^- (H^{2+}, H^+, O^+) + H_2O \rightarrow H_2O+ + 2e^-$$

$$H_2O^+ + H_2O \rightarrow H_2O{\cdot}H^+ + OH^-$$

Subsequently, protonated water ($H_2O{\cdot}H^+$) is introduced into the reaction chamber (PTR drift tube) through a Venturi-type inlet. The sample gas, which is steadily supplied and contains volatile organic compounds (VOCs), predominantly experiences non-dissociative proton transfer from $H_2O{\cdot}H^+$ during the collisions, provided that the colliding VOCs possess a higher proton affinity, as:

$$\mathbf{H_2O{\cdot}H^+ + VOCs \rightarrow VOCs{\cdot}H^+}$$

Since O_2, CO_2, N_2, Ar, and other similar gases exhibit a reduced proton affinity, the $H_2O{\cdot}H^+$ ions do not engage in reactions with any of these predominant constituents found within the atmosphere characterized as pristine. Protonated volatile organic compounds (VOCs) are introduced into the Time-of-Flight Mass Spectrometry (ToF-MS) system for the purpose of mass analysis via a Transfer Lens System. The Transfer Lens System is responsible for rectifying the trajectory of $VOCs{\cdot}H^+$ as they enter the ToF-MS apparatus. ToF-MS constitutes a mass spectrometric technique whereby the mass-to-charge ratio (m/z) is ascertained through the measurement of time and intensity. Specifically, within an electric or magnetic field, the duration required for the ion to traverse to a detector positioned at a predetermined distance is recorded. This duration is determined by the ion's velocity, which in turn is influenced by the m/z, thereby serving as an indicator of its mass-to-charge ratio.

The phenomenon of acceleration takes place within a designated area known as the Time-of-Flight (ToF) extractor; subsequently, ions traverse to the distal end of the flight chamber, where

they encounter a reflectron that alters their trajectory and redirects them towards the detector, which is typically a microchannel plate (MCP). Ions possessing lower energy levels, yet identical mass-to-charge ratios (m/z), penetrate a reduced distance into the reflectron and, consequently, follow a more abbreviated trajectory to the detector. Consequently, the temporal interval between the initiation of the impulse and the subsequent collision with the detector is meticulously recorded. A location characterized by the simultaneous arrival of ions exhibiting the same m/z but differing energy levels is commonly referred to as the *ToF focus*. The aggregate signals encompass both intensity and time subsequent to the ion acceleration event, which are subsequently amplified and systematically recorded by a computational device. The continuous data array that encapsulates the observed signal intensities at all respective times of flight is designated as the ToF spectrum.

In Proton Transfer Reaction Time-of-Flight Mass Spectrometry (PTR-ToF-MS), the Time-of-Flight (ToF) component facilitates the analysis of an entire mass spectrum within a fraction of a second, achieving a mass resolution of roughly 5000 m/Δm (full width at half maximum).

Quantitative analysis is achievable through known proton transfer reaction rate constants combined with accurate control of drift tube conditions (pressure, temperature, E/N). Although PTR-ToF-MS allows for absolute quantification without external standards, empirical calibration using certified gas mixtures is routinely applied to enhance accuracy and correct for instrumental transmission efficiencies.

5 Product studies of the OH radicals with cyclohexane oxide

Abstract

The chemical pathway of atmospheric epoxides degradation is dependent upon the specific site of hydrogen abstraction. As elucidated in the preceding chapters and supported by theoretical and empirical evidence related to the epoxides under investigation, it is expected that the β-position predominates as the favored abstraction channel. This assertion holds true for epoxydiols as well. In their research, Bates et al. (2014) identified that cis-β- and trans-β-epoxydiols collectively represent over 97% of the epoxydiols detected from the reaction of isoprene with OH radicals. Furthermore, Paulot et al. (2009) documented an extraordinarily high epoxide yield (75%) in their study, which involved the irradiation of isoprene under NOx conditions analogous to those prevalent in tropical regions.

An additional significant revelation of this research was that the identical mechanisms responsible for generating epoxide concurrently regenerate OH radicals. This phenomenon is of paramount importance in the domain of atmospheric chemistry research, as traditional paradigms have posited that radical-radical reactions yielding organic peroxides were entirely chain-terminating (Kleindienst et al., 2009).

The principal aim of this section is to investigate these possibilities by considering the products acquired. The selection of epoxides for this study is justified by their direct association with anthropogenic activities and their extensive presence in the atmosphere.

Initial investigations on cyclohexane oxide were conducted in the 480 L indoor simulation chamber located in Wuppertal, Germany, to identify the predominant reaction products. A comprehensive product analysis concerning the OH- initiated oxidation of cyclohexene oxide was subsequently undertaken within the indoor simulation chamber-7.3 m^3 situated in ICARE, France. Product formation studies were conducted in the chamber in ICARE using PTR-TOF-MS.

5.1 Introduction

The primary objective of the research delineated in this chapter was to qualitatively ascertain the products resulting from the gas-phase oxidation of epoxides, specifically focusing on cyclohexane oxide, initiated by OH radicals. As stated in previous investigations concerning ethylene oxide and propylene oxide, it is anticipated that the alkoxy radicals generated after the hydrogen abstraction will facilitate the ring-opening through C-C bond cleavage, thereby leading to the formation of peroxy radicals. These peroxy radicals are expected to engage in additional reactions, yielding products such as acetic formic anhydride, acetic acid, and formic acid (Chen et al., 1995; Middala et al., 2011).

The oxidation products of isoprene-derived epoxides through reactions with OH radicals have been examined under both high and low nitric oxide concentration conditions (Bates et al., 2014; Jacobs et al., 2013). Middala et al. (2011) investigated the mechanistic pathways governing the reaction of propylene oxide with hydroxyl (OH) radicals and nitrogen monoxide (NO) utilizing a 142-L reaction chamber in conjunction with long-path Fourier transform infrared spectroscopy at atmospheric pressure and a temperature of 298 K. The resultant products observed are congruent with hydrogen abstraction, succeeded by the addition of oxygen to yield a peroxy radical. The subsequent transformation of the peroxy radicals leads to the generation of an alkoxy radical, which preferentially undergoes ring-opening via cleavage of the carbon-carbon (C-C) bond. This finding aligns with the results reported by Chen et al. (1995).

In the context of propylene oxide, hydrogen abstraction can occur from any of the three distinct atoms within the molecular structure, resulting in the formation of three diverse peroxy radicals. The generated peroxy radicals exhibit a tendency to react with NO (when present) to produce alkoxy radicals. Consequently, the chemical fate of the epoxides is contingent upon the specific site of hydrogen atom abstraction. Based on the observed product yields and measured rate coefficients from the reaction of propylene oxide with OH radicals, it can be inferred that hydrogen atom abstraction predominantly occurs at the β-position (Middala et al., 2011).This conclusion is consistent with the findings documented in our work (Tovar et al., 2021, 2022).

The alkoxy radical produced through abstraction at the β-position can interact with oxygen, leading to the formation of an aldehyde while maintaining the integrity of the ring structure. Alternatively, the alkoxy radical produced could decompose, yielding formaldehyde and the initial peroxy radical formed at the commencement of the reaction. This branching ratio was not quantified by Middala et al. (2011) due to the unavailability of a standard for the anticipated product. Furthermore, ACUCHEM simulations suggested that approximately 80% of the aldehyde generated would subsequently react with OH under the employed reaction conditions.

5.2 Experimental and Material

In experiments conducted within the chambers at Wuppertal University, the quantification of identified products is generally performed by subtracting calibrated reference FTIR spectra. However, due to the limitations in product identification when utilizing only the 480 L chamber at Wuppertal, the present study will focus exclusively on the qualitative analysis of the reaction products of cyclohexene oxide with OH radicals. Through complementary studies conducted in the chambers at ICARE Orléans, France, several compounds were identified and confirmed, allowing for the proposal of a tentative reaction mechanism. Furthermore, the cross-sections of all epoxides were determined in the chambers at Wuppertal University to support future research studies. The absorption cross sections of *trans*-2,3-epoxybutane, *cis*-2,3-epoxybutane, 1,2-epoxybutane, 1,2-epoxyhexane and cyclohexane oxide were determined by injecting different volumes of the pure compounds into the chambers.

All experiments for product elucidation in Wuppertal university, were conducted in a 480 L reaction chamber at 298 ± 2 K and a total pressure of 760 ± 10 Torr of synthetic air (760 Torr = 101.325 kPa). Hydroxyl radicals were generated by the photolysis of the mixture CH_3ONO/NO/air at 360 nm.

Methyl nitrite was prepared through the gradual introduction of 50% sulfuric acid into a saturated solution of sodium nitrite dissolved in methanol, followed by purification via vacuum

distillation until a product with a purity of 99% was achieved, as verified by infrared spectroscopy.

As the design, configuration, and operation of the atmospheric simulation chambers have been comprehensively addressed in earlier chapters, they will not be reiterated in this section.

5.2.1 Indoor simulation chamber-480 L

The initial mixing ratios for the experiments conducted within the 480 L chamber are expressed in parts per million by volume (ppmV) (1 ppmV = 2.46×10^{13} molecules cm^{-3} at 298 K) and are as follows: 6.6–7.2 for cyclohexane oxide and 23 for methyl nitrite.

The target compound and the reaction products, investigated for mechanistic insights, were monitored using FTIR spectroscopy. Typically, 50–70 interferograms were co-added per spectrum, with 15–20 spectra recorded per experiment. During each experiment, the first five spectra were collected in the absence of light over a period of 10–20 minutes to assess potential wall loss of the epoxides. Subsequently, the reaction was initiated by activating the lamps. In product study experiments, the reaction was terminated after a maximum of 10 spectra had been recorded. No changes in reactant concentration or formation of new products were detected during this dark aging period.

5.2.2 Indoor simulation chamber-7.3 m^3 (CSA)

The experimental investigation concerning the products resulting from the reaction between cyclohexane oxide with hydroxyl radicals was conducted within a 7.3 m^3 chamber (ICARE, France) constructed from Teflon foil and maintained under ambient temperature and a pressure of 760 Torr of purified air (relative humidity <2%).

Known volumes of liquid compounds, such as epoxides under study, are introduced into a tri-path glass tube, while calibrated concentrations of gaseous species, including SF_6, are introduced into a calibrated cylinder with a volume of 0.9 L, which is outfitted with two pressure gauges calibrated to 0–10 Torr and 0–100 Torr (MKS Baratron). The contents of the cylinder are subsequently transported into the chamber via a stream of purified air. The concentrations

of reactants within the chamber are determined utilizing the ideal gas law. In the CSA, the generation of hydroxyl (OH) radicals is primarily achieved by introducing methyl nitrite (CH_3ONO) and subsequently photolyzing it is using a 365 nm wavelength light source. Following the incorporation of all reactants and SF_6, the initiation of the reaction is accomplished through the introduction of the precursor oxidant.

Chemical analyses were executed utilizing an online Proton Transfer Reaction - Time of Flight - Mass Spectrometer (PTR-ToF-MS, IONICON 8000). The analysis of the PTR-ToF-MS spectra was carried out using the PTR-ToF Data Analyzer (Müller et al., 2013).

5.2.3 Chemicals

The reagents utilized, along with their reported purities, were as follows: cyclohexane oxide (Sigma-Aldrich, 98%), sulfur hexafluoride (SF_6) (Mitry-Mory, 99.95%), purified air (Alphagaz, ≥99.9999%), and oxygen (O_2) (Alphagaz, 99.9999%), synthetic air (Messer, 99.9999%), and nitrogen (Messer, 99.9999%). For the synthesis of CH_3ONO, the following gases and chemicals were employed: nitrogen (N_2) (Alphagaz, ≥99.9999%), sulfuric acid (H_2SO_4) (Normapur, >95%), sodium nitrite ($NaNO_2$) (Sigma-Aldrich, ≥97.0%), methanol (Carlo Erba, 95%), and phosphorus pentoxide (P_2O_5) (Fluka, >98%).

5.3 Results

Figure 20 presents detailed findings obtained from the analysis of infrared (IR) spectra recorded during an experiment involving the reaction between cyclohexane oxide and OH radicals in the indoor simulation chamber-480 L (Wuppertal). The references utilized for the identification of reaction products are also included. The infrared (IR) spectrum of cyclohexene oxide is also presented in Figure 32. For the sake of clarity, the spectral range of 2000–900 cm^{-1} was specifically selected. Additional spectra focusing on different spectral regions is available in Figure 21. The residual absorption features observed after subtracting the spectral contributions of cyclohexane oxide, methyl nitrite, methyl nitrate, HNO_3, HONO, formaldehyde (HCHO) and NO_2 can be unequivocally assigned to formic acid. Additionally, the formation of CO_2 was distinctly identified through the examination of its absorption characteristics in Figure 21. The yield of formic acid produced during the experiments conducted in a 480 L chamber at Wuppertal University was determined by plotting its mixing ratio against the mixing ratio of the consumed cyclohexene oxide. The resulting yield was calculated to be 31%, with the data adjusted solely to account for the wall loss of epoxide. These plots are shown in Figure 30 and Figure 31 and exhibit a high linearity for formic acid. The non-linearity is a strong indication for further oxidation and secondary processes in the investigated reaction systems.

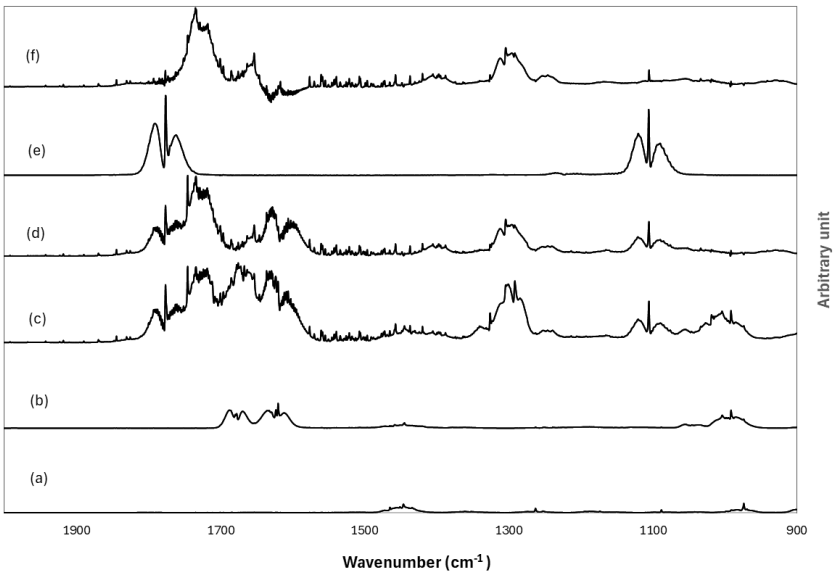

Figure 20 - Representative FTIR spectra from a product study experiment involving the reaction of CHO with OH are presented as follows: (a) the reference spectrum of CHO (b) the reaction mixture prior to irradiation, (c) the reaction mixture at the conclusion of the irradiation period, (d) the residual spectrum obtained after subtracting methyl nitrite, methyl nitrate, HNO_3 HONO and NO_2 from the reference spectrum (e) the reference spectrum of formic acid (f) the residual spectrum obtained after subtracting formaldehyde, CO and formic acid from (d). For clarity, the spectra have been individually shifted and scaled.

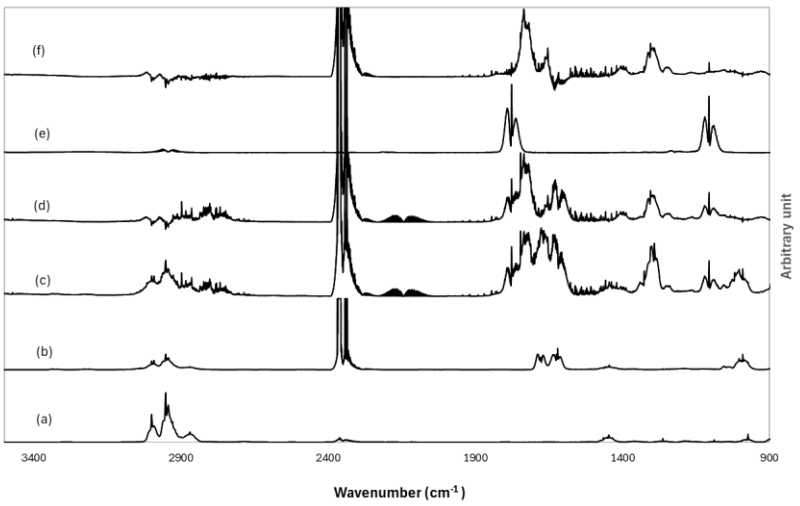

Figure 21 - Spectral data obtained in the frequency region 900-3400 cm^{-1} obtained from the reaction of CHO with OH are presented as follows: (a) the reference spectrum of CHO (b) the reaction mixture prior to irradiation, (c) the reaction mixture at the conclusion of the irradiation period, (d) the residual spectrum obtained after subtracting methyl nitrite, methyl nitrate, HNO_3 HONO and NO_2 from the reference spectrum (e) the reference spectrum of formic acid (f) the residual spectrum obtained after subtracting formaldehyde, CO and formic acid from (d). For clarity, the spectra have been individually shifted and scaled.

After removing all clearly identified spectral features, the remaining spectrum exhibits strong absorption bands centered at 1734 cm^{-1}, 1717 cm^{-1}, 1652 cm^{-1}, 1664 cm^{-1},1404 cm^{-1}, 1311 cm^{-1},1304 cm^{-1}, 1291 cm^{-1}, 1245 cm^{-1}, 1104 cm^{-1}, 854 cm^{-1}, 793 cm^{-1}, 734 $cm^{-1}$and 720 cm^{-1} (Figure 22).

As discussed in the following paragraphs, certain infrared (IR) bands may suggest the presence of ring-retaining compounds, which exhibit characteristic absorption bands associated with the vibrational modes of their functional groups, particularly the epoxide (-C-O-C-) and the carbonyl (C=O) group.

The absorption band at 1734 cm^{-1} is indicative of the stretching vibrations of the carbonyl (C=O) group in aldehydes, which are typically observed within the range of 1740–1720 cm^{-1}. The C=O stretching band at 1664 cm^{-1} and the C=C stretching band at 1652 cm^{-1} are characteristic of α, β-unsaturated ketones (Figure 22). This conjugation effect delocalizes electron density, stabilizing the carbonyl and shifting its absorption to lower wavenumbers. Besides, band around 734 cm^{-1} is characteristic of C-H out-of-plane bending vibrations in cyclohexene or disubstituted alkene rings.

A band at 1404 cm^{-1} suggests O-H bending, which is mostly observed in carboxylic acids, phenols, or alcohols. Conversely, the spectral band observed at approximately 1104 cm^{-1} is indicative of C-O stretching vibrations commonly associated with secondary alcohols. Also, the bands around 1252 cm^{-1} and 1245 cm^{-1} correspond to strong C-O stretching in esters or alcohols. This may serve as a dual validation regarding the existence of an alcohol within one of the reaction products, at least in a preliminary context.

A key distinguishing feature of epoxy compound are the epoxide (-C-O-C-) stretching vibrations. The absorption pattern of the bands 1311 cm^{-1}, 1304 cm^{-1}, and 1291 cm^{-1} are associated with C-O stretching in cyclic ethers, epoxides, or esters. Another evidence of the epoxide compound is the band centred on 793 cm^{-1} which is commonly attributed to epoxide ring deformation or C-H out-of-plane bending in substituted cyclohexane or cyclohexene

rings. The spectral characteristic identified at 720 cm^{-1} is acknowledged as a vibrational mode of the CH_2 rocking motion, which pertains to long-chain hydrocarbons, cyclic alkanes, and CH_2 units existing in cyclohexane derivatives (Figure 22).

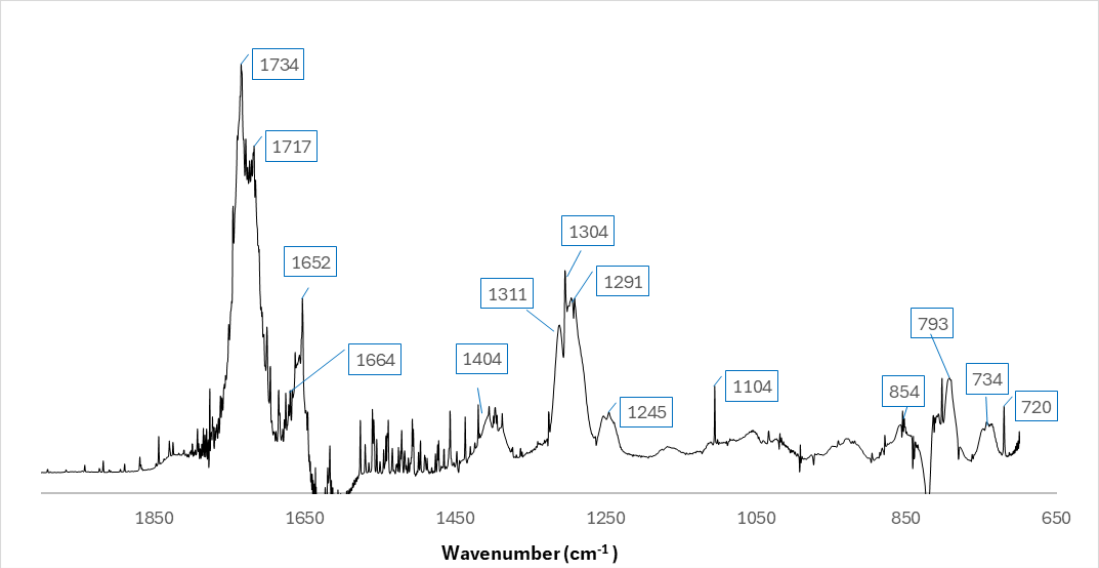

Figure 22 - IR residual spectra of the products of the reaction of CHO with OH after removing all clearly identified spectral features in 760 ± 10 Torr of synthetic air.

To validate the potential chemical structures corresponding to these absorption bands, as identified in studies conducted within the Wuppertal chamber, an experiment was conducted in the 7.3 m^3 (CSA) facility in Orléans, France. The results of this experiment are illustrated in Figure 23. The identification and characterization of reaction products were carried out using proton transfer reaction time-of-flight mass spectrometry (PTR-ToF-MS) as the analytical technique.

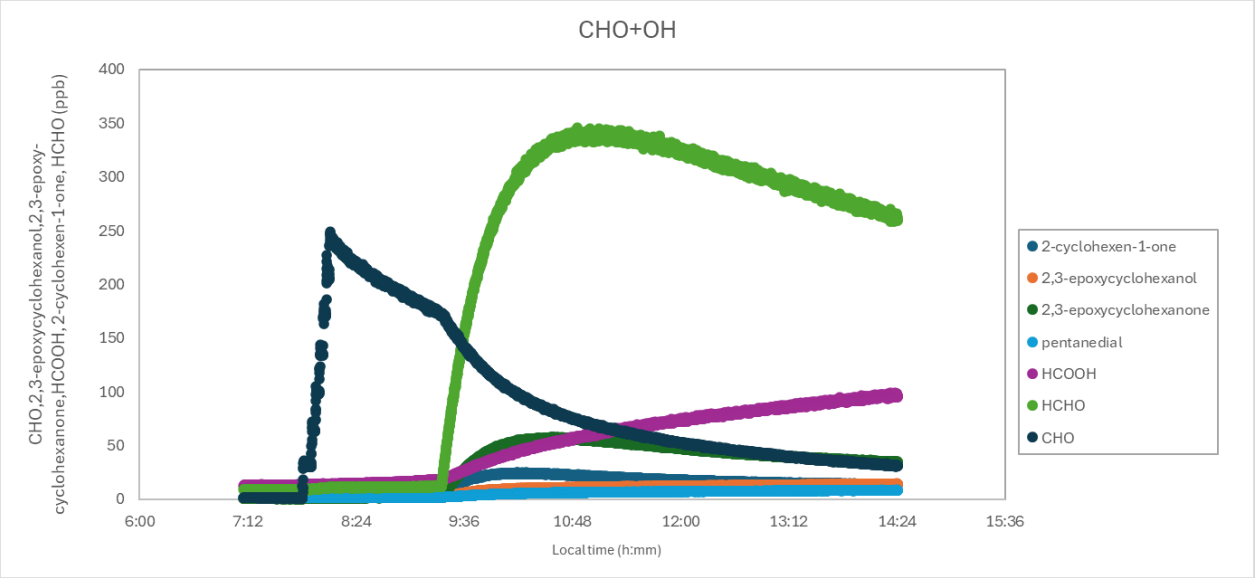

Figure 23 – Concentration-reaction time profiles of CHO and the products formed during the investigation of CHO reaction with OH radical.

The most prevalent products detected by PTR-ToF-MS (Figure 23) appeared at *m/z*, 31, 47,97, 99, 101, 113 and 115.

5.3.1 Products formation from cyclohexane oxide + OH radicals

The comprehensive examination of the infrared (IR) spectral bands in conjunction with the PTR-TOF mass fragmentation data robustly indicates the formation of the following compounds: 2,3-epoxycyclohexanone, 2,3-epoxycyclohexanol, 2-cyclohexen-1-one, pentanedial (glutaraldehyde), formic acid and formaldehyde (Figure 23). The identification of fragments at *m/z* 31 and *m/z* 47 serves to further validate the presence of formaldehyde and formic acid, respectively.

In the case of 2,3-epoxycyclohexanone, infrared (IR) spectroscopic analysis demonstrates prominent carbonyl stretching vibrations at 1734 and 1717 cm^{-1}, accompanied by characteristic C–O stretching bands at 1245 and 1104 cm^{-1}. Complementarily, mass spectrometric analysis employing proton transfer reaction time-of-flight (PTR-TOF) spectrometry reveals fragment ions at *m/z* 101 and 113. These ions are diagnostic of cyclic ketone structures incorporating epoxide functionalities.

Accordingly, protonated 2,3-epoxycyclohexanone ($C_6H_8O_2 \cdot H^+$) corresponds well to the m/z 113.05968. The prominent C=O absorption at 1734 cm^{-1} is characteristic of a non-conjugated ketone. Analysis of the IR bands confirms the presence of epoxy groups, which typically exhibit C–O–C stretching in the 1250–950 cm^{-1} range, as supported by the observed absorptions at 1245 cm^{-1} and 1104 cm^{-1}. Additionally, a notable epoxide ring deformation is observed at 803 cm^{-1} (Figure 22).

The m/z 115.07536 matches the protonated form of 2,3-epoxycyclohexanol ($C_6H_{10}O_2 \cdot H^+$). This indicates the presence of an additional hydroxyl group compared to the ketone. The broad O–H bending bands between 1400–1300 cm^{-1} and the strong C–O stretching bands at 1104 cm^{-1} support the existence of alcohol functionalities.

The protonated form of the compound 2-cyclohexen-1-one ($C_6H_8O \cdot H^+$) corresponds to the m/z 97.06480. This suggests a conjugated ketone structure. The C=O stretching band at 1664 cm^{-1} and the C=C stretching band at 1652 cm^{-1} are characteristic of α, β-unsaturated ketones. Such conjugation lowers the C=O stretching frequency compared to non-conjugated ketones.

Protonated pentanedial ($C_5H_8O_2 \cdot H^+$) is associated with the m/z 101.05968. This molecular ion aligns with the structural attributes of a dialdehyde. In Figure 22, the observed dual C=O stretching vibrations at 1734 cm^{-1} and 1717 cm^{-1} indicate the existence of two aldehyde moieties.

The oxidation of cyclohexane oxide in atmospheric and laboratory conditions involves complex radical-driven mechanisms. The presence of formic acid as the dominant product and 2,3-epoxycyclohexanone as the second most abundant product in both OH radical and Cl atom reactions provide insights into the reaction pathways (Figure 27).

5.3.1.1 Infrared absorption cross section

The integrated absorption cross sections σ have been ascertained in accordance with the Beer-Lambert law. This was accomplished by graphing the integrated absorption band within the spectral range υ1 to υ2 in relation to the concentration c. These findings are compiled in Table 9. To the best of the author's knowledge, there are no existing publications in the literature that

report infrared (IR) cross sections for trans-2,3-epoxybutane, cis-2,3-epoxybutane, 1,2-epoxybutane, 1,2-epoxyhexane, or cyclohexene oxide.

Table 9 - Integrated absorption cross sections determined within this work (resolution: 1 cm^{-1})

Compound	***Wavelengths [cm^{-1}]***	***σ_{10} [$ppmV^{-1}{\cdot}m^{-1}$]***
t-EB	3063.900-2778.000	$(6.96\pm0.12)\times10^{-4}$
	1546.655-1359.108	$(1.25\pm0.07)\times10^{-4}$
	1550.512-1360.073	$(1.19\pm0.06)\times10^{-4}$
	1530.745-1306.557	$(1.97\pm0.11)\times10^{-4}$
	1358.626-1305.593	$(1.13\pm0.06)\times10^{-4}$
	1207.721-1066.459	$(1.08\pm0.06)\times10^{-4}$
	1063.084-931.946	$(1.18\pm0.08)\times10^{-4}$
	935.803-855.289	$(9.14\pm0.05)\times10^{-5}$
	852.396-773.327	$(8.00\pm0.05)\times10^{-5}$
c-EB	3078.364-2814.160	$(3.53\pm0.20)\times10^{-4}$
	1565.940-1322.949	$(1.15\pm0.06)\times10^{-4}$
	1537.495-1327.770	$(1.05\pm0.06)\times10^{-4}$
	1547.619-1312.825	$(1.97\pm0.11)\times10^{-4}$
	1542.316-1317.646	$(1.44\pm0.01)\times10^{-5}$
	1321.594-1233.274	$(2.69\pm0.02)\times10^{-5}$
	1225.078-1049.103	$(8.27\pm0.05)\times10^{-5}$
	1041.389-929.536	$(7.32\pm0.04)\times10^{-5}$
	1047.656-928.571	$(9.57\pm0.05)\times10^{-5}$
	927.607-820.094	$(7.30\pm0.04)\times10^{-5}$
	822.504-702.937	$(1.20\pm0.07)\times10^{-4}$
12-EB	3110.184-2811.267	$(2.06\pm0.12)\times10^{-4}$
	3101.506-2803.553	$(4.42\pm0.26)\times10^{-4}$
	984.016-698.116	$(1.40\pm0.08)\times10^{-4}$
	871.681-781.523	$(1.46\pm0.08)\times10^{-4}$
EHX	3085.114-3024.366	$(1.84\pm0.08)\times10^{-4}$
	3099.095-2808.856	$(5.72\pm0.26)\times10^{-4}$
	3086.560-2780.893	$(5.64\pm0.25)\times10^{-4}$
	3092.827-2769.804	$(2.55\pm0.12)\times10^{-4}$
	894.341-792.130	$(1.23\pm0.06)\times10^{-4}$
CHO	3047.990-2828.623	$(6.59\pm0.23)\times10^{-4}$
	3040.758-2818.017	$(1.22\pm0.40)\times10^{-3}$
	3035.937-2822.356	$(9.03\pm0.30)\times10^{-4}$
	3038.347-2816.088	$(2.36\pm0.08)\times10^{-4}$
	1490.728-1394.786	$(9.49\pm0.03)\times10^{-5}$
	1504.228-1401.535	$(1.78\pm0.06)\times10^{-4}$
	1302.700-1223.149	$(8.07\pm0.02)\times10^{-5}$
	1015.354-941.107	$(1.95\pm0.06)\times10^{-4}$
	860.110-811.415	$(2.11\pm0.07)\times10^{-4}$
	810.933-720.294	$(2.79\pm0.09)\times10^{-4}$

5.4 Discussion

Both chlorine (Cl) atom and hydroxyl (OH) radical oxidation mechanisms contribute to the formation of key oxidation products, including 2,3-epoxycyclohexanone, 2,3-epoxycyclohexanol, 2-cyclohexen-1-one, pentanedial, formaldehyde, and formic acid. While oxidation mediated by Cl atoms is primarily relevant in marine and polluted atmospheric environments, the OH radical pathway represents a globally dominant oxidation process. These pathways will be further explored in the subsequent section, as all the aforementioned products have been observed during oxidation by both OH and Cl atoms. Notably, formic acid formation occurs independently of NOx species (e.g., methylnitrite), underscoring a significant mechanistic distinction.

The study by Orlando et al. (2000) provides critical insights into the atmospheric oxidation mechanisms of cyclohexane derivatives, with a particular focus on the reactivity of the cyclohexoxy radical. Their findings offer a comprehensive understanding of the pathways leading to formic acid formation. The results obtained in this study are in strong agreement with previous observations and offer a more detailed elucidation of the proposed mechanism.

5.5 Atmospheric implications

The predominance of formic acid, followed by 2,3-epoxycyclohexanone, in the oxidation of cyclohexane oxide by OH radicals reveal key mechanistic insights. This observation has significant environmental implications, as the formation of formic acid, a major atmospheric organic acid, contributes to acid rain formation and influences aerosol chemistry through its partitioning into atmospheric particles. Additionally, the consistent formation of 2,3-epoxycyclohexanone suggests potential pathways for secondary organic aerosol (SOA) formation via acid-catalyzed ring-opening reactions in the particulate phase. These findings are essential for atmospheric modeling, as they highlight the need to incorporate oxidative fragmentation pathways and epoxide formation mechanisms into models predicting air quality, climate interactions, and radical cycling in the atmosphere.

5.6 Conclusion and future work

The oxidation of epoxides by OH radicals result in significant amounts of ring-retaining compounds alongside fragmentation products. This suggests that both mechanistic pathways ring opening and ring retention are competitive under atmospheric conditions. The presence of both pathways indicates the involvement of multiple reaction mechanisms, with their relative contributions influenced by various factors.

For instance, if hydrogen abstraction occurs at significant rates, ring-retaining pathways can compete with fragmentation. In this case, H-abstraction preserves the ring structure by forming peroxy radicals (RO_2), which can undergo further oxidation to yield ring-retaining products. The fate of these peroxy radicals depends on their reaction environment:

RO_2 + HO_2 → Hydroperoxides (ROOH): This pathway often favors the formation of ring-retaining compounds.

RO_2 + NO → Alkoxy Radicals (RO): These radicals can either undergo fragmentation via C–C bond scission or experience intramolecular rearrangement that preserves the ring structure.

If the alkoxy radical exhibits sufficient internal stabilization, ring-retaining pathways may outcompete fragmentation. Under high-NO_x conditions, as described in the experiments in this chapter, alkoxy radicals may undergo isomerization prior to fragmentation, allowing ring-retaining pathways to persist even in NO-rich environments. Finally, if multiple fragmentation pathways are available, each with distinct energy requirements, the less energetic ring-retaining pathways may still contribute significantly to the overall reaction.

The following chapter will provide a detailed description of these potential pathways.

6 Product studies of the chlorine atoms with cyclohexane oxide

Abstract

To elucidate the chemical mechanisms governing the atmospheric degradation of epoxides, comprehensive data concerning the identity and yield of reaction products is imperative. This investigation presents qualitative insights derived from laboratory experiments examining the interactions between a series of epoxides and chlorine atoms under conditions that simulate the atmosphere, employing diverse reaction chambers and a range of analytical methodologies.

Up to the present, there has been a scarcity of investigations on product formation resulting from the gas-phase reactions of chlorine atoms with epoxides under ambient conditions in the present literature. Bartels, Hoyermann, and Lange (1989) documented the interaction of chlorine atoms with ethylene oxide at ambient temperature and reduced pressure, utilizing the discharge flow-mass spectrometric technique at 298 K in a 1 Torr diluent of helium.

The findings of this study contribute to bridging the existing knowledge gap regarding the atmospheric fate of epoxides in the presence of chlorine atoms. By expanding the understanding of product formation and reaction pathways under ambient conditions, these results hold significance for refining atmospheric chemical models and assessing the impact of epoxide degradation on air quality and climate dynamics. Further research involving a broader range of epoxides, as well as investigations into secondary reactions and their environmental implications, is essential for developing a comprehensive perspective on their atmospheric transformation processes.

6.1 Introduction

Few investigations have addressed the gas-phase oxidation of epoxides by chlorine atoms. The interaction between chlorine atoms and ethylene oxide was examined under ambient temperature conditions using the discharge flow-mass spectrometric technique, with experiments conducted at 298 K and a helium diluent pressure of 1 Torr (Bartels et al., 1989). This work determined that chlorine atoms are capable of engaging ethylene oxide through mechanisms of abstraction, addition, and substitution. Nonetheless, this investigation yielded evidence exclusively for the abstraction and addition pathways. The identification of bioxirane as a reaction product suggests that the ring structure of the primary radical is preserved to some extent. The elucidation of the reaction mechanism of ethylene oxide in the presence of chlorine atoms was incomplete due to the absence of data regarding the branching ratios of abstraction versus addition and decomposition versus substitution. Subsequently, a Fourier Transform Infrared (FTIR) product analysis was performed to study the chlorine atom-initiated reactions of ethylene oxide at 297 K in an atmosphere of 700 Torr of nitrogen and nitrogen–oxygen mixtures (Chen et al., 1995).

In experiments conducted at 700 Torr of nitrogen, the sole primary product identified was monochloroethylene oxide, a ring-retaining product characterized by the formula C_2H_3ClO, while hydrochloric acid (HCl) and HC(O)Cl were recognized as byproducts, where spectral bands at 921 and 1312 cm^{-1} corresponded to the C-O-C ring deformation, and bands at 747 and 801 cm^{-1} were attributed to C-Cl stretching modes. In this analysis, approximately 97% of the carbon-containing products consisted of chlorinated ethylene oxides. The formation of these compounds was attributed to hydrogen atom abstraction by chlorine atoms. The resulting cyclic oxiranyl radical demonstrated a sufficiently long lifetime to react with Cl_2, consistent with predictions reported by Bartels et al. (1989).

However, Chen et al. (1995) did not report any products resulting from the addition of chlorine atoms followed by unimolecular dissociation. The addition pathway was characterized by the signal corresponding to the CH_2Cl radical, with supporting evidence for the isomerization of the oxiranyl radical to vinoxy (CH_2CHO) and acetyl (CH_3CO) radicals (Bartels et al., 1989).

These species were observed below the 0.5 yield detection limit, a discrepancy that Chen and co-workers (Chen et al., 1995) ascribed to the comparatively high Cl_2 pressures (0.5–2 Torr) used in their study versus the much lower concentrations (10^{-5}–10^{-4} Torr) investigated by Bartels et. al (1989).

In the reactions conducted in the presence of air, approximately 70% of the consumed ethylene oxide resulted in the production of acyclic compounds characterized by the presence of C-O-C bonds, while the remaining compounds consisted solely of a single carbon atom. This degradation of the three-membered ring structure of ethylene oxide stands in stark contrast to the findings observed under nitrogen conditions, where the ring structure remained predominantly unaltered. Furthermore, the current investigation did not yield any products that contained C-C bonds, thereby suggesting that under conditions of 700 Torr of air, the oxiranyl radical primarily engaged in reactions with O_2. The oxiranylperoxy radical undergoes a self-reaction process, predominantly yielding the formation of the oxiranyloxy radical.

The major products resulting from the ring-opening reactions identified in this investigation (such as formic anhydride) signify the cleavage of the C-C bond rather than that of the C-O bond within the oxiranyloxy radical.

More recently, the reaction mechanisms of cis-2,3-dimethyloxirane, trans-2,3-dimethyloxirane, and ethyloxirane with chlorine atoms were elucidated under conditions of 10 Torr pressure and elevated temperatures of 650 K and 800 K (Christianson et al., 2021; Doner et al., 2021).

6.2 Experimental and Material

To elucidate the reaction products formed from the oxidative degradation of cyclohexane oxide under atmospheric conditions, two complementary experimental systems and analytical techniques were employed. In an initial set of experiments, the 480 L indoor simulation chamber at Wuppertal University was utilized to preliminarily assess the primary products of the gas-phase Cl reaction with cyclohexane oxide. After subtracting the contributions of CHO and chlorine-related species (e.g., HCl), CO_2 formation was detected via absorption features in the 2400–2250 cm^{-1} range (Figure 24). Although this analysis provided some indications regarding the functional groups present in the mixture, definitive product identification was hindered by the complexity of the product distribution and overlapping IR bands.

A subsequent series of experiments was then conducted in the HELIOS chamber in Orléans, France, aimed at qualitatively evaluating the products from the Cl oxidation of cyclohexane oxide. This dual approach allowed a robust structural interpretation of the oxidation products, facilitated by the integration of Fourier-transform infrared spectroscopy (FTIR) and proton-transfer-reaction time-of-flight mass spectrometry (PTR-TOF-MS).

Although experiments were conducted in different laboratories under varying conditions, the comparability of core findings enabled a qualitative cross-validation of product identity and mechanistic consistency.

Despite differences in precursor chemistry (Cl_2 vs. $(COCl)_2$), both systems promoted Cl-initiated oxidation, allowing for the assessment of convergent product formation under varied but atmospherically relevant conditions. FTIR and PTR-TOF-MS provide orthogonal but complementary information. FTIR enables detection of functional group signatures (e.g., carbonyls, alcohols, epoxides, halogenated species) through their characteristic vibrational bands. Particularly, bands around 1735 and 1781 cm^{-1} were used to identify carbonyl functionalities resulting from epoxide ring-opening and further oxidation. In contrast, PTR-TOF-MS offers molecular-level detection of trace volatile compounds, including low-

molecular-weight oxygenates such as formic acid, through precise m/z measurements and fragmentation profiles.

The consistency of product detection across both analytical platforms, including both cyclic epoxides and non-cyclic oxidation products, notably formic acid, strongly supports the robustness of the proposed reaction pathways. The formation of formic acid in both systems despite different radical sources indicates the presence of shared secondary oxidation mechanisms, likely involving ring opening followed by C–C bond scission and hydroxylation.

Since the atmospheric simulation chambers have been thoroughly described in previous chapters, a detailed description will not be provided in the following section.

6.2.1 Indoor simulation chamber-480 L

Gas-phase experiments were carried out in a horizontal borosilicate glass simulation chamber with a total volume of 480 L, designed as a cylindrical reactor measuring 3.0 meters in length and 0.45 meters in inner diameter. FTIR spectra were recorded using a spectrometer operating in the range of 4000–600 cm^{-1} with a resolution of 1 cm^{-1}.

The reactor was used to study the photooxidation of cyclohexane oxide initiated by chlorine atoms, which were generated in situ by photolysis of molecular chlorine (Cl_2) under UV irradiation. The formation of gas-phase products was monitored over time, with particular attention to the emergence of absorption bands in the carbonyl stretching region (1735 and 1781 cm^{-1}). These bands were assigned to aldehydes, ketones, or carboxylic acids formed through epoxide ring opening and subsequent oxidation. Broader and less resolved absorption features observed between 805 and 1450 cm^{-1} were attributed to overlapping vibrational modes such as C–O stretching, CH_2 wagging, and C–Cl bending, consistent with the formation of multiple oxygenated and halogenated secondary products.

The initial mixing ratios, expressed in ppmV (with 1 ppmV corresponding to 2.46×10^{13} molecules cm^{-3} at 298 K), were as follows: 6.6 for cyclohexane oxide and for 42 for chlorine, respectively.

6.2.2 Outdoor simulation chamber (HELIOS) -90 m^3 (ICARE-ORLEANS)

Experiments were conducted using the large-scale simulation chamber, HELIOS at CNRS-Orléans. The HELIOS chamber has been described in detail in chapter 2.1.4 of this work. Briefly, the facility comprises a 90 m^3 hemispherical outdoor simulation chamber fabricated from FEP Teflon film. Two fans within the chamber ensured rapid homogenization of reactants, achieving complete mixing within 90 seconds. Purified air was provided by a dedicated air generation system (AADCO Instruments, Inc., 737 series). Pressure, relative humidity, and temperature were continuously monitored using a three-axis ultrasonic anemometer (Delta Ohm, HD 2003) centrally positioned in the chamber. Additionally, six spatially distributed PT-100 thermocouples continuously measured the temperature distribution, with variations maintained within ±1 K. The chamber is protected against adverse weather conditions, such as rain and strong winds, by mobile protective housing.

This housing can be automatically retracted within 30 seconds to allow full exposure to sunlight when necessary. The organic compounds were systematically evaluated using PTR-ToF-MS (Proton Transfer Reaction - Time of Flight Mass Spectrometer, IONICON 8000). The spectra generated by the PTR-ToF-MS were examined utilizing the PTR-ToF Data Analyzer (Müller et al., 2013). Oxalyl chloride, $(ClCO)_2$, has been used as a photolytic Cl atoms precursor for product studies.

Oxalyl chloride $(ClCO)_2$ is widely used as a source of photolytically generated Cl atoms in kinetic and photochemical experiments. Initially, an excited ClCO* radical is produced, and then depending on the photolysis wavelength, a portion of this ClCO* rapidly decomposes into Cl and CO. This mechanism can be summarized as follows:

$$(ClCO)_2 + h\nu \rightarrow ClCO^* + CO + Cl$$

$$ClCO^* \rightarrow Cl + CO$$

The PTR-ToF-MS method typically detected the key compounds at concentrations as low as 0.1–0.2 ppb. Known amounts of cyclohexane oxide (CHO) were introduced into the chamber by placing measured liquid volumes into a bubbler and flushing them with purified air. Their

concentrations were calculated using the ideal gas law based on the introduced volume, pressure, and temperature. Gaseous reactants like SF_6 were added using a calibrated gas cylinder equipped with capacitance manometers. To counteract sampling flows and potential leaks, a continuous low flow of purified air (15–25 L/min) was maintained during experiments, keeping the chamber slightly overpressurized and preventing outside contamination. Between experiments, the chamber was thoroughly cleaned by flushing it with pure air at 800 L/min for at least 12 hours. Regular checks confirmed that background levels in the chamber were below the detection limits of the analytical instruments (e.g., [NOx] < 1.3×10^{10}, [O_3] < 1.3×10^{10}, and [VOC] < 1.3×10^{8} molecules cm^{-3}). The initial mixing ratios in the HELIOS chamber experiments in ppb were: 137.1 for CHO and 181 for oxalyl chloride.

6.2.3 Chemicals

Cyclohexane oxide (Sigma-Aldrich, 98%), synthetic air synthetic air (Messer GmbH, 99.9999 %), and SF6 (Mitry-Mory, 99.95%).

6.3 Results

(IR) spectroscopy provides crucial insights into the structural features of the resulting compounds, particularly in identifying functional groups and elucidating reaction pathways. Figure 24 presents detailed findings obtained from the analysis of infrared (IR) spectra recorded during an experiment involving the reaction between cyclohexane oxide and Cl atoms in the indoor simulation chamber-480 L (Wuppertal). For the sake of clarity, the spectral range of 3200–700 cm^{-1} was specifically selected. Additionally, the formation of CO_2 was distinctly identified through the examination of its absorption characteristics in Figure 24. Different spectral regions are available in Figure 25.

One of the most critical indicators in this study is the identification of O–H stretching vibrations, which indicate the presence of hydroxyl functional groups. A prominent absorption band at 3602 cm^{-1} supports this observation, confirming the existence of hydroxyl-containing compounds typically associated with alcohol functional groups. A plausible compound corresponding to this finding is 2,3-epoxycyclohexanol. Notably, this compound has also been identified during the oxidation of cyclohexane oxide in the presence of OH radicals. The formation of 2,3-epoxycyclohexanol suggests the occurrence of a hydroxylation reaction, likely taking place alongside the preservation of the epoxide ring.

Besides, the presence of strong absorption bands at 1781 cm^{-1} and 1735 cm^{-1} corresponds to C=O stretching vibrations (Figure 25). The high-frequency C=O absorption at 1781 cm^{-1} suggests the formation of strained cyclic ketones, such as 2,3-epoxycyclohexanone. The strain within the cyclic structure elevates the C=O stretching frequency compared to typical open-chain ketones.

As shown in Figure 25, the absorption band at 1735 cm^{-1} is indicative of aldehydic carbonyl groups, consistent with the formation of glutaraldehyde. The concurrent appearance of these bands implies oxidative cleavage processes and ring strain-induced modifications, resulting in both ketonic and aldehydic functionalities.

C–H bending can be evidenced by absorption bands at 1450 cm^{-1}, 1324 cm^{-1}, and 1245 cm^{-1}, which are typical in saturated hydrocarbons such as cyclohexane derivatives. Additionally, these frequencies may also represent vibrations associated with the epoxide ring, underscoring the persistence of the oxirane functionality despite oxidative conditions. These bands provide evidence of epoxide ring stability and the presence of chlorinated derivatives maintaining the epoxide moiety.

Also, the bands observed at 1157 cm^{-1}, 1094 cm^{-1}, and 1037 cm^{-1} correspond to C–O stretching vibrations. These absorptions are consistent with the presence of alcohol and epoxide functionalities, supporting the identification of 2,3-epoxycyclohexanol and related derivatives. The observation of these bands highlights the coexistence of oxygen-containing functional groups resulting from partial oxidation and substitution reactions mediated by chlorine atoms.

Characteristic absorption bands at 995 cm^{-1} and 937 cm^{-1} correspond to epoxide ring deformation vibrations. These bands confirm the structural integrity of the epoxide ring in certain oxidation products, such as 2,3-epoxycyclohexanol and 2,3-epoxycyclohexanone. The retention of these features signifies that epoxide cleavage is not the only reaction pathway under the employed oxidative conditions.

An absorption band at 805 cm^{-1} is attributed to out-of-plane C–H bending vibrations, which are typically observed in substituted cyclohexane derivatives. The presence of this band suggests that substitution reactions have occurred on the cyclohexane ring, potentially involving chlorine atoms. This substitution could account for the formation of chlorinated epoxide derivatives, which are relevant in understanding the overall oxidation mechanism.

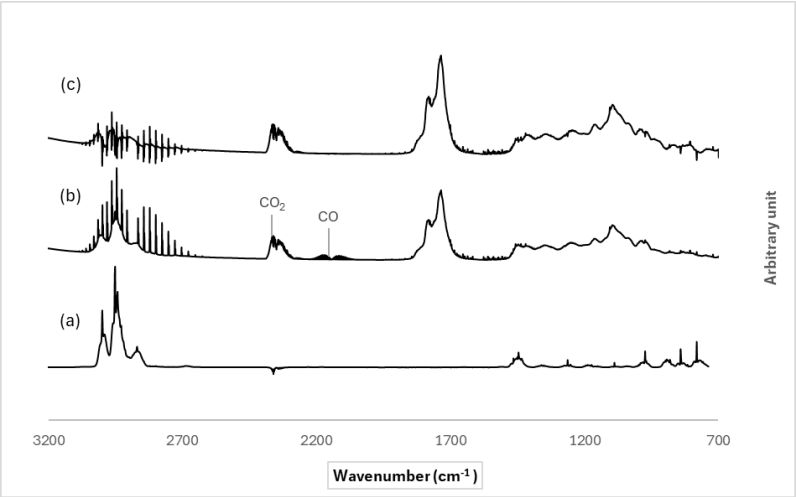

Figure 24 - Representative FTIR spectra from a product study experiment involving the reaction of CHO with OH are presented as follows: (a) the reaction mixture prior to irradiation, (b) the reaction mixture at the conclusion of the irradiation period, (c) the residual spectrum obtained after subtracting HCl *and* CO *from the reference. For clarity, the spectra have been individually shifted and scaled.*

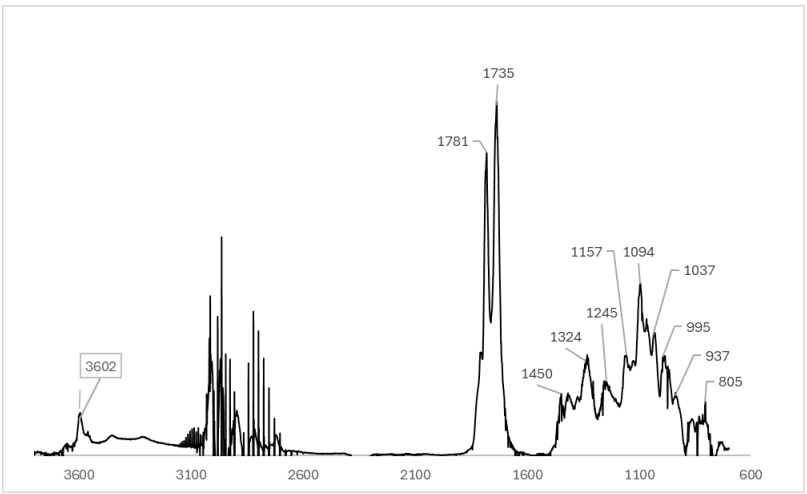

Figure 25 - IR residual spectra of the products of the reaction of CHO with Cl after removing all clearly identified spectral features in 760 ± 10 Torr of synthetic air.

To validate the potential chemical structures corresponding to these absorption bands, as identified in studies conducted within the Wuppertal chamber, an experiment was conducted in HELIOS chamber facility in Orléans, France. The results of this experiment are illustrated in Figure 26 . The identification and characterization of reaction products were carried out using proton transfer reaction time-of-flight mass spectrometry (PTR-ToF-MS) as the analytical technique.

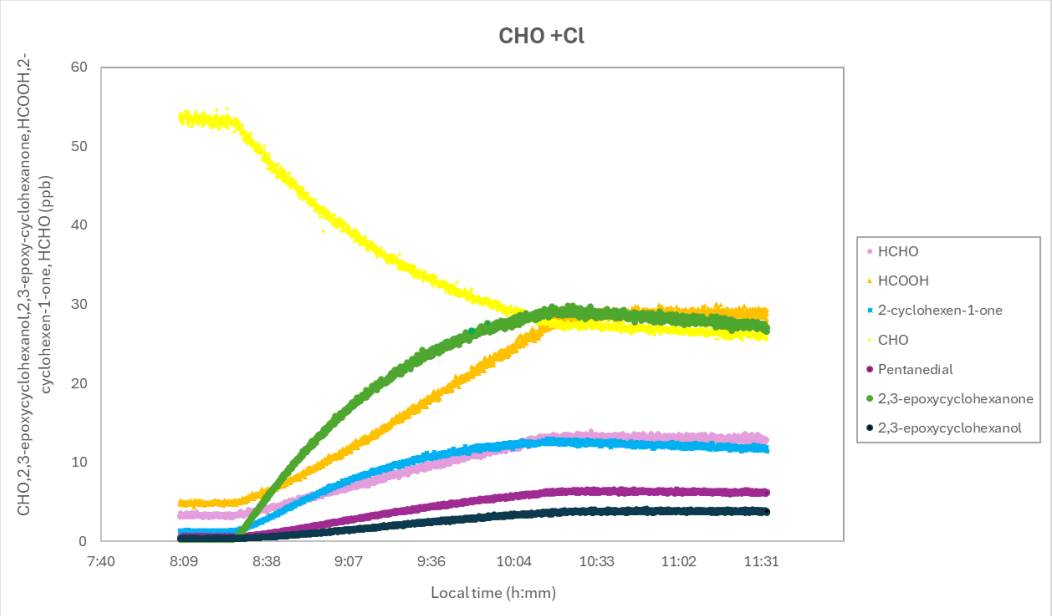

Figure 26 - Concentration-reaction time profiles of CHO and the products formed during the investigation of CHO reaction with Cl atom

6.3.1 Products formation from cyclohexane oxide + Cl atoms

The subsequent segment delineates a comprehensive analysis of specific *m/z* values, their potentially associated compounds, and the mechanistic basis confirming their identification.

The observed m/z value of 31.01784 corresponds to the protonated form of formaldehyde ($CH_2O{\cdot}H^+$) (Figure 26). This indicates the formation of formaldehyde during the oxidation process. The formation of formaldehyde indicates the partial oxidation of cyclohexane oxide by Cl atoms, potentially involving hydrogen abstraction and subsequent rearrangement.

The m/z value of 47.01276 matches protonated formic acid ($CH_2O_2{\cdot}H^+$). The detection of formic acid is significant, as shown in Figure 26 and indicates further oxidation beyond formaldehyde. A detailed mechanistic explanation of the formation of formic acid, involving peroxy radical intermediates is shown in Figure 27.

The mass spectral data show a peak at m/z 97.06480. According to the evaluation this could correspond to protonated 2-cyclohexen-1-one ($C_6H_8O{\cdot}H^+$). This suggests hydrogen abstraction at β-position of cyclohexane oxide and subsequent C-O cleavage, resulting in the formation of an α, β-unsaturated ketone. Such transformations are indicative of rearrangement and selective oxidation pathway (Figure 27).

The m/z value of 101.05968, aligns with protonated pentanedial ($C_5H_8O_2 \cdot H^+$). The presence of glutaraldehyde suggests ring-opening oxidation pathway, potentially involving the cleavage of six-membered cyclic structures as shown in Figure 27 . The formation of dialdehydes reflects advanced oxidation stages and may indicate selective cleavage at specific carbon-carbon bonds.

In the mechanism outlined in Figure 27, the m/z at 113.05968 can be attributed to protonated 2,3-epoxycyclohexanone ($C_6H_8O_2 \cdot H^+$), an epoxide-ketone derivative of cyclohexane oxide.

The formation of this compound, as depicted in Figure 27, involves the abstraction of hydrogen at position 1 by chlorine atoms, followed by the generation of a peroxy radical through the addition of molecular oxygen (O_2). The resulting peroxy radical (RO_2) then reacts with another RO_2 radical, forming an alkoxy radical. In the presence of O_2, this alkoxy radical undergoes further oxidation, yielding 2,3-epoxycyclohexanone along with the elimination of hydroperoxyl radicals (HO_2). This sequence of reactions highlights the intricate nature of oxidative rearrangement processes.

Furthermore, the HO_2 radicals produced can react with NO, O_3, or other radicals, thereby playing a crucial role in ozone formation and degradation.

Finally, the observed m/z value of 115.07536 ($C_6H_{10}O_2 \cdot H^+$), with two additional hydrogens relative to the ketone derivative, indicates an epoxide-alcohol structure, corresponding to 2,3-epoxycyclohexanol.

6.4 Discussion

The mechanism initiates with hydrogen abstraction by chlorine atoms at the 1, 2, or 3 positions (Figure 27). For abstractions at positions 2 and 3 (β and γ, respectively), the addition of O_2 leads to peroxy radical formation, which can undergo various transformations. Specifically, at position 3, reaction with NO yields an alkoxy radical, resulting in epoxy ring-containing compounds following C–C bond cleavage and subsequent O_2 addition. These compounds were detected by PTR-TOF-MS at m/z 129.055, albeit in minor quantities compared to other pathways. Consequently, they are not depicted in Figure 26.

At position 2, the alkoxy radical undergoes further oxidation, leading to the formation of protonated 2,3-epoxycyclohexanone with m/z 113.060. The reaction initiates with β-hydrogen abstraction from cyclohexane oxide, followed by the addition of O_2, resulting in the formation of a peroxy radical. This peroxy radical subsequently reacts with another radical species, such as RO_2 or NO, yielding an alkoxy radical at the β-position relative to the epoxide ring.

The alkoxy radical then reacts with O_2, leading to the elimination of HO_2. Alternatively, it can undergo a 1,2-hydrogen shift, wherein a hydrogen atom from the adjacent carbon migrates to the oxygen radical site. This hydrogen shift stabilizes the radical intermediate by converting the alkoxy radical into a carbonyl group (C=O) at the β-position. This transformation reduces the radical character on oxygen while simultaneously oxidizing the adjacent carbon, ultimately resulting in ketone (C=O) formation.

During this rearrangement, the epoxide ring within the cyclohexane structure remains intact due to the high activation barrier preventing epoxide ring opening under these radical conditions. This intramolecular rearrangement selectively facilitates the formation of 2,3-epoxycyclohexanone.

As depicted in Figure 26, the formation of 2,3-epoxycyclohexanone and 2,3-epoxycyclohexanol occurs via competing pathways originating from common radical intermediates, such as peroxy (RO_2) and alkoxy (RO) radicals. The divergence in product formation is influenced by the subsequent reactions of the alkoxy radical and the availability of radical species that facilitate

hydrogen transfer or rearrangement. Specifically, the peroxy radical may react to form a hydroperoxide (ROOH) instead of an RO radical, followed by hydrogen atom transfer, ultimately yielding 2,3-epoxycyclohexanol.

Under low NO_x conditions, the conversion of RO_2 to RO radicals proceeds more slowly, allowing sufficient time for the formation of organic hydroperoxides (ROOH). Additionally, the presence of ozone (O_3) in the reaction chamber can generate secondary radicals that facilitate hydrogen atom transfer, thereby favouring the pathway leading to alcohol formation. If ROOH intermediates accumulate, radical recombination processes may reduce them to alcohols rather than exclusively forming alkoxy radicals. Moreover, heterogeneous reactions on the chamber walls might provide surface-mediated pathways for hydrogen transfer.

The ion at m/z 97.06480 corresponds to protonated 2-cyclohexen-1-one. The formation mechanism involves preferential hydrogen abstraction at the β-position relative to the epoxide oxygen, generating a β-position radical intermediate. This radical exerts an electronic influence that weakens the adjacent C–O bond, leading to epoxide ring cleavage and the formation of an unsaturated radical intermediate with a double bond between the C2 and C3 carbons. The intermediate is stabilized by conjugation between the newly formed C=C bond and the radical center, reducing the activation energy required for subsequent oxidation steps.

The detection of formic acid indicates that ring-opening is a significant pathway for the unsaturated cyclohexoxy radical under the experimental conditions. This finding is crucial as it demonstrates a non-NO-mediated oxidation route, suggesting that chlorine radicals can efficiently facilitate C–C bond cleavage. The unsaturated cyclohexoxy radical is highly reactive and can undergo various transformations, including C–C bond scission and isomerization. Specifically, the alkoxy radical may experience C–C bond cleavage adjacent to the oxygen-bearing carbon, resulting in the formation of smaller aldehydic fragments, such as formaldehyde, and an unsaturated fragment.

The unsaturated fragment can undergo intramolecular hydrogen shifts or rearrangements to stabilize the radical center. This isomerization is facilitated by the conjugated C=C bond,

lowering the activation energy required for these transformations. The stabilized radical intermediate formed can subsequently react with O_2, continuing the oxidation process. The aldehydic fragment (formaldehyde) undergoes further oxidation through the formic acid formation. The formation of an alkoxy radical introduces additional pathways for C–C bond cleavage and rearrangement compared to direct peroxy radical decomposition. The isomerization steps are more feasible in the unsaturated radical scenario due to the lower energy requirements provided by conjugation.

An alternative pathway leading to the formation of formic acid and pentanedial, as illustrated in Figure 27, occurs when a radical initiator (e.g., Cl or OH) abstracts a hydrogen atom from the β-position of cyclohexane oxide. This abstraction results in the formation of a peroxy radical in the presence of O_2. The β-position peroxy radical can undergo multiple transformations, including reactions with molecular oxygen (HO_2), NO, or RO_2, leading to the formation of an alkoxy radical. This radical subsequently fragments, producing a C_6 radical that retains the epoxy ring.

In the presence of O_2, the C_6 radical leads to two primary fragments:

Fragment A: This fragment contains a terminal aldehyde group (–CHO) and a radical on an alkoxy group. It undergoes unimolecular decomposition via a 1,5-hydrogen shift from the aldehyde formyl hydrogen (–CHO) to the oxygen radical, forming a hydroxyalkyl radical. This 1,5-H shift is a crucial rearrangement step, converting the alkoxy radical into a hydroxyalkyl radical, which then undergoes β-scission. The reaction is driven by the thermodynamic stability of the resulting products, particularly the formation of CO and the stable dialdehyde, glutaraldehyde.

Fragment B: In this pathway, hydrogen abstraction results in the formation of an alkoxy radical while maintaining the integrity of the epoxy ring due to the selective site of hydrogen abstraction. Subsequently, the β-position alkoxy radical rapidly reacts with molecular oxygen (O_2), forming a peroxy radical (ROO). The epoxy ring remains intact during this step, likely because the reactive site is spatially distant from the ring structure. The peroxy radical then

undergoes C–C bond cleavage adjacent to the radical center. The resulting linear chain, containing an aldehyde group, further oxidizes into a peroxy radical through a self-arrangement process involving a cyclic transition state. This cyclic rearrangement facilitates molecular decomposition, ultimately yielding pentanedial and formic acid.

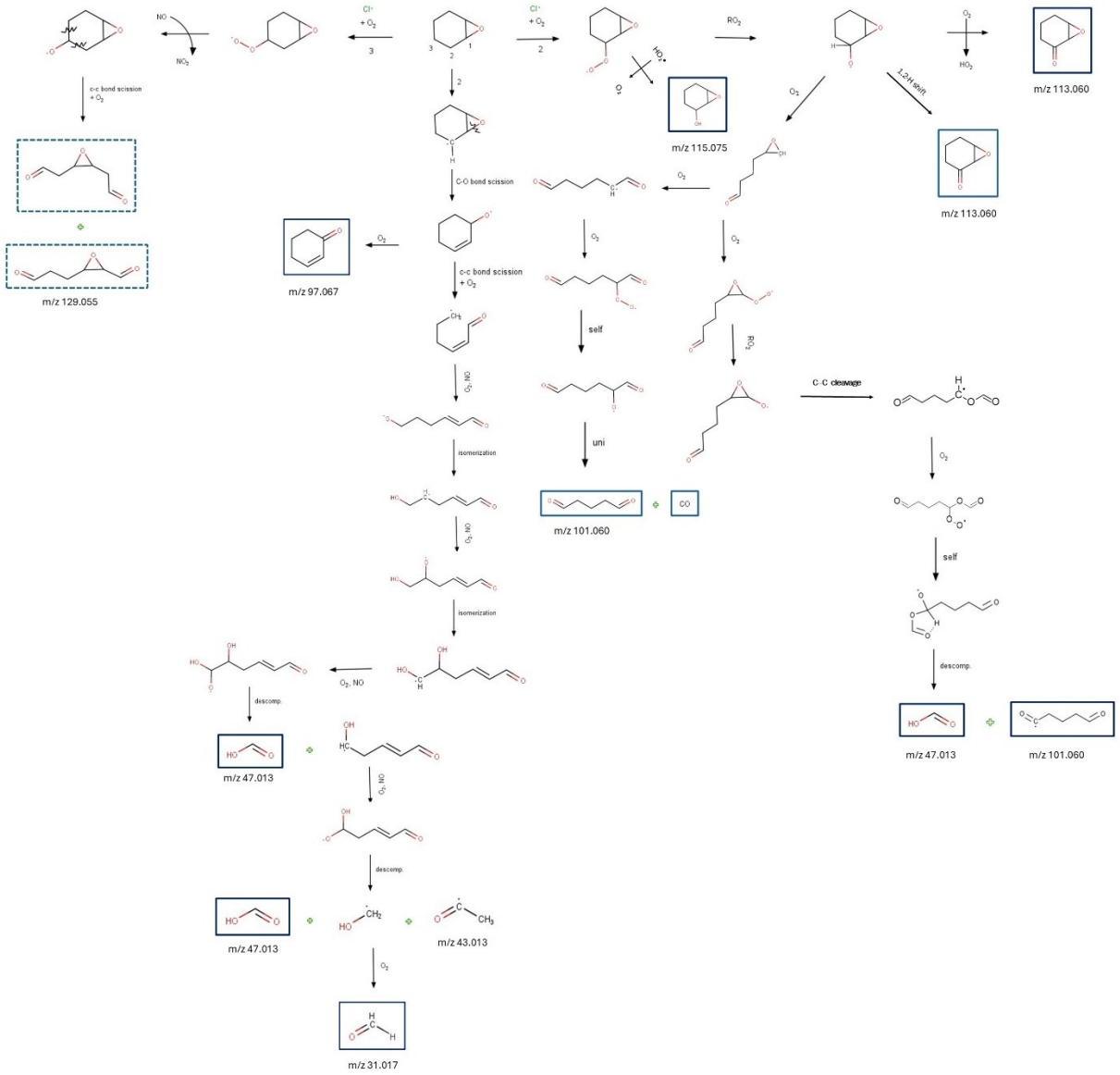

Figure 27 - Proposed mechanism for the Cl initiated oxidation of cyclohexane oxide. Proposed first generation products are outlined in blue boxes. Products observed but not in significant quantities are in dashed boxes.

6.5 Atmospheric implications

While 2,3-epoxycyclohexanone predominates due to its oxidative stability, the minor formation of 2,3-epoxycyclohexanol indicates that reductive pathways can compete, particularly under low-NO_x or VOC-rich conditions. Hydroperoxide intermediates may serve as key precursors to various atmospheric products, suggesting that even minor alcohol products could influence secondary organic aerosol (SOA) formation and atmospheric reactivity.

The generation of 2-cyclohexen-1-one via the β-position cleavage pathway implies that chlorine atoms significantly promote unsaturation during the oxidation of cyclic epoxides. Such unsaturated ketones enhance atmospheric reactivity, affecting photochemical smog formation and SOA generation.

6.6 Conclusion

Chlorine radicals are potent hydrogen abstractors, efficiently facilitating β-hydrogen abstraction. However, they do not significantly promote rapid formation of alkoxy radicals through reactions with NO. Consequently, chlorine-driven oxidation cycles often result in longer-lived peroxy radicals (RO_2), creating conditions conducive to the accumulation of hydroperoxides (ROOH). This environment favors partial reduction to alcohol and introduces competition with oxidation pathways leading to ketone formation.

In the formation of formic acid, the β-position pathway—entailing alkoxy radical formation and isomerization—is more feasible due to enhanced conjugation and a lower activation energy for C–C bond cleavage. In contrast, the α-position pathway lacks similar stabilization, rendering the β-position mechanism the preferred route under chlorine-rich atmospheric conditions.

7 Conclusions and Perspectives

The findings of this study provide novel insights into the behaviour of epoxides under oxidative conditions. The results indicate that the abstraction pathway is the predominant mechanism in both OH- and Cl-initiated oxidation of epoxides. Specifically, β-hydrogen abstraction adjacent to the epoxide ring serves as the primary step, generating a carbon-centered radical. This step is rate-determining and dictates the subsequent oxidation pathway, whether leading to ketones, alcohols, or further oxidation products.

The preference for β-H abstraction, extensively discussed in Chapters 2 and 3, underscores the unique reactivity of β-H bonds adjacent to the epoxide ring. The pseudo-ethylenic nature of the epoxide ring introduces subtle but crucial variations in reaction pathways, influencing competitive processes. The extended lifetime of radical intermediates, attributed to pseudo-π stabilization, allows alternative reaction routes to occur, explaining the minor formation of alcohols instead of ketones.

The minor formation of 2,3-epoxycyclohexanol is likely due to pseudo-π stabilization, which decelerates the 1,2-hydrogen shift, providing sufficient time for hydroperoxide formation and subsequent reduction to alcohol. This competition between reaction pathways, though subtle, is detectable and contributes to the minor product distribution. When the rearrangement process is slowed, radical intermediates have an increased probability of interacting with hydrogen donors, leading to the formation of alcohols (e.g., 2,3-epoxycyclohexanol) or undergoing alternative radical recombination and disproportionation reactions.

To further elucidate these reaction mechanisms, additional studies incorporating radical balance experiments are recommended. Investigations modifying NO_x/OH/O_3 ratios could provide further insight into how these variables influence product distribution.

Additionally, temperature-dependent studies are suggested to determine whether lower temperatures enhance alcohol formation by suppressing the 1,2-hydrogen shift. Small but significant presence of 2,3-epoxycyclohexanol highlights the delicate interplay of oxidation and

reduction in atmospheric radical chemistry, where kinetics, radical availability, and environmental factors dictate product distributions.

The concurrent formation of formic acid in both OH and Cl oxidation experiments indicates that its primary source is the oxidation of the organic compounds, rather than CH_3ONO photolysis. This observation suggests that the oxidation mechanism efficiently cleaves carbon–carbon bonds, yielding low-molecular-weight products such as formic acid. Atmospherically, formic acid plays a significant role in acid rain formation and affects aerosol chemistry by contributing to the acidity of cloud and rainwater, thereby influencing processes like aerosol growth and cloud development.

The consistent detection of 2,3-epoxycyclohexanone indicates that ring-retaining compounds are significant in the oxidation of cyclohexane oxide. This compound, possessing an epoxide functional group, is prone to acid-catalyzed ring-opening reactions in atmospheric particulate matter. Such reactions can yield more polar, low-volatility products that contribute to the growth of secondary organic aerosols (SOAs). The acid-catalyzed transformation of epoxides into diols or organosulfates has been well-documented in atmospheric chemistry, highlighting the role of acidic aerosols in facilitating these processes. Therefore, the presence of 2,3-epoxycyclohexanone in the atmosphere could enhance SOA formation through similar mechanisms, impacting air quality and climate.

Although instrumentation and conditions differed between the two laboratories, the comparability of results was ensured by focusing on:

- The qualitative agreement of detected products, rather than absolute concentrations.
- The presence of consistent mass spectral features and IR absorbance bands associated with chlorinated and oxygenated degradation products.
- The interpretation of observed products in the context of known Cl- and OH-initiated atmospheric oxidation mechanisms.

This approach allowed a consolidated analysis of the product spectrum and the elucidation of the degradation mechanism of cyclohexane oxide under atmospheric radical attack. The convergence of results from both systems enhances the confidence in the structural identification of the products and supports the environmental relevance of the observed transformations.

8 References

Abraham, K. M., Goldman, J. L., & Natwig, D. L. (1982). Characterization of Ether Electrolytes for Rechargeable Lithium Cells. *Journal of The Electrochemical Society*, *129*(11), 2404. https://doi.org/10.1149/1.2123556

Acker, K., Möller, D., Wieprecht, W., Meixner, F. X., Bohn, B., Gilge, S., Plass-Dülmer, C., & Berresheim, H. (2006). Strong daytime production of OH from HNO_2 at a rural mountain site. *Geophysical Research Letters*, *33*(2). https://doi.org/10.1029/2005GL024643

Ager, D. J., Prakash, I., & Schaad, D. R. (1996). 1,2-Amino Alcohols and Their Heterocyclic Derivatives as Chiral Auxiliaries in Asymmetric Synthesis. *Chemical Reviews*, *96*(2), 835–876. https://doi.org/10.1021/cr9500038

Akimoto, H. (2016). Tropospheric Reaction Chemistry. In H. Akimoto (Ed.), *Atmospheric Reaction Chemistry* (pp. 285–386). Springer Japan. https://doi.org/10.1007/978-4-431-55870-5_7

Almatarneh, M. H., Elayan, I. A., Abu-Saleh, A. A.-A. A., Altarawneh, M., & Ariya, P. A. (2019). The gas-phase ozonolysis reaction of methylbutenol: A mechanistic study. *International Journal of Quantum Chemistry*, *119*(10), e25888. https://doi.org/10.1002/qua.25888

Almatarneh, M. H., Elayan, I. A., Altarawneh, M., & Hollett, J. W. (2019). A computational study of the ozonolysis of sabinene. *Theoretical Chemistry Accounts*, *138*(2), 30. https://doi.org/10.1007/s00214-019-2420-7

Altway, S., Taha, M., & Lee, M.-J. (2015). (Liquid+liquid), (solid+liquid), and (solid+liquid+liquid) equilibria of systems containing cyclic ether (tetrahydrofuran or 1,3-dioxolane), water, and a biological buffer MOPS. *The Journal of Chemical Thermodynamics*, *82*, 93–98. https://doi.org/10.1016/j.jct.2014.11.002

Alvarado, A., Tuazon, E. C., Aschmann, S. M., Atkinson, R., & Arey, J. (1998). Products of the gas-phase reactions of O (^{3} P) atoms and O_3 with a-pinene and 1,2-dimethyl-1-cyclohexene. *Journal of Geophysical Research: Atmospheres*, *103*(D19), 25541–25551. https://doi.org/10.1029/98JD00524

Anaya de Parrodi, C. J., Eusebio. (2006). Chiral 1,2-Amino Alcohols and 1,2-Diamines Derived from Cyclohexene Oxide: Recent Applications in Asymmetric Synthesis. *Synlett*, *2006*(17), 2699–2715. https://doi.org/10.1055/s-2006-950259

Andrea, K. A., & Kerton, F. M. (2021). Iron-catalyzed reactions of CO2 and epoxides to yield cyclic and polycarbonates. *Polymer Journal*, *53*(1), 29–46. https://doi.org/10.1038/s41428-020-00395-6

Appaturi, J., Ramalingam, R., Gnanamani, M., Periyasami, G., Arunachalam, P., Adnan, R., Adam, F., Wasmiah, M., & Al-Lohedan, H. (2021). Review on Carbon Dioxide Utilization for Cycloaddition of Epoxides by Ionic Liquid-Modified Hybrid Catalysts: Effect of Influential Parameters and Mechanisms Insight. *Catalysts*, *11*(1). https://doi.org/10.3390/catal11010004

Aschmann, S. M., & Atkinson, R. (1995). Rate constants for the gas-phase reactions of alkanes with Cl atoms at 296 ± 2 K. *International Journal of Chemical Kinetics*, *27*(6), 613–622. https://doi.org/10.1002/kin.550270611

Atkinson, R. (1986a). Estimations of OH radical rate constants from H-atom abstraction from C-H and O-H bonds over the temperature range 250-1000 K. *International Journal of Chemical Kinetics*, *18*(5), 555–568. https://doi.org/10.1002/kin.550180506

Atkinson, R. (1986b). Kinetics and mechanisms of the gas-phase reactions of the hydroxyl radical with organic compounds under atmospheric conditions. *Chemical Reviews*, *86*(1), 69–201. https://doi.org/10.1021/cr00071a004

Atkinson, R. (1987). A structure-activity relationship for the estimation of rate constants for the gas-phase reactions of OH radicals with organic compounds. *International Journal of Chemical Kinetics*, *19*(9), 799–828. https://doi.org/10.1002/kin.550190903

Atkinson, R. (1997). Atmospheric reactions of alkoxy and β-hydroxyalkoxy radicals. *International Journal of Chemical Kinetics*, *29*(2), 99–111. https://doi.org/10.1002/(SICI)1097-4601(1997)29:2<99::AID-KIN3>3.0.CO;2-F

Atkinson, R. (2000). Atmospheric chemistry of VOCs and NOx. *Atmospheric Environment*, *34*(12), 2063–2101.

Atkinson, R., Arey, J., Aschmann, S. M., & Tuazon, E. C. (1994). Formation of $O(^3P)$ atoms and epoxides from the gas- phase reaction of O_3 with isoprene. *Research on Chemical Intermediates*, *20*(3), 385–394. https://doi.org/10.1163/156856794X00388

Atkinson, R., Aschmann, S. M., Arey, J., & Tuazon, E. C. (1994). Formation yields of epoxides and O(^{3}P) atoms from the gas-phase reactions of O_3 with a series of alkenes. *International Journal of Chemical Kinetics*, *26*(9), 945–950. https://doi.org/10.1002/kin.550260908

Auzmendi-Murua, I., & Bozzelli, J. W. (2014). Thermochemical Properties and Bond Dissociation Enthalpies of 3- to 5-Member Ring Cyclic Ether Hydroperoxides, Alcohols, and Peroxy Radicals: Cyclic Ether Radical + $3O_2$ Reaction Thermochemistry. *The Journal of Physical Chemistry A*, *118*(17), 3147–3167. https://doi.org/10.1021/jp412590g

Bader, R. F. W., Popelier, P. L. A., & Keith, T. A. (1994). Theoretical Definition of a Functional Group and the Molecular Orbital Paradigm. *Angewandte Chemie International Edition in English*, *33*(6), 620–631. https://doi.org/10.1002/anie.199406201

Barnes, I., Becker, K. H., & Mihalopoulos, N. (1994). An FTIR product study of the photooxidation of dimethyl disulfide. *Journal of Atmospheric Chemistry*, *18*(3), 267–289. https://doi.org/10.1007/BF00696783

Barnes, I., Wiesen, P., & Gallus, M. (2016). Kinetics and mechanism of the OH-radical and Cl-atom oxidation of propylene carbonate. *RSC Adv.*, *6*(100), 98234–98242. https://doi.org/10.1039/C6RA21952G

Bartels, M., Hoyermann, K., & Lange, U. (1989). An Experimental Study of the Reactions CH_3CHO + Cl, C_2H_4O + Cl, and C_2H_4O + F in the Gas-Phase. *Berichte Der*

Bunsengesellschaft Für Physikalische Chemie, *93*(4), 423–427. https://doi.org/10.1002/bbpc.19890930403

Bates, K. H., Crounse, J. D., St Clair, J. M., Bennett, N. B., Nguyen, T. B., Seinfeld, J. H., Stoltz, B. M., & Wennberg, P. O. (2014). Gas phase production and loss of isoprene epoxydiols. *The Journal of Physical Chemistry. A*, *118*(7), 1237–1246. https://doi.org/10.1021/jp4107958

Becke, A. D. (1993). Density-functional thermochemistry. III. The role of exact exchange. *The Journal of Chemical Physics*, *98*(7), 5648–5652. https://doi.org/10.1063/1.464913

Belaribi, F. B., Abdouche, N., Boussebissi, A., Amireche, F., & Boukais-Belaribi, G. (2015). Excess molar enthalpies of binary mixtures of n-octane, isooctane and cyclooctane with morpholine, 1,4-dioxane, piperidine, oxane, N-methyl piperidine and cyclohexane. Experimental results and DISQUAC modelling. *Journal of Molecular Liquids*, *212*, 650–655. https://doi.org/10.1016/j.molliq.2015.10.020

Budisulistiorini, S. H., Canagaratna, M. R., Croteau, P. L., Marth, W. J., Baumann, K., Edgerton, E. S., Shaw, S. L., Knipping, E. M., Worsnop, D. R., Jayne, J. T., Gold, A., & Surratt, J. D. (2013). Real-time continuous characterization of secondary organic aerosol derived from isoprene epoxydiols in downtown Atlanta, Georgia, using the Aerodyne Aerosol Chemical Speciation Monitor. *Environmental Science & Technology*, *47*(11), 5686–5694. https://doi.org/10.1021/es400023n

Budisulistiorini, S. H., Li, X., Bairai, S. T., Renfro, J., Liu, Y., Liu, Y. J., McKinney, K. A., Martin, S. T., McNeill, V. F., Pye, H. O. T., Nenes, A., Neff, M. E., Stone, E. A., Mueller,

S., Knote, C., Shaw, S. L., Zhang, Z., Gold, A., & Surratt, J. D. (2015). Examining the effects of anthropogenic emissions on isoprene-derived secondary organic aerosol formation during the 2013 Southern Oxidant and Aerosol Study (SOAS) at the Look Rock, Tennessee ground site. *Atmospheric Chemistry and Physics*, *15*(15), 8871–8888. https://doi.org/10.5194/acp-15-8871-2015

Calvert, G., Atkinson, R., Kerr, A., Madronich, S., Moortgat, G., Wallington, J., & Yarwood, G. (2000). *The Mechanisms of Atmospheric Oxidation of the Alkenes*. https://opensky.ucar.edu/islandora/object/books%3A153/

Calvert, J. G., Orlando, J. J., Stockwell, W. R., & Wallington, T. J. (2015). *The Mechanisms of Reactions Influencing Atmospheric Ozone*. Oxford University Press.

Calvert, J., Mellouki, A., Orlando, J., Pilling, M., & Wallington, T. (2011). *Mechanisms of Atmospheric Oxidation of the Oxygenates*. Oxford University Press.

Cappa, C. D., Zhang, X., Loza, C. L., Craven, J. S., Yee, L. D., & Seinfeld, J. H. (2013). Application of the Statistical Oxidation Model (SOM) to Secondary Organic Aerosol formation from photooxidation of C_{12} alkanes. *Atmospheric Chemistry and Physics*, *13*(3), 1591–1606. https://doi.org/10.5194/acp-13-1591-2013

Carter, W. P. L., Atkinson, R., Winer, A. M., & Pitts Jr., J. N. (1982). Experimental investigation of chamber-dependent radical sources. *International Journal of Chemical Kinetics*, *14*(10), 1071–1103. https://doi.org/10.1002/kin.550141003

Chen, J., Young, V., Hooshiyar, P. A., Niki, H., & Hurley, M. D. (1995). FTIR Spectroscopic Study of the Cl-Atom-Initiated Reactions of Ethylene Oxide in O_2/N_2 Diluent. *The Journal of Physical Chemistry*, *99*(12), 4071–4077. https://doi.org/10.1021/j100012a030

Christianson, M. G., Doner, A. C., Davis, M. M., Koritzke, A. L., Turney, J. M., Schaefer III, H. F., Sheps, L., Osborn, D. L., Taatjes, C. A., & Rotavera, B. (2021). Reaction mechanisms of a cyclic ether intermediate: Ethyloxirane. *International Journal of Chemical Kinetics*, *53*(1), 43–59. https://doi.org/10.1002/kin.21423

Cichowicz, R., Wielgosiński, G., & Fetter, W. (2017). Dispersion of atmospheric air pollution in summer and winter season. *Environmental Monitoring and Assessment*, *189*(12), 605. https://doi.org/10.1007/s10661-017-6319-2

Claeys, M. (2010). Comment on "Unexpected Epoxide Formation in the Gas-Phase Photooxidation of Isoprene". *Science*, *327*(5966), 644. https://doi.org/10.1126/science.1180942

Coppens, P. (2005). Charge Densities Come of Age. *Angewandte Chemie International Edition*, *44*(42), 6810–6811. https://doi.org/10.1002/anie.200501734

Coulson, C. A., & Moffitt, W. E. (1947). Strain in Non-Tetrahedral Carbon Atoms. *The Journal of Chemical Physics*, *15*(3), 151. https://doi.org/10.1063/1.1746450

Coulson, C., A. & Moffitt, W., E. (1949). I. The properties of certain strained hydrocarbons. *The London, Edinburgh, and Dublin Philosophical Magazine and Journal of Science*, *40*(300), 1–35. https://doi.org/10.1080/14786444908561208

Cromwell, N. H., & Graff, M. A. (1952). Three-Ring carbonyl hyperconjugation in cis and trans aryl-aroylL ethylene imines and related compounds. *J. Org. Chem.*, *17*(3), 414-425. https://doi.org/10.1021/jo01137a014

Cromwell, N. H., & Hudson, G. V. (1953). The Steric Requirements for Three-Ring Carbonyl Hyperconjugation1. *Journal of the American Chemical Society*, *75*(4), 872–874. https://doi.org/10.1021/ja01100a031

Daimari, S. R., Changmai, R. R., & Sarma, M. (2024). Investigating the Atmospheric Fate and Kinetics of OH Radical-Initiated Oxidation Reactions for Epoxybutane Isomers: Theoretical Insight. *The Journal of Physical Chemistry. A*, *128*(30), 6240–6253. https://doi.org/10.1021/acs.jpca.4c00379

Dayan, U., Ricaud, P., Zbinden, R., & Dulac, F. (2017). Atmospheric pollution over the eastern Mediterranean during summer – a review. *Atmospheric Chemistry and Physics*, *17*(21), 13233–13263. https://doi.org/10.5194/acp-17-13233-2017

DeMore, W.B., Sander, S.P., Golden, D.M., Hampson, R.F., Kurylo, M.J., Howard, C.J., Ravishankara, A.R., Kolb, C.E., & Molina, M.J. (1997, January 15). *Chemical Kinetics and Photochemical Data for use in Stratospheric Modeling, Evaluation No. 12, NASA Panel for Data Evaluation, Jet Propulsion Laborat- ory Publication 97-4*.

Dennington, Roy, Keith, Todd A., & Millam, John M. (2019). *GaussView6* (Lee) [Computer software].

Derwent, R. G., Powlson, D. S., & Conrad, R. (1995). Air Chemistry and Terrestrial Gas Emissions: A Global Perspective [and Discussion]. *Philosophical Transactions: Physical Sciences and Engineering*, *351*(1696), 205–217.

Doner, A. C., Davis, M. M., Koritzke, A. L., Christianson, M. G., Turney, J. M., Schaefer III, H. F., Sheps, L., Osborn, D. L., Taatjes, C. A., & Rotavera, B. (2021). Isomer-dependent reaction mechanisms of cyclic ether intermediates: Cis-2,3-dimethyloxirane and trans-2,3-dimethyloxirane. *International Journal of Chemical Kinetics*, *53*(1), 127–145. https://doi.org/10.1002/kin.21429

Doussin, J.-F. (2023). Conclusions. In J.-F. Doussin, H. Fuchs, A. Kiendler-Scharr, P. Seakins, & J. Wenger (Eds.), *A Practical Guide to Atmospheric Simulation Chambers* (pp. 331–339). Springer International Publishing. https://doi.org/10.1007/978-3-031-22277-1_9

Dusanter, S., Vimal, D., Stevens, P. S., Volkamer, R., Molina, L. T., Baker, A., Meinardi, S., Blake, D., Sheehy, P., Merten, A., Zhang, R., Zheng, J., Fortner, E. C., Junkermann, W., Dubey, M., Rahn, T., Eichinger, B., Lewandowski, P., Prueger, J., & Holder, H. (2009). Measurements of OH and HO_2 concentrations during the MCMA-2006 field campaign – Part 2: Model comparison and radical budget. *Atmospheric Chemistry and Physics*, *9*(18), 6655–6675. https://doi.org/10.5194/acp-9-6655-2009

Duuren, B. L. V. (1972). Epoxides, Hydroperoxides and Peroxides in Air Pollution. *International Journal of Environmental Analytical Chemistry*, *1*(3), 233–241. https://doi.org/10.1080/03067317208076374

Ehrenberg, L., & Hussain, S. (1981). Genetic toxicity of some important epoxides. *Mutation Research/Reviews in Genetic Toxicology*, *86*(1), 1–113. https://doi.org/10.1016/0165-1110(81)90034-8

El Othmani, H., Ren, Y., Bedjanian, Y., El Hajjaji, S., Tovar, C., Wiesen, P., Mellouki, A., McGillen, M. R., & Daële, V. (2021). Gas-Phase Rate Coefficient of OH + 1,2-Epoxybutane Determined between 220 and 950 K. *ACS Earth and Space Chemistry*, *5*(4), 960–968. https://doi.org/10.1021/acsearthspacechem.1c00050

El Othmani, H., Ren, Y., Mellouki, A., Daële, V., & McGillen, M. R. (2021). Gas-phase rate coefficient of OH + cyclohexene oxide measured from 251 to 373 K. *Chemical Physics Letters*, *783*, 139056. https://doi.org/10.1016/j.cplett.2021.139056

Elshorbany, Y. F., Kleffmann, J., Kurtenbach, R., Lissi, E., Rubio, M., Villena, G., Gramsch, E., Rickard, A. R., Pilling, M. J., & Wiesen, P. (2010). Seasonal dependence of the oxidation capacity of the city of Santiago de Chile. *Atmospheric Chemical Mechanisms: Selected Papers from the 2008 Conference*, *44*(40), 5383–5394. https://doi.org/10.1016/j.atmosenv.2009.08.036

Elshorbany, Y. F., Kurtenbach, R., Wiesen, P., Lissi, E., Rubio, M., Villena, G., Gramsch, E., Rickard, A. R., Pilling, M. J., & Kleffmann, J. (2009). Oxidation capacity of the city air of Santiago, Chile. *Atmospheric Chemistry and Physics*, *9*(6), 2257–2273. https://doi.org/10.5194/acp-9-2257-2009

Ervens, B., Turpin, B. J., & Weber, R. J. (2011). Secondary organic aerosol formation in cloud droplets and aqueous particles (aqSOA): A review of laboratory, field and model

studies. *Atmospheric Chemistry and Physics*, *11*(21), 11069–11102. https://doi.org/10.5194/acp-11-11069-2011

Finlayson-Pitts, B. J., & Pitts, J. N. (2000). CHAPTER 1—Overview of the Chemistry of Polluted and Remote Atmospheres. In B. J. Finlayson-Pitts & J. N. Pitts (Eds.), *Chemistry of the Upper and Lower Atmosphere* (pp. 1–14). Academic Press. https://doi.org/10.1016/B978-012257060-5/50003-4

Fokin, V. V., & Wu, P. (2006). Epoxides and Aziridines in Click Chemistry. In *Aziridines and Epoxides in Organic Synthesis* (pp. 443–477). John Wiley & Sons, Ltd. https://doi.org/10.1002/3527607862.ch12

Förster, T. (1939). Die gegenseitige Beeinflussung der Valenzen im Kohlenstoffatom. *Zeitschrift für Physikalische Chemie*, *43B*(1), 58–78. https://doi.org/10.1515/zpch-1939-4306

Frisch, M. J., Trucks, G. W., Schlegel, H. B., Scuseria, G. E., Robb, M. A., Cheeseman, J. R., Scalmani, G., Barone, V., Petersson, G. A., Nakatsuji, H., Li, X., Caricato, M., Marenich, A. V., Bloino, J., Janesko, B. G., Gomperts, R., Mennucci, B., Hratchian, H. P., Ortiz, J. V., … Fox, D. J. (2016). *Gaussian 16 Rev. A.03* [Computer software].

Fuzzi, S., Baltensperger, U., Carslaw, K., Decesari, S., Denier van der Gon, H., Facchini, M. C., Fowler, D., Koren, I., Langford, B., Lohmann, U., Nemitz, E., Pandis, S., Riipinen, I., Rudich, Y., Schaap, M., Slowik, J. G., Spracklen, D. V., Vignati, E., Wild, M., … Gilardoni, S. (2015). Particulate matter, air quality and climate: Lessons learned and

future needs. *Atmospheric Chemistry and Physics*, *15*(14), 8217–8299. https://doi.org/10.5194/acp-15-8217-2015

Gao, S., Ng, N. L., Keywood, M., Varutbangkul, V., Bahreini, R., Nenes, A., He, J., Yoo, K. Y., Beauchamp, J. L., Hodyss, R. P., Flagan, R. C., & Seinfeld, J. H. (2004). Particle Phase Acidity and Oligomer Formation in Secondary Organic Aerosol. *Environmental Science & Technology*, *38*(24), 6582–6589. https://doi.org/10.1021/es049125k

Grabowsky, S., Jayatilaka, D., Mebs, S., & Luger, P. (2010). The Electron Localizability Indicator from X-Ray Diffraction Data—A First Application to a Series of Epoxide Derivatives. *Chemistry – A European Journal*, *16*(43), 12818–12821. https://doi.org/10.1002/chem.201002061

Grigoropoulou, G., Clark, J. H., & Elings, J. A. (2003). Recent developments on the epoxidation of alkenes using hydrogen peroxide as an oxidant. *Green Chemistry*, *5*(1), 1–7. https://doi.org/10.1039/B208925B

Grimme, S., Ehrlich, S., & Goerigk, L. (2011). Effect of the damping function in dispersion corrected density functional theory. *Journal of Computational Chemistry*, *32*(7), 1456–1465. https://doi.org/10.1002/jcc.21759

Guenther, A., Karl, T., Harley, P., Wiedinmyer, C., Palmer, P. I., & Geron, C. (2006). Estimates of global terrestrial isoprene emissions using MEGAN (Model of Emissions of Gases and Aerosols from Nature). *Atmospheric Chemistry and Physics*, *6*(11), 3181–3210. https://doi.org/10.5194/acp-6-3181-2006

Guo, L., J. Lamb, K., & North, M. (2021). Recent developments in organocatalysed transformations of epoxides and carbon dioxide into cyclic carbonates. *Green Chemistry*, *23*(1), 77–118. https://doi.org/10.1039/D0GC03465G

Hallquist, M., Wenger, J. C., Baltensperger, U., Rudich, Y., Simpson, D., Claeys, M., Dommen, J., Donahue, N. M., George, C., Goldstein, A. H., Hamilton, J. F., Herrmann, H., Hoffmann, T., Iinuma, Y., Jang, M., Jenkin, M. E., Jimenez, J. L., Kiendler-Scharr, A., Maenhaut, W., … Wildt, J. (2009). The formation, properties and impact of secondary organic aerosol: Current and emerging issues. *Atmospheric Chemistry and Physics*, *9*(14), 5155–5236. https://doi.org/10.5194/acp-9-5155-2009

Hereijgers, B. P. C., Parton, R. F., & Weckhuysen, B. M. (2012). Mechanistic insights in the olefin epoxidation with cyclohexyl hydroperoxide. *Catalysis Science & Technology*, *2*(5), 951–960. https://doi.org/10.1039/C2CY00455K

Hidy, G. M. (2019). Atmospheric Chemistry in a Box or a Bag. *Atmosphere*, *10*(7). https://doi.org/10.3390/atmos10070401

Hu, W. W., Campuzano-Jost, P., Palm, B. B., Day, D. A., Ortega, A. M., Hayes, P. L., Krechmer, J. E., Chen, Q., Kuwata, M., Liu, Y. J., de Sá, S. S., McKinney, K., Martin, S. T., Hu, M., Budisulistiorini, S. H., Riva, M., Surratt, J. D., St. Clair, J. M., Isaacman-Van Wertz, G., … Jimenez, J. L. (2015). Characterization of a real-time tracer for isoprene epoxydiols-derived secondary organic aerosol (IEPOX-SOA) from aerosol mass spectrometer measurements. *Atmospheric Chemistry and Physics*, *15*(20), 11807–11833. https://doi.org/10.5194/acp-15-11807-2015

Huang, X.-F., Zhang, B., Xia, S.-Y., Han, Y., Wang, C., Yu, G.-H., & Feng, N. (2020). Sources of oxygenated volatile organic compounds (OVOCs) in urban atmospheres in North and South China. *Environmental Pollution*, *261*, 114152. https://doi.org/10.1016/j.envpol.2020.114152

Hui, L., Feng, X., Yuan, Q., Chen, Y., Xu, Y., Zheng, P., Lee, S., & Wang, Z. (2023). Abundant oxygenated volatile organic compounds and their contribution to photochemical pollution in subtropical Hong Kong. *Environmental Pollution*, *335*, 122287. https://doi.org/10.1016/j.envpol.2023.122287

Impey, G. A., Shepson, P. B., Hastie, D. R., Barrie, L. A., & Anlauf, K. G. (1997). Measurements of photolyzable chlorine and bromine during the Polar Sunrise Experiment 1995. *Journal of Geophysical Research: Atmospheres*, *102*(D13), 16005–16010. https://doi.org/10.1029/97JD00851

IUPAC Task Group on Atmospheric Chemical Kinetic Data Evaluation. (n.d.). Retrieved 26 October 2021, from https://iupac-aeris.ipsl.fr/

Jacobs, M. I., Darer, A. I., & Elrod, M. J. (2013). Rate Constants and Products of the OH Reaction with Isoprene-Derived Epoxides. *Environmental Science & Technology*, *47*(22), 12868–12876. https://doi.org/10.1021/es403340g

Jelliss, P. A., Buckner, S. W., Chung, S. W., Patel, A., Guliants, E. A., & Bunker, C. E. (2013). The use of 1,2-epoxyhexane as a passivating agent for core–shell aluminum nanoparticles with very high active aluminum content. *Solid State Sciences*, *23*, 8–12. https://doi.org/10.1016/j.solidstatesciences.2013.06.001

Jenkin, M. E., Valorso, R., Aumont, B., Rickard, A. R., & Wallington, T. J. (2018a). Estimation of rate coefficients and branching ratios for gas-phase reactions of OH with aliphatic organic compounds for use in automated mechanism construction. *Atmospheric Chemistry and Physics*, *18*(13), 9297–9328. https://doi.org/10.5194/acp-18-9297-2018

Jenkin, M. E., Valorso, R., Aumont, B., Rickard, A. R., & Wallington, T. J. (2018b). Estimation of rate coefficients and branching ratios for gas-phase reactions of OH with aromatic organic compounds for use in automated mechanism construction. *Atmospheric Chemistry and Physics*, *18*(13), 9329–9349. https://doi.org/10.5194/acp-18-9329-2018

Jenkin, M. E., Young, J. C., & Rickard, A. R. (2015). The MCM v3.3.1 degradation scheme for isoprene. *Atmospheric Chemistry and Physics*, *15*(20), 11433–11459. https://doi.org/10.5194/acp-15-11433-2015

Jiang, X., Tsona, N. T., Jia, L., Liu, S., Zhang, H., Xu, Y., & Du, L. (2019). Secondary organic aerosol formation from photooxidation of furan: Effects of NOx and humidity. *Atmospheric Chemistry and Physics*, *19*(21), 13591–13609. https://doi.org/10.5194/acp-19-13591-2019

Kaminski, M., Fuchs, H., Acir, I.-H., Bohn, B., Brauers, T., Dorn, H.-P., Häseler, R., Hofzumahaus, A., Li, X., Lutz, A., Nehr, S., Rohrer, F., Tillmann, R., Vereecken, L., Wegener, R., & Wahner, A. (2017). Investigation of the β-pinene photooxidation by \chemOH in the atmosphere simulation chamber SAPHIR. *Atmospheric Chemistry and Physics*, *17*(11), 6631–6650. https://doi.org/10.5194/acp-17-6631-2017

Kanakidou, M., Seinfeld, J. H., Pandis, S. N., Barnes, I., Dentener, F. J., Facchini, M. C., Dingenen, R. V., Ervens, B., Nenes, A., Nielsen, C. J., Swietlicki, E., Putaud, J. P., Balkanski, Y., Fuzzi, S., Horth, J., Moortgat, G. K., Winterhalter, R., Myhre, C. E. L., Tsigaridis, K., … Wilson, J. (2005). Organic aerosol and global climate modelling: A review. *Atmospheric Chemistry and Physics*, *5*(4), 1053–1123. https://doi.org/10.5194/acp-5-1053-2005

Kiendler-Scharr, A., Becker, K.-H., Doussin, J.-F., Fuchs, H., Seakins, P., Wenger, J., & Wiesen, P. (2023). Introduction to Atmospheric Simulation Chambers and Their Applications. In J.-F. Doussin, H. Fuchs, A. Kiendler-Scharr, P. Seakins, & J. Wenger (Eds.), *A Practical Guide to Atmospheric Simulation Chambers* (pp. 1–72). Springer International Publishing. https://doi.org/10.1007/978-3-031-22277-1_1

Kleindienst, T. E., Lewandowski, M., Offenberg, J. H., Jaoui, M., & Edney, E. O. (2009). The formation of secondary organic aerosol from the isoprene + OH reaction in the absence of NO_x. *Atmospheric Chemistry and Physics*, *9*(17), 6541–6558. https://doi.org/10.5194/acp-9-6541-2009

Klotz, B., Barnes, I., Becker, K. H., & Golding, B. T. (1997). Atmospheric chemistry of benzeneoxide/oxepin. *Journal of the Chemical Society, Faraday Transactions*, *93*(8), 1507–1516. https://doi.org/10.1039/A606152D

Klotz, B., Volkamer, R., Hurley, M. D., Andersen, M. P. S., Nielsen, O. J., Barnes, I., Imamura, T., Wirtz, K., Becker, K.-H., Platt, U., Wallington, T. J., & Washida, N. (2002). OH-

initiated oxidation of benzene. *Physical Chemistry Chemical Physics*, *4*(18), 4399–4411. https://doi.org/10.1039/B204398J

Kohout, M. (2004). A measure of electron localizability. *International Journal of Quantum Chemistry*, *97*(1), 651–658. https://doi.org/10.1002/qua.10768

Kolb, H. C., Finn, M. G., & Sharpless, K. B. (2001). Click Chemistry: Diverse Chemical Function from a Few Good Reactions. *Angewandte Chemie International Edition*, *40*(11), 2004–2021. https://doi.org/10.1002/1521-3773(20010601)40:11%3C2004::AID-ANIE2004%3E3.0.CO;2-5

Koritsanszky, T. S., & Coppens, P. (2001). Chemical Applications of X-ray Charge-Density Analysis. *Chemical Reviews*, *101*(6), 1583–1628. https://doi.org/10.1021/cr990112c

Kutzelnigg, W. (1993). Book Review: Atoms in Molecules. A Quantum Theory. (International Series Monographs on Chemistry, Vol. 22). By R. F. W. Bader. *Angewandte Chemie International Edition in English*, *32*(1), 128–129. https://doi.org/10.1002/anie.199301282

Kwok, E. S. C., & Atkinson, R. (1995). Estimation of hydroxyl radical reaction rate constants for gas-phase organic compounds using a structure-reactivity relationship: An update. *Atmospheric Environment*, *29*(14), 1685–1695. https://doi.org/10.1016/1352-2310(95)00069-B

Lal, V., Khalizov, A. F., Lin, Y., Galvan, M. D., Connell, B. T., & Zhang, R. (2012). Heterogeneous Reactions of Epoxides in Acidic Media. *The Journal of Physical Chemistry A*, *116*(24), 6078–6090. https://doi.org/10.1021/jp2112704

Lee, C., Yang, W., & Parr, R. G. (1988). Development of the Colle-Salvetti correlation-energy formula into a functional of the electron density. *Physical Review. B, Condensed Matter*, *37*(2), 785–789. https://doi.org/10.1103/physrevb.37.785

Legreid, G., Lööv, J. B., Staehelin, J., Hueglin, C., Hill, M., Buchmann, B., Prevot, A. S. H., & Reimann, S. (2007). Oxygenated volatile organic compounds (OVOCs) at an urban background site in Zürich (Europe): Seasonal variation and source allocation. *Atmospheric Environment*, *41*(38), 8409–8423. https://doi.org/10.1016/j.atmosenv.2007.07.026

Legreid, G., Reimann, S., Steinbacher, M., Staehelin, J., Young, D., & Stemmler, K. (2007). 'Measurements of OVOCs and NMHCs in a Swiss Highway Tunnel for Estimation of Road Transport Emissions. *Environmental Science & Technology*, *41*(20), 7060–7066. https://doi.org/10.1021/es062309+

Lelieveld, J., Gromov, S., Pozzer, A., & Taraborrelli, D. (2016). Global tropospheric hydroxyl distribution, budget and reactivity. *Atmospheric Chemistry and Physics*, *16*(19), 12477–12493. https://doi.org/10.5194/acp-16-12477-2016

Lemaire, O., Ribaucour, M., Carlier, M., & Minetti, R. (2001). The production of benzene in the low-temperature oxidation of cyclohexane, cyclohexene, and cyclohexa-1,3-diene. *Combustion and Flame*, *127*(1), 1971–1980. https://doi.org/10.1016/S0010-2180(01)00301-7

Li, M., Liu, Y., & Wang, L. (2018). Gas-phase ozonolysis of furans, methylfurans, and dimethylfurans in the atmosphere. *Physical Chemistry Chemical Physics*, *20*(38), 24735–24743. https://doi.org/10.1039/C8CP04947E

Liao, J., Huey, L. G., Liu, Z., Tanner, D. J., Cantrell, C. A., Orlando, J. J., Flocke, F. M., Shepson, P. B., Weinheimer, A. J., Hall, S. R., Ullmann, K., Beine, H. J., Wang, Y., Ingall, E. D., Stephens, C. R., Hornbrook, R. S., Apel, E. C., Riemer, D., Fried, A., … Nowak, J. B. (2014). High levels of molecular chlorine in the Arctic atmosphere. *Nature Geoscience*, *7*(2), 91–94. https://doi.org/10.1038/ngeo2046

Lin, Y.-H., Knipping, E. M., Edgerton, E. S., Shaw, S. L., & Surratt, J. D. (2013). Investigating the influences of SO_2 and NH_3 levels on isoprene-derived secondary organic aerosol formation using conditional sampling approaches. *Atmospheric Chemistry and Physics*, *13*(16), 8457–8470. https://doi.org/10.5194/acp-13-8457-2013

Lin, Y.-H., Zhang, H., Pye, H. O. T., Zhang, Z., Marth, W. J., Park, S., Arashiro, M., Cui, T., Budisulistiorini, S. H., Sexton, K. G., Vizuete, W., Xie, Y., Luecken, D. J., Piletic, I. R., Edney, E. O., Bartolotti, L. J., Gold, A., & Surratt, J. D. (2013a). Epoxide as a precursor to secondary organic aerosol formation from isoprene photooxidation in the presence of nitrogen oxides. *Proceedings of the National Academy of Sciences*, *110*(17), 6718–6723. https://doi.org/10.1073/pnas.1221150110

Lin, Y.-H., Zhang, H., Pye, H. O. T., Zhang, Z., Marth, W., J., Park, S., Arashiro, M., Cui, T., Budisulistiorini, S. H., Sexton, K. G., Vizuete, W., Xie, Y., Luecken, D., J., Piletic, I., R., Edney, E., O., Bartolotti, L., J., Gold, A., & Surratt, J., D. (2013b). Epoxide as a

precursor to secondary organic aerosol formation from isoprene photooxidation in the presence of nitrogen oxides. *Proceedings of the National Academy of Sciences*, *110*(17), 6718–6723. https://doi.org/10.1073/pnas.1221150110

Liu, P., Ye, C., Zhang, C., He, G., Xue, C., Liu, J., Liu, C., Zhang, Y., Song, Y., Li, X., Wang, X., Chen, J., He, H., Herrmann, H., & Mu, Y. (2021). Photochemical Aging of Atmospheric Fine Particles as a Potential Source for Gas-Phase Hydrogen Peroxide. *Environmental Science & Technology*, *55*(22), 15063–15071. https://doi.org/10.1021/acs.est.1c04453

Liu, X., Qu, H., Huey, L. G., Wang, Y., Sjostedt, S., Zeng, L., Lu, K., Wu, Y., Hu, M., Shao, M., Zhu, T., & Zhang, Y. (2017). High Levels of Daytime Molecular Chlorine and Nitryl Chloride at a Rural Site on the North China Plain. *Environmental Science & Technology*, *51*(17), 9588–9595. https://doi.org/10.1021/acs.est.7b03039

Liu, Z., Wang, Y., Gu, D., Zhao, C., Huey, L. G., Stickel, R., Liao, J., Shao, M., Zhu, T., Zeng, L., Amoroso, A., Costabile, F., Chang, C.-C., & Liu, S.-C. (2012). Summertime photochemistry during CAREBeijing-2007: RO_x budgets and O_3 formation. *Atmospheric Chemistry and Physics*, *12*(16), 7737–7752. https://doi.org/10.5194/acp-12-7737-2012

Liu, Z., Wang, Y., Gu, D., Zhao, C., Huey, L. G., Stickel, R., Liao, J., Shao, M., Zhu, T., Zeng, L., Liu, S.-C., Chang, C.-C., Amoroso, A., & Costabile, F. (2010). Evidence of Reactive Aromatics As a Major Source of Peroxy Acetyl Nitrate over China. *Environmental Science & Technology*, *44*(18), 7017–7022. https://doi.org/10.1021/es1007966

Malik, S., Sharma, D., & Sharma, V. K. (2016). Topological investigations of mixtures containing cyclic ether and cyclic alkanones. *Journal of Molecular Liquids*, *223*, 1158–1171. https://doi.org/10.1016/j.molliq.2016.09.025

McGillen, M. R., Carter, W. P. L., Mellouki, A., Orlando, J. J., Picquet-Varrault, B., & Wallington, T. J. (2020). Database for the kinetics of the gas-phase atmospheric reactions of organic compounds. *Earth System Science Data*, *12*(2), 1203–1216. https://doi.org/10.5194/essd-12-1203-2020

Mellouki, A., Wallington, T. J., & Chen, J. (2015). Atmospheric Chemistry of Oxygenated Volatile Organic Compounds: Impacts on Air Quality and Climate. *Chemical Reviews*, *115*(10), 3984–4014. https://doi.org/10.1021/cr500549n

Middala, S., Campbell, S., Olea, C., Scruggs, A., & Hasson, A. S. (2011). Kinetics and mechanism of the reaction of propylene oxide with chlorine atoms and hydroxy radicals. *International Journal of Chemical Kinetics*, *43*(9), 507–521. https://doi.org/10.1002/kin.20580

Min, S., Bin, W., Sihua, L., Bin, Y., & Ming, W. (2011). Effects of Beijing Olympics Control Measures on Reducing Reactive Hydrocarbon Species. *Environmental Science & Technology*, *45*(2), 514–519. https://doi.org/10.1021/es102357t

Minerath, E. C., & Elrod, M. J. (2009). Assessing the Potential for Diol and Hydroxy Sulfate Ester Formation from the Reaction of Epoxides in Tropospheric Aerosols. *Environmental Science & Technology*, *43*(5), 1386–1392. https://doi.org/10.1021/es8029076

Minerath, E. C., Schultz, M. P., & Elrod, M. J. (2009). Kinetics of the Reactions of Isoprene-Derived Epoxides in Model Tropospheric Aerosol Solutions. *Environmental Science & Technology*, *43*(21), 8133–8139. https://doi.org/10.1021/es902304p

Molina, L. T., & Molina, M. J. (1987). Production of chlorine oxide (Cl2O2) from the self-reaction of the chlorine oxide (ClO) radical. *The Journal of Physical Chemistry*, *91*(2), 433–436. https://doi.org/10.1021/j100286a035

Molina, M. J., & Rowland, F. S. (1974). Stratospheric sink for chlorofluoromethanes: Chlorine atom-catalysed destruction of ozone. *Nature*, *249*(5460), 810–812. https://doi.org/10.1038/249810a0

Müller, M., Mikoviny, T., Jud, W., D'Anna, B., & Wisthaler, A. (2013). A new software tool for the analysis of high resolution PTR-TOF mass spectra. *Chemometrics and Intelligent Laboratory Systems*, *127*, 158–165. https://doi.org/10.1016/j.chemolab.2013.06.011

Nguyen, T. B., Bates, K. H., Crounse, J. D., Schwantes, R. H., Zhang, X., Kjaergaard, H. G., Surratt, J. D., Lin, P., Laskin, A., Seinfeld, J. H., & Wennberg, P. O. (2015). Mechanism of the hydroxyl radical oxidation of methacryloyl peroxynitrate (MPAN) and its pathway toward secondary organic aerosol formation in the atmosphere. *Phys. Chem. Chem. Phys.*, *17*(27), 17914–17926. https://doi.org/10.1039/C5CP02001H

Notario, A., Mellouki, A., & Bras, G. L. (2000). Rate constants for the gas-phase reactions of Cl atoms with a series of ethers. *International Journal of Chemical Kinetics*, *32*, 105–110.

Orlando, J. J., Iraci, L. T., & Tyndall, G. S. (2000). Chemistry of the Cyclopentoxy and Cyclohexoxy Radicals at Subambient Temperatures. *The Journal of Physical Chemistry A*, *104*(21), 5072–5079. https://doi.org/10.1021/jp0002648

Oshima, T., Asahara, H., Kubo, E., Miyamoto, S., & Togaya, K. (2008). Conformational Effects in Acid-Mediated Ring Opening of Epoxides: A Prominent Role of the Oxirane Walsh Orbital. *Organic Letters*, *10*(12), 2413–2416. https://doi.org/10.1021/ol800535c

Otto, H.-H., & Schirmeister, T. (1997). Cysteine Proteases and Their Inhibitors. *Chemical Reviews*, *97*(1), 133–172. https://doi.org/10.1021/cr950025u

Oyama, S. T. (2008). Chapter 1—Rates, Kinetics, and Mechanisms of Epoxidation: Homogeneous, Heterogeneous, and Biological Routes. In S. T. Oyama (Ed.), *Mechanisms in Homogeneous and Heterogeneous Epoxidation Catalysis* (pp. 3–99). Elsevier. https://doi.org/10.1016/B978-0-444-53188-9.00001-8

Pagliaro, M. (2006). Supercritical Carbon Dioxide in Polymer Reaction Engineering. Edited by Maartje F. Kemmere and Thierry Meyer. *Angewandte Chemie International Edition*, *45*(37), 6079–6079. https://doi.org/10.1002/anie.200585386

Pang, C., Ding, F., Sun, W., Liu, J., Hao, M., Wang, Y., Liu, X., & Xu, Q. (2015). A novel dimethyl sulfoxide/1,3-dioxolane based electrolyte for lithium/carbon fluorides batteries with a high discharge voltage plateau. *Electrochimica Acta*, *174*, 230–237. https://doi.org/10.1016/j.electacta.2015.06.004

Parker, R. E., & Isaacs, N. S. (1959). Mechanisms Of Epoxide Reactions. *Chemical Reviews*, *59*(4), 737–799. https://doi.org/10.1021/cr50028a006

Paulot, F., Crounse, J. D., Kjaergaard, H. G., Kürten, A., St Clair, J. M., Seinfeld, J. H., & Wennberg, P. O. (2009). Unexpected epoxide formation in the gas-phase photooxidation of isoprene. *Science (New York, N.Y.)*, *325*(5941), 730—733. https://doi.org/10.1126/science.1172910

Paulson, S. E., Flagan, R. C., & Seinfeld, J. H. (1992a). Atmospheric photooxidation of isoprene part I: The hydroxyl radical and ground state atomic oxygen reactions. *International Journal of Chemical Kinetics*, *24*(1), 79–101. https://doi.org/10.1002/kin.550240109

Paulson, S. E., Flagan, R. C., & Seinfeld, J. H. (1992b). Atmospheric photooxidation of isoprene part II: The ozone-isoprene reaction. *International Journal of Chemical Kinetics*, *24*(1), 103–125. https://doi.org/10.1002/kin.550240110

Peeters, J., Müller, J.-F., Stavrakou, T., & Nguyen, V. S. (2014). Hydroxyl Radical Recycling in Isoprene Oxidation Driven by Hydrogen Bonding and Hydrogen Tunneling: The Upgraded LIM1 Mechanism. *The Journal of Physical Chemistry A*, *118*(38), 8625–8643. https://doi.org/10.1021/jp5033146

Peng, X., Wang, T., Wang, W., Ravishankara, A. R., George, C., Xia, M., Cai, M., Li, Q., Salvador, C. M., Lau, C., Lyu, X., Poon, C. N., Mellouki, A., Mu, Y., Hallquist, M., Saiz-Lopez, A., Guo, H., Herrmann, H., Yu, C., … Chen, J. (2022). Photodissociation of particulate nitrate as a source of daytime tropospheric Cl2. *Nature Communications*, *13*(1), 939. https://doi.org/10.1038/s41467-022-28383-9

Piletic, I. R., Edney, E. O., & Bartolotti, L. J. (2017). Barrierless Reactions with Loose Transition States Govern the Yields and Lifetimes of Organic Nitrates Derived from Isoprene. *The Journal of Physical Chemistry A*, *121*(43), 8306–8321. https://doi.org/10.1021/acs.jpca.7b08229

Placet, M., Mann, C. O., Gilbert, R. O., & Niefer, M. J. (2000). Emissions of ozone precursors from stationary sources: A critical review. *Atmospheric Environment*, *34*(12), 2183–2204. https://doi.org/10.1016/S1352-2310(99)00464-1

Potter, C., Klooster, S., Bubenheim, D., Singh, H. B., & Myneni, R. (2003). Modeling Terrestrial Biogenic Sources of Oxygenated Organic Emissions. *Earth Interactions*, *7*(7), 1–15. https://doi.org/10.1175/1087-3562(2003)007<0001:MTBSOO>2.0.CO;2

Powers, J. C., Asgian, J. L., Ekici, Ö. D., & James, K. E. (2002). Irreversible Inhibitors of Serine, Cysteine, and Threonine Proteases. *Chemical Reviews*, *102*(12), 4639–4750. https://doi.org/10.1021/cr010182v

Priestley, M., le Breton, M., Bannan, T. J., Worrall, S. D., Bacak, A., Smedley, A. R. D., Reyes-Villegas, E., Mehra, A., Allan, J., Webb, A. R., Shallcross, D. E., Coe, H., & Percival, C. J. (2018). Observations of organic and inorganic chlorinated compounds and their contribution to chlorine radical concentrations in an urban environment in northern Europe during the wintertime. *Atmospheric Chemistry and Physics*, *18*(18), 13481–13493. https://doi.org/10.5194/acp-18-13481-2018

Prinn, R. G., Huang, J., Weiss, R. F., Cunnold, D. M., Fraser, P. J., Simmonds, P. G., McCulloch, A., Harth, C., Reimann, S., Salameh, P., O'Doherty, S., Wang, R. H. J., Porter, L. W.,

Miller, B. R., & Krummel, P. B. (2005). Evidence for variability of atmospheric hydroxyl radicals over the past quarter century. *Geophysical Research Letters*, *32*(7). https://doi.org/10.1029/2004GL022228

Qu, H., Wang, Y., Zhang, R., Liu, X., Huey, L. G., Sjostedt, S., Zeng, L., Lu, K., Wu, Y., Shao, M., Hu, M., Tan, Z., Fuchs, H., Broch, S., Wahner, A., Zhu, T., & Zhang, Y. (2021). Chemical Production of Oxygenated Volatile Organic Compounds Strongly Enhances Boundary-Layer Oxidation Chemistry and Ozone Production. *Environmental Science & Technology*, *55*(20), 13718–13727. https://doi.org/10.1021/acs.est.1c04489

Read, K. A., Carpenter, L. J., Arnold, S. R., Beale, R., Nightingale, P. D., Hopkins, J. R., Lewis, A. C., Lee, J. D., Mendes, L., & Pickering, S. J. (2012). Multiannual Observations of Acetone, Methanol, and Acetaldehyde in Remote Tropical Atlantic Air: Implications for Atmospheric OVOC Budgets and Oxidative Capacity. *Environmental Science & Technology*, *46*(20), 11028–11039. https://doi.org/10.1021/es302082p

Re-evaluation of Some Organic Chemicals, Hydrazine and Hydrogen Peroxide (Part 1, Part 2, Part 3). IARC Monographs on the Evaluation of Carcinogenic Risks to Humans Volume 71. (1999). https://publications.iarc.fr/Book-And-Report-Series/Iarc-Monographs-On-The-Identification-Of-Carcinogenic-Hazards-To-Humans/Re-evaluation-Of-Some-Organic-Chemicals-Hydrazine-And-Hydrogen-Peroxide-Part-1-Part-2-Part-3--1999

Ren, X., Brune, W. H., Mao, J., Mitchell, M. J., Lesher, R. L., Simpas, J. B., Metcalf, A. R., Schwab, J. J., Cai, C., Li, Y., Demerjian, K. L., Felton, H. D., Boynton, G., Adams, A.,

Perry, J., He, Y., Zhou, X., & Hou, J. (2006). Behavior of OH and HO2 in the winter atmosphere in New York City. *Particulate Matter Supersites Program and Related Studies*, *40*, 252–263. https://doi.org/10.1016/j.atmosenv.2005.11.073

Ren, X., Harder, H., Martinez, M., Lesher, R. L., Oliger, A., Simpas, J. B., Brune, W. H., Schwab, J. J., Demerjian, K. L., He, Y., Zhou, X., & Gao, H. (2003). OH and HO2 Chemistry in the urban atmosphere of New York City. *Atmospheric Environment*, *37*(26), 3639–3651. https://doi.org/10.1016/S1352-2310(03)00459-X

Richters, S., Herrmann, H., & Berndt, T. (2016). Different pathways of the formation of highly oxidized multifunctional organic compounds (HOMs) from the gas-phase ozonolysis of \beta -caryophyllene. *Atmospheric Chemistry and Physics*, *16*(15), 9831–9845. https://doi.org/10.5194/acp-16-9831-2016

Riedel, T. P., Bertram, T. H., Crisp, T. A., Williams, E. J., Lerner, B. M., Vlasenko, A., Li, S.-M., Gilman, J., de Gouw, J., Bon, D. M., Wagner, N. L., Brown, S. S., & Thornton, J. A. (2012). Nitryl Chloride and Molecular Chlorine in the Coastal Marine Boundary Layer. *Environmental Science & Technology*, *46*(19), 10463–10470. https://doi.org/10.1021/es204632r

Riedel, T. P., Wagner, N. L., Dubé, W. P., Middlebrook, A. M., Young, C. J., Öztürk, F., Bahreini, R., VandenBoer, T. C., Wolfe, D. E., Williams, E. J., Roberts, J. M., Brown, S. S., & Thornton, J. A. (2013). Chlorine activation within urban or power plant plumes: Vertically resolved $ClNO_2$ and Cl_2 measurements from a tall tower in a polluted

continental setting. *Journal of Geophysical Research: Atmospheres*, *118*(15), 8702–8715. https://doi.org/10.1002/jgrd.50637

Rogers, M. T. (1947). The Electric Moments and Ultraviolet Absorption Spectra of Some Derivatives of Cyclopropane and of Ethylene Oxide. *Journal of the American Chemical Society*, *69*(10), 2544–2548. https://doi.org/10.1021/ja01202a081

Rosowsky, A. (1964). Ethylene Oxides. In *Chemistry of Heterocyclic Compounds* (pp. 1–523). John Wiley & Sons, Ltd. https://doi.org/10.1002/9780470239704.ch1

Sandhiya, L., Kolandaivel, P., & Senthilkumar, K. (2013). Mechanism and Kinetics of the Atmospheric Oxidative Degradation of Dimethylphenol Isomers Initiated by OH Radical. *The Journal of Physical Chemistry A*, *117*(22), 4611–4626. https://doi.org/10.1021/jp3120868

Sawyer, R. F., Harley, R. A., Cadle, S. H., Norbeck, J. M., Slott, R., & Bravo, H. A. (2000). Mobile sources critical review: 1998 NARSTO assessment. *Atmospheric Environment*, *34*(12), 2161–2181. https://doi.org/10.1016/S1352-2310(99)00463-X

Schirmeister, T., & Klockow, A. (2003). Cysteine Protease Inhibitors Containing Small Rings. *Mini-Reviews in Medicinal Chemistry*, *3*(6), 585–596.

Schwantes, R. H., Schilling, K. A., McVay, R. C., Lignell, H., Coggon, M. M., Zhang, X., Wennberg, P. O., & Seinfeld, J. H. (2017). Formation of highly oxygenated low-volatility products from cresol oxidation. *Atmospheric Chemistry and Physics*, *17*(5), 3453–3474. https://doi.org/10.5194/acp-17-3453-2017

Seakins, P., Allanic, A., Jammoul, A., Mellouki, A., Muñoz, A., Rickard, A. R., Doussin, J.-F., Kleffmann, J., Kangasluoma, J., Lehtipalo, K., Cain, K., Dada, L., Kulmala, M., Cazaunau, M., Newland, M. J., Ródenas, M., Wiesen, P., Jorga, S., Pandis, S., & Petäjä, T. (2023). Analysis of Chamber Data. In J.-F. Doussin, H. Fuchs, A. Kiendler-Scharr, P. Seakins, & J. Wenger (Eds.), *A Practical Guide to Atmospheric Simulation Chambers* (pp. 241–291). Springer International Publishing. https://doi.org/10.1007/978-3-031-22277-1_7

Searles, S., & Tamres, M. (1951). Hydrogen Bond Formation with Saturated Cyclic Ethers1. *Journal of the American Chemical Society*, *73*(8), 3704–3706. https://doi.org/10.1021/ja01152a041

Searles, S., Tamres, M., & Lippincott, E. R. (1953). Hydrogen Bonding Ability and Structure of Ethylene Oxides. *Journal of the American Chemical Society*, *75*(11), 2775–2777. https://doi.org/10.1021/ja01107a517

Seinfeld, J. H., & Pandis, S. N. (n.d.). Atmospheric Chemistry and Physics: From Air Pollution to Climate Change, 3rd Edition | Wiley. *Wiley.Com*. https://www.wiley.com/en-us/Atmospheric+Chemistry+and+Physics%3A+From+Air+Pollution+to+Climate+Change%2C+3rd+Edition-p-9781118947401

Shrivastava, M., Andreae, M. O., Artaxo, P., Barbosa, H. M. J., Berg, L. K., Brito, J., Ching, J., Easter, R. C., Fan, J., Fast, J. D., Feng, Z., Fuentes, J. D., Glasius, M., Goldstein, A. H., Alves, E. G., Gomes, H., Gu, D., Guenther, A., Jathar, S. H., … Zhao, C. (2019). Urban pollution greatly enhances formation of natural aerosols over the Amazon rainforest.

Nature Communications, *10*(1), 1046–1046. https://doi.org/10.1038/s41467-019-08909-4

Singh, H. B., & Hanst, P. L. (1981). Peroxyacetyl nitrate (PAN) in the unpolluted atmosphere: An important reservoir for nitrogen oxides. *Geophysical Research Letters*, *8*(8), 941–944. https://doi.org/10.1029/GL008i008p00941

Singh, H. B., Kanakidou, M., Crutzen, P. J., & Jacob, D. J. (1995). High concentrations and photochemical fate of oxygenated hydrocarbons in the global troposphere. *Nature*, *378*(6552), 50–54. https://doi.org/10.1038/378050a0

Skov, H., Benter, Th., Schindler, R. N., Hjorth, J., & Restelli, G. (1994). Epoxide formation in the reactions of the nitrate radical with 2,3-dimethyl-2-butene, cis- and trans-2-butene and isoprene. *Atmospheric Environment*, *28*(9), 1583–1592. https://doi.org/10.1016/1352-2310(94)90304-2

Solomon, S., Garcia, R. R., Rowland, F. S., & Wuebbles, D. J. (1986). On the depletion of Antarctic ozone. *Nature*, *321*(6072), 755–758. https://doi.org/10.1038/321755a0

Soni, M., Sander, R., Sahu, L. K., Taraborrelli, D., Liu, P., Patel, A., Girach, I. A., Pozzer, A., Gunthe, S. S., & Ojha, N. (2023). Comprehensive multiphase chlorine chemistry in the box model CAABA/MECCA: Implications to atmospheric oxidative capacity. *EGUsphere*, *2023*, 1–24. https://doi.org/10.5194/egusphere-2023-652

Starit, L. A., Ketcham, Roger., Jambotkar, D., & Shah, V. P. (1964). Three-Membered Rings. I. Conjugative Properties and Electrinic Spectra of Arylcyclopropanes, Oxiranes, and

Thiiranes. *Journal of the American Chemical Society*, *86*(21), 4628–4630. https://doi.org/10.1021/ja01075a022

Stevenson, D. S., Zhao, A., Naik, V., O'Connor, F. M., Tilmes, S., Zeng, G., Murray, L. T., Collins, W. J., Griffiths, P. T., Shim, S., Horowitz, L. W., Sentman, L. T., & Emmons, L. (2020). Trends in global tropospheric hydroxyl radical and methane lifetime since 1850 from AerChemMIP. *Atmospheric Chemistry and Physics*, *20*(21), 12905–12920. https://doi.org/10.5194/acp-20-12905-2020

Stropoli, S. J., Miner, C. R., Hill, D. R., & Elrod, M. J. (2019). Assessing Potential Oligomerization Reaction Mechanisms of Isoprene Epoxydiols on Secondary Organic Aerosol. *Environmental Science & Technology*, *53*(1), 176–184. https://doi.org/10.1021/acs.est.8b05247

Surratt, J. D., Chan, A. W. H., Eddingsaas, N. C., Chan, M., Loza, C. L., Kwan, A. J., Hersey, S. P., Flagan, R. C., Wennberg, P. O., & Seinfeld, J. H. (2010). Reactive intermediates revealed in secondary organic aerosol formation from isoprene. *Proceedings of the National Academy of Sciences*, *107*(15), 6640–6645. https://doi.org/10.1073/pnas.0911114107

Tamres, M., Searles, S., Leighly, E. M., & Mohrman, D. W. (1954). Hydrogen Bond Formation with Pyridines and Aliphatic Amines1. *Journal of the American Chemical Society*, *76*(15), 3983–3985. https://doi.org/10.1021/ja01644a035

Tovar, C. M., Barnes, I., Bejan, I. G., & Wiesen, P. (2022). Kinetic study of the atmospheric oxidation of a series of epoxy compounds by OH radicals. *Atmospheric Chemistry and Physics*, *22*(10), 6989–7004. https://doi.org/10.5194/acp-22-6989-2022

Tovar, C. M., Haack, A., Barnes, I., Bejan, I. G., & Wiesen, P. (2021). Experimental and theoretical study of the reactivity of a series of epoxides with chlorine atoms at 298 K. *Physical Chemistry Chemical Physics*, *23*(9), 5176–5186. https://doi.org/10.1039/D0CP06033J

Vereecken, L. (2018). Reaction Mechanisms for the Atmospheric Oxidation of Monocyclic Aromatic Compounds. In *Advances in Atmospheric Chemistry: Vol. Volume 2* (pp. 377–527). WORLD SCIENTIFIC. https://doi.org/10.1142/9789813271838_0006

Vereecken, L., Glowacki, D. R., & Pilling, M. J. (2015). Theoretical Chemical Kinetics in Tropospheric Chemistry: Methodologies and Applications. *Chemical Reviews*, *115*(10), 4063–4114. https://doi.org/10.1021/cr500488p

Villanueva, F., Cabañas, B., Monedero, E., Salgado, S., Bejan, I., & Martin, P. (2009). Atmospheric degradation of alkylfurans with chlorine atoms: Product and mechanistic study. *Atmospheric Environment*, *43*(17), 2804–2813. https://doi.org/10.1016/j.atmosenv.2009.02.030

Virmani, A., Walavalkar, M. P., Sharma, A., Sengupta, S., Saha, A., & Kumar, A. (2020). Kinetic studies of the gas phase reaction of 1,2-propylene oxide with the OH radical over a temperature range of 261–335 K. *Atmospheric Environment*, *237*, 117709. https://doi.org/10.1016/j.atmosenv.2020.117709

Wallington, T. J., Dagaut, P., & Kurylo, M. J. (1988). Correlation between gas-phase and solution-phase reactivities of hydroxyl radicals towards saturated organic compounds. *J. Phys. Chem.*, *92*(17), 5024–5028. https://doi.org/10.1021/j100328a039

Wallington, T. J., Liu, R., Dagaut, P., & Kurylo, M. J. (1988). The gas phase reactions of hydroxyl radicals with a series of aliphatic ethers over the temperature range 240–440 K. *International Journal of Chemical Kinetics*, *20*(1), 41–49. https://doi.org/10.1002/kin.550200106

Walsh, A. D. (1947). Structures of Ethylene Oxide and Cyclopropane. *Nature*, *159*(4047), 712–713. https://doi.org/10.1038/159712a0

Walsh, A. D. (1949). The structures of ethylene oxide, cyclopropane, and related molecules. *Transactions of the Faraday Society*, *45*(0), 179–190. https://doi.org/10.1039/TF9494500179

Wang, D. S., & Ruiz, L. H. (2017). Secondary organic aerosol from chlorine-initiated oxidation \hack\newline of isoprene. *Atmospheric Chemistry and Physics*, *17*(22), 13491–13508. https://doi.org/10.5194/acp-17-13491-2017

Wang, Q., Ni, S., Bai, F., & Pan, X. (2022). Theoretical investigation on atmospheric reaction mechanism, kinetics and SAR estimations of four-carbon ketones and alcohols. *Atmospheric Environment*, *271*, 118915. https://doi.org/10.1016/j.atmosenv.2021.118915

Wang, X., Jacob, D. J., Eastham, S. D., Sulprizio, M. P., Zhu, L., Chen, Q., Alexander, B., Sherwen, T., Evans, M. J., Lee, B. H., Haskins, J. D., Lopez-Hilfiker, F. D., Thornton, J.

A., Huey, G. L., & Liao, H. (2019). The role of chlorine in global tropospheric chemistry. *Atmospheric Chemistry and Physics*, *19*(6), 3981–4003. https://doi.org/10.5194/acp-19-3981-2019

Wayne, R. P. (1985). *Chemistry of atmospheres*. https://www.osti.gov/biblio/6852065

Weigend, F., & Ahlrichs, R. (2005). Balanced basis sets of split valence, triple zeta valence and quadruple zeta valence quality for H to Rn: Design and assessment of accuracy. *Phys. Chem. Chem. Phys.*, *7*(18), 3297–3305. https://doi.org/10.1039/B508541A

Wiberg, K. B. (1996). Bent Bonds in Organic Compounds. *Accounts of Chemical Research*, *29*(5), 229–234. https://doi.org/10.1021/ar950207a

Worton, D. R., Surratt, J. D., Lafranchi, B. W., Chan, A. W. H., Zhao, Y., Weber, R. J., Park, J.-H., Gilman, J. B., de Gouw, J., Park, C., Schade, G., Beaver, M., Clair, J. M. S., Crounse, J., Wennberg, P., Wolfe, G. M., Harrold, S., Thornton, J. A., Farmer, D. K., … Goldstein, A. H. (2013). Observational insights into aerosol formation from isoprene. *Environmental Science & Technology*, *47*(20), 11403–11413. https://doi.org/10.1021/es4011064

Xu, L., Guo, H., Boyd, C. M., Klein, M., Bougiatioti, A., Cerully, K. M., Hite, J. R., Isaacman-VanWertz, G., Kreisberg, N. M., Knote, C., Olson, K., Koss, A., Goldstein, A. H., Hering, S. V., de Gouw, J., Baumann, K., Lee, S.-H., Nenes, A., Weber, R. J., & Ng, N. L. (2015). Effects of anthropogenic emissions on aerosol formation from isoprene and monoterpenes in the southeastern United States. *Proceedings of the National Academy*

of Sciences of the United States of America, *112*(1), 37–42. https://doi.org/10.1073/pnas.1417609112

Xue, L. K., Saunders, S. M., Wang, T., Gao, R., Wang, X. F., Zhang, Q. Z., & Wang, W. X. (2015). Development of a chlorine chemistry module for the Master Chemical Mechanism. *Geoscientific Model Development*, *8*(10), 3151–3162. https://doi.org/10.5194/gmd-8-3151-2015

Young, C. J., Washenfelder, R. A., Edwards, P. M., Parrish, D. D., Gilman, J. B., Kuster, W. C., Mielke, L. H., Osthoff, H. D., Tsai, C., Pikelnaya, O., Stutz, J., Veres, P. R., Roberts, J. M., Griffith, S., Dusanter, S., Stevens, P. S., Flynn, J., Grossberg, N., Lefer, B., … Brown, S. S. (2014). Chlorine as a primary radical: Evaluation of methods to understand its role in initiation of oxidative cycles. *Atmospheric Chemistry and Physics*, *14*(7), 3427–3440. https://doi.org/10.5194/acp-14-3427-2014

Zhang, F., Wang, Y., Zhang, X., Zhang, X., Liu, H., & Han, B. (2020). Recent advances in the coupling of CO_2 and epoxides into cyclic carbonates under halogen-free condition. *Green Chemical Engineering*, *1*(2), 82–93. https://doi.org/10.1016/j.gce.2020.09.008

Zhang, Q., Jimenez, J. L., Worsnop, D. R., & Canagaratna, M. (2007). A Case Study of Urban Particle Acidity and Its Influence on Secondary Organic Aerosol. *Environmental Science & Technology*, *41*(9), 3213–3219. https://doi.org/10.1021/es061812j

Zhang, X., Ortega, J., Huang, Y., Shertz, S., Tyndall, G. S., & Orlando, J. J. (2018). A steady-state continuous flow chamber for the study of daytime and nighttime chemistry

under atmospherically relevant NO levels. *Atmospheric Measurement Techniques*, *11*(5), 2537–2551. https://doi.org/10.5194/amt-11-2537-2018

Zhou, S., Yeung, L. W., Y., Forbes, M., W., Mabury, S., & Abbatt, J., P. ,. D. (2017). Epoxide formation from heterogeneous oxidation of benzo[a]pyrene with gas-phase ozone and indoor air. *Environmental Science: Processes & Impacts*, *19*(10), 1292–1299. https://doi.org/10.1039/C7EM00181A

Zou, B., & Hu, C. (2017). Halogen-free processes for organic carbonate synthesis from CO2. *Current Opinion in Green and Sustainable Chemistry*, *3*, 11–16. https://doi.org/10.1016/j.cogsc.2016.10.007

9 Illustrations

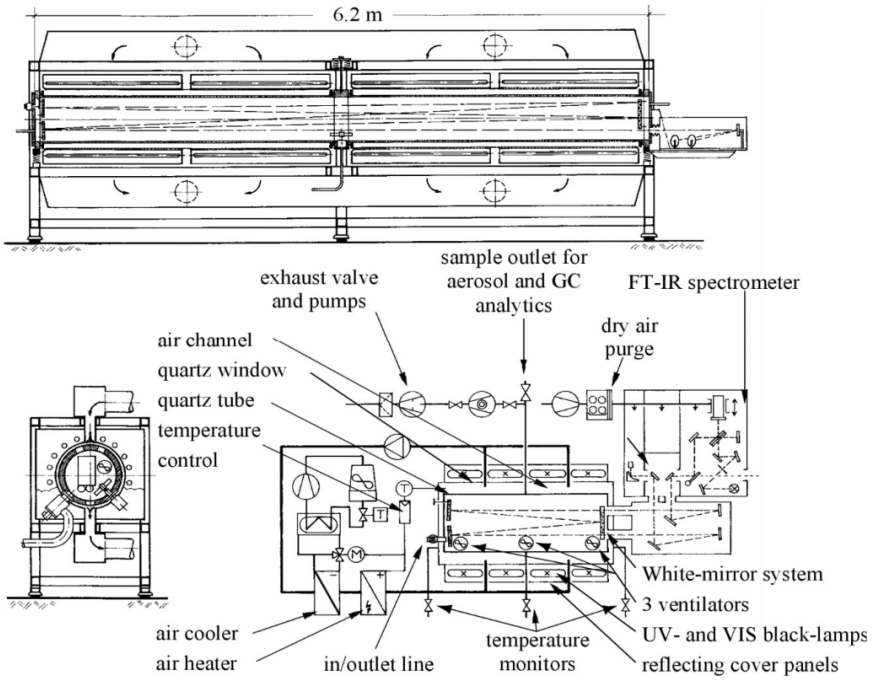

Figure 28 Scheme of the 1080 L chamber (QUAREC), adapted from Barnes et al. (1994).

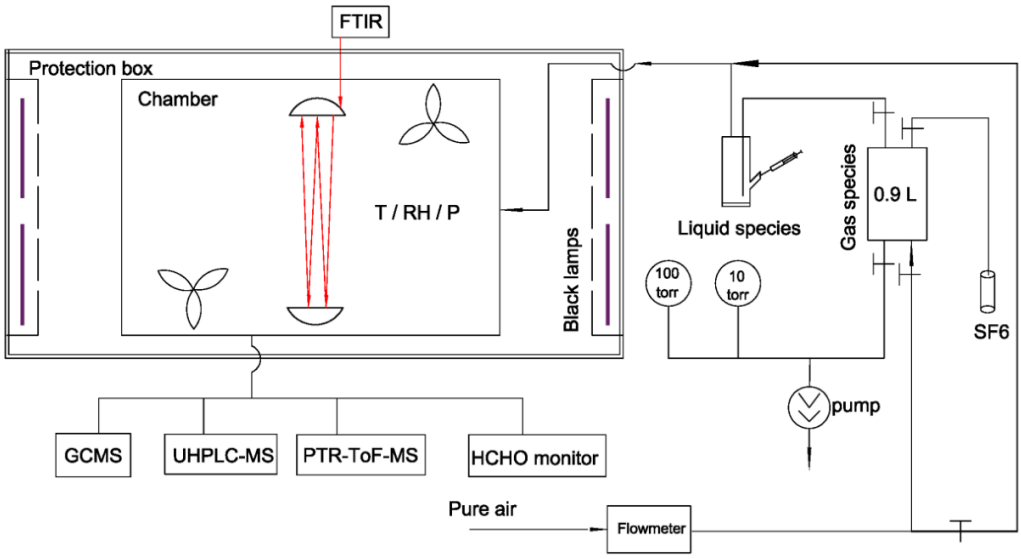

Figure 29 Schematic diagram of the 7.3 m³ simulation chamber facility (This figure has been adapted from Yangang REN, Atmospheric degradation of VOCs: Isoprene and its ozonolysis products, a perfluoro-ketone and long chain ketones (2017), with permission. The original figure was obtained from the author's thesis and has been included in this work for illustrative purposes.

10 Glossary

Volatile Organic Compounds (VOCs)

Organic compounds with high vapor pressure that easily evaporate into the atmosphere. VOCs play a crucial role in atmospheric chemistry, leading to the formation of ozone and secondary organic aerosols (SOAs).

Epoxides

A class of cyclic ethers characterized by a three-membered oxygen-containing ring. Epoxides are highly reactive intermediates in oxidation reactions and contribute to secondary organic aerosol formation.

Master Chemical Mechanism (MCM)

A comprehensive reaction mechanism used to model the atmospheric degradation of VOCs and their transformation into oxidation products and secondary pollutants.

C–C Cleavage

The breaking of a carbon–carbon bond during oxidation, leading to smaller fragment molecules. This process significantly influences the formation of low-volatility oxidation products and atmospheric reactivity.

C–O Cleavage

The breaking of a carbon–oxygen bond, which can alter the oxidation products and affect the volatility of atmospheric organic compounds. This type of cleavage is relevant in epoxide degradation and oxidation processes.

Rearrangement

A chemical process in which atoms or groups within a molecule shift to form a different structural configuration, often occurring during oxidation and radical reactions in atmospheric chemistry.

Isomerization

The transformation of a molecule into another structural form with the same molecular formula but different connectivity or spatial arrangement. Isomerization is a key step in oxidation pathways, affecting product distribution.

1,2-Shift

A specific type of rearrangement where an atom or functional group moves from one carbon to an adjacent carbon within a molecule. This process plays a role in radical and ionic mechanisms during atmospheric oxidation.

Secondary Organic Aerosols (SOAs)

Particulate matter formed from the oxidation of VOCs, contributing to air pollution, cloud formation, and climate effects by modifying atmospheric radiative properties.

11 Annex

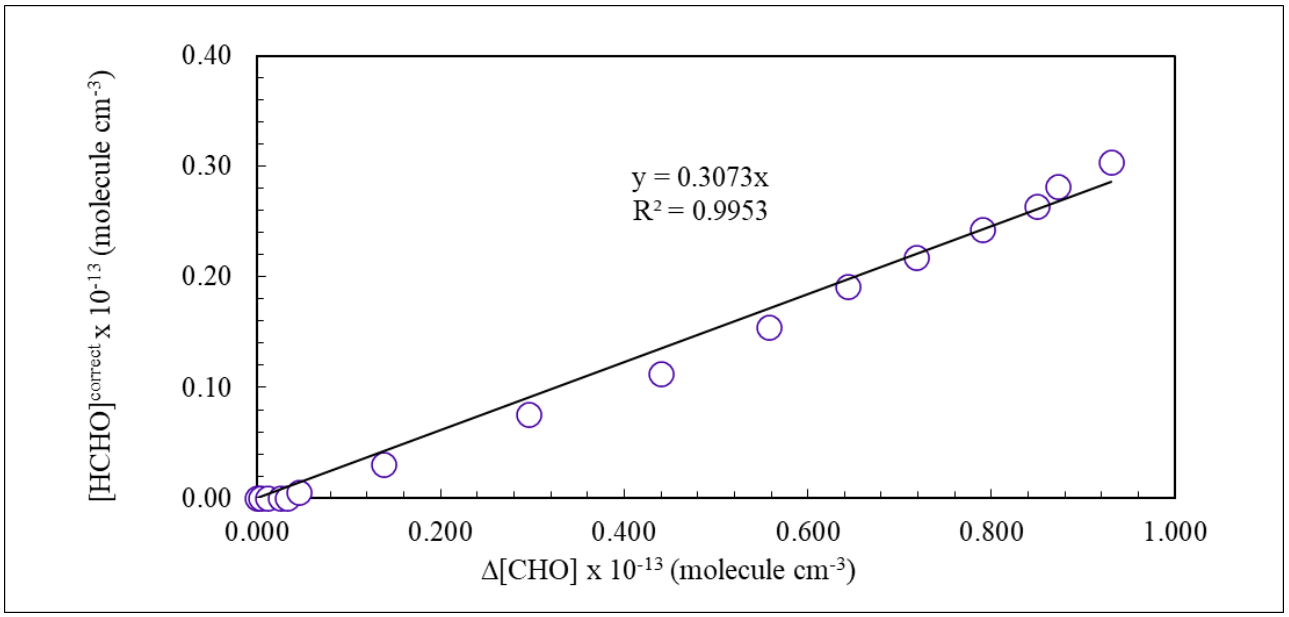

Figure 30 Yield plots of HCHO in the CHO + OH reaction where the consumption of CHO is corrected for the wall loss. Experiment performed at University of Wuppertal-480L chamber

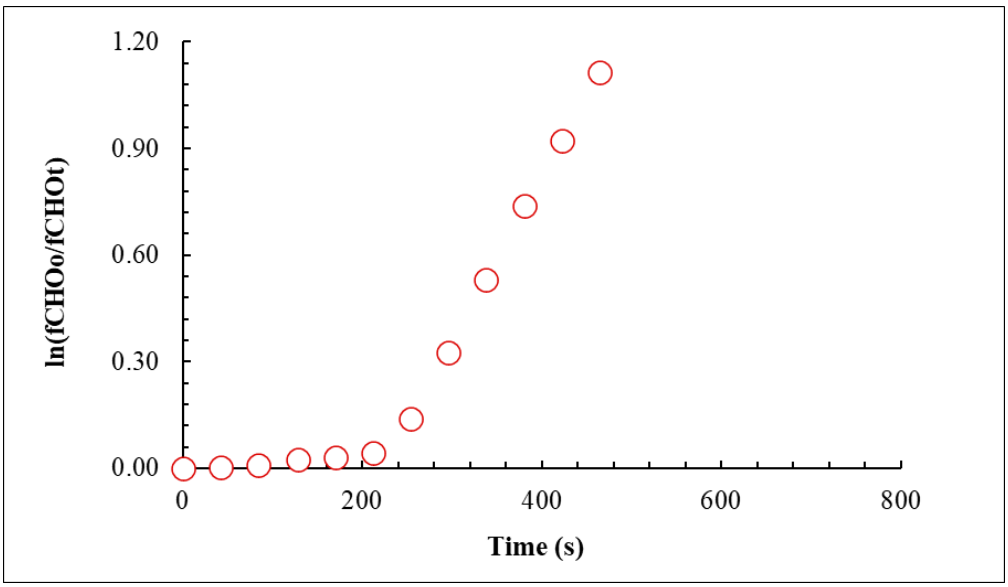

Figure 31 Plot for [OH] in the CHO + OH reaction where the consumption of CHO is corrected for the wall loss. Experiment performed at University of Wuppertal-480L chamber

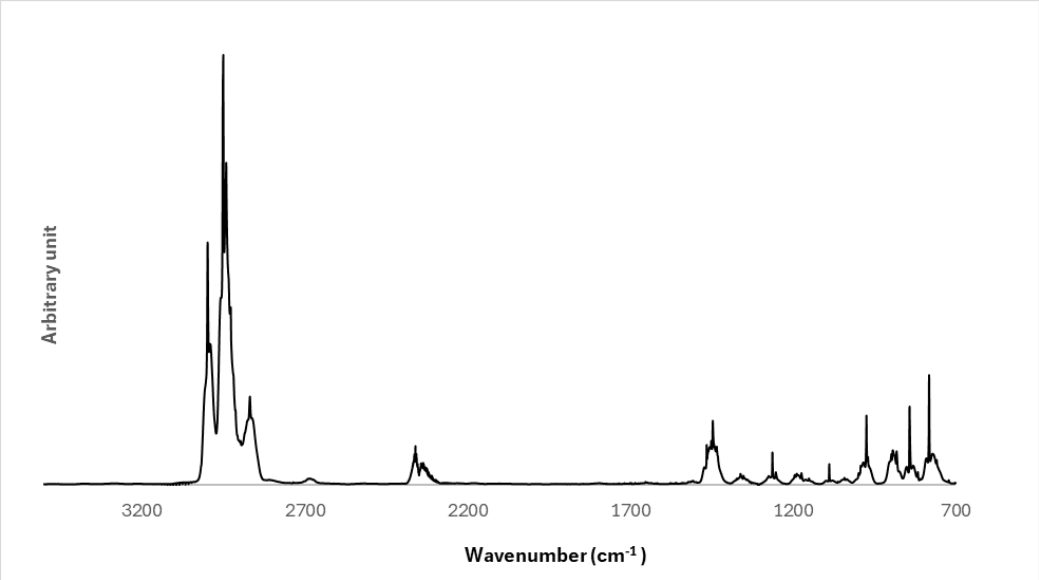

Figure 32 FTIR spectra of cyclohexane oxide (CHO) in the gas-phase